2015-01-01

Defeating Anisotropy In Material Extrusion 3d Printing Via Materials Development

Ángel Ramón Torrado Pérez
University of Texas at El Paso, artorradoperez@miners.utep.edu

DEFEATING ANISOTROPY
IN MATERIAL EXTRUSION 3D PRINTING
VIA MATERIALS DEVELOPMENT

ÁNGEL RAMÓN TORRADO PÉREZ,

Doctoral Program in Materials Science and Engineering

APPROVED:

David A. Roberson, Ph.D., Chair

Jose Nuñez, Ph.D.

Cristian Botez, Ph.D.

Stephen Stafford, Ph.D.

Charles Ambler, Ph.D.
Dean of the Graduate School

DEDICATION

A mi mujer, mis padres y mi abuelo.

Por ser las estrellas que me muestran el camino a través del desierto que es la vida.

To my wife, my parents and my grandfather.

For being the stars showing me the path through the dessert that is life.

DEFEATING ANISOTROPY
IN MATERIAL EXTRUSION 3D PRINTING
VIA MATERIALS DEVELOPMENT

by

ÁNGEL RAMÓN TORRADO PÉREZ
Ingeniería Industrial: Mecánica
U.P.M.

DISSERTATION

Presented to the Faculty of the Graduate School of
The University of Texas at El Paso
in Partial Fulfillment
of the Requirements
for the Degree of

DOCTOR OF PHILOSOPHY

Materials Science and Engineering
THE UNIVERSITY OF TEXAS AT EL PASO
May 2015

ACKNOWLEDGEMENTS

Not very often do you have the chance to express your gratitude sincerely. It has become an everyday ritual in our society habits to routinely say “thank you” and hopefully receive a “you are welcome” in return, but it is quite rare to have the opportunity to sit down and come up with the words to really express “thanks” for something. Due to the busy lives we live nowadays, sometimes we take for granted a lot of the things that surround us, and do not stop to really appreciate them.

Thanks to Dr. David A. Roberson. Starting your life in a new country can be one of the toughest and most discouraging situations somebody could have to face. He has guided me in my research, letting me choose my path in many aspects, and supported me during my whole time at UTEP.

Thanks to all my friends in El Paso: They have helped me enjoy this city from a different perspective: Gilberto Siqueiros, Carmen Rocha, Nubia Zuverza, Max Winter and Esteban Salcedo. They have made my life in El Paso much easier and have been true friends at all times. They strangely found that spending time with me was worth it.

Thanks to the rest of my collegues: Brenda Arellano, Adriana Ramirez, Joel English and Fabian Álvarez-Primo. They helped me get to the end of this journey.

Thanks to the students and staff in the Keck Center for letting me borrow their equipment, and involving me with their team. Especially to Corey Shemelya for the support and the writing advice.

Thanks to my committee and professors at UTEP for providing me with the right directions and tools needed for the journey that is research.

Thanks to every institution, department and person responsible for the funding support for research that I have received during my time at UTEP.

Thanks to all my family. My family in Spain that has always found a way to stay together even considering their individual differences. And my new parents and brother in law that made possible my stay in the United States, that I can’t thank them enough for being so blindly and kindly supportive with a total stranger.

Thanks to my parents and my brother for always believing, supporting and being there for me with any decision I've made, even if they weren't completely satisfied with them.

Thanks to my grandfather: a model to follow, who has always known how to balance success in all different aspects of life: work, family and enjoyment.

And last but not definitely not least the most sincere thanks to my wife Stephanie Diebold, my real supporter, the one that has truly been there all the time, in the good and the bad moments, tolerating my bad moods and believing in me the whole time. You are the yang in my yin.

Thanks to all of you and to the people not explicitly mentioned here: You all deserve a place here. There is no combination of words able to express the gratitude I have for you.

ABSTRACT

Additive Manufacturing technologies has been in continuous development for more than 35 years. Specifically, the later denominated Material Extrusion Additive Manufacturing (MEAM), was first developed by S. Scott Crump around 1988 and trademarked later as Fused Deposition Modeling (FDM). Although all of these technologies have been around for a while, it was not until recently that they have been more accessible to everyone. Today, the market of 3D printers covers all ranges of price, from very specialized, heavy and expensive machines, to desktop printers of only a few cubic inches in volume. Until recently, FDM technology had remained somewhat stagnant in terms of developments; however, with the new market boom, scholars and hobbyists have opened new doors for investigation in this area. The technology is now better understood from a software, mechanical, electrical and not less important, materials point of view.

The current availability of materials for MEAM is very broad: PLA (Polylactic Acid), ABS (Acrylonitrile Butadiene Styrene), PC (Polycarbonate), PEEK (Polyether Ether Ketone), nylon, polyurethanes, and many others. Even so, these are all materials that were used before for other technologies, adapted but not specifically developed for MEAM. The processes that take place during the production of a part are currently not very well understood, and the final properties exhibited are long ways away from reaching the potential of more traditional manufacturing techniques. Due to the nature of the process, all the material properties always display a certain level of anisotropy.

The research covered in these pages aims to shed some light on understanding the different mechanics taking place during the extrusion process of additive manufacturing. The development of new materials for MEAM has been explored. Several blends and composites have been developed, and their tensile properties and fracture mechanics evaluated. The blending of different combinations of ABS, UHMWPE (Ultra High Molecular Weight Polyethylene) and SEBS (Styrene Ethylene Butylene Styrene) were further examined due to the potential they demonstrated as low anisotropic materials in terms of strength. Also, the geometrical influence of different standard tensile specimens was studied.

The development of materials that lead to lowered anisotropy on the strength of 3D printed parts has been successfully demonstrated, and alternative methodologies for the evaluation of anisotropic characteristics has been proposed as well. The present work shows the beginning to a better understanding of the mechanics taking place during the fusion of deposited material in MEAM.

TABLE OF CONTENTS

LIST OF TABLES

LIST OF FIGURES

CHAPTER 1: INTRODUCTION

1.1. Statement of the problem

Build orientation-caused mechanical property anisotropy is one of the biggest challenges to overcome in material extrusion 3D printing (ME3DP). The difference in mechanical properties (typically measured by differences in tensile test specimens) of the resulting parts fabricated by ME3DP has been reported multiple times in literature [1-11]. The parts fabricated by additive manufacturing usually exhibit different mechanical properties depending on the given direction. The anisotropic nature of the building process already suggests that the mechanical properties will present certain anisotropy as well (Figure 1.1 a and b). This makes the design process difficult as it forces the designer to think on the optimal way to position the part in the 3D printer that will lead to the most robust part. In some situations, the ideal positioning is not possible due to the manufacturing difficulty. Thus, a compromise in either the design or the final properties of the part must be made [10].

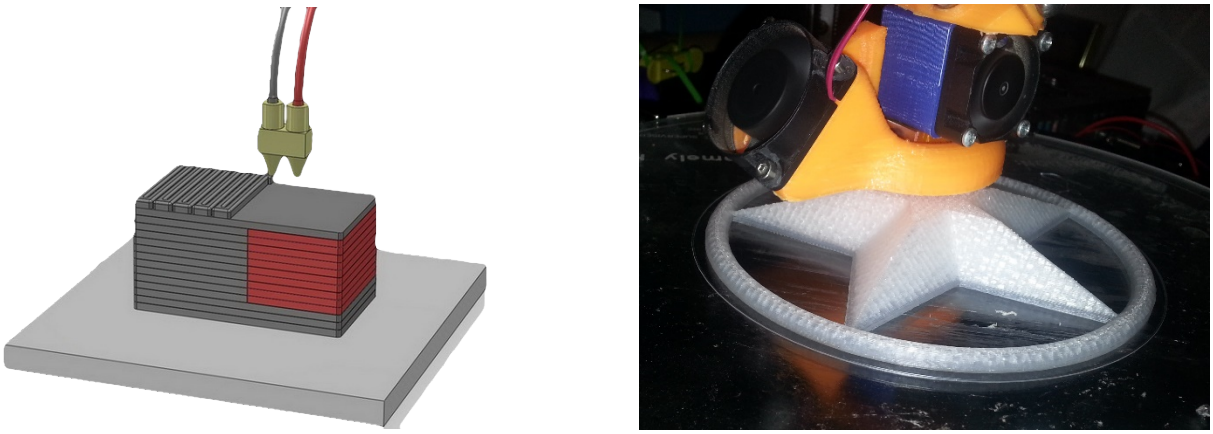

Figure 1.1: Extrusion-based additive manufacturing: (a) Material Extrusion Process [20] (b) Example of a Printed Part

Most of the documents that we can find in our literature research bases their studies in the mechanical design of the process and while this plays a very important role in the final properties of the part, it seems that most of the researches are obviating the impact of the different materials in these final properties. Only a recent publication by Shaffer *et al*. [11] attacks the problem with a completely different

and novel approach in which PLA was blended with triallyisocyanurate (TAIC), a radiation sensitizers that improves crosslinkage in rubbery materials. The final parts produced with these novel materials are then irradiated with gamma rays. They demonstrated and increase of a 70% of the tensile strength for the most unfavorable direction. The drawback of the process was the increase of the standard deviation of the UTS by more than 4 times [11]. On the other hand, the diminished anisotropy appears only when heated is applied to the specimens, and therefore it is unclear if it´s a result of the use of radiation on the samples or the heat applied to the samples, that could have led to a better bonding between the rasters.

3D printing is in continuous expansion to specialized wide variety of industries such as the aerospace, automotive, and health care. Moreover, adoption of this manufacturing method is growing even faster in the personal use spectrum. At the same time it moves from being considered only as a rapid prototyping centered technique to a rapid manufacturing process that generates completely functional and finished or a few steps back from finished products. The total market for all the manufacturing techniques is estimated to grow at a 30% annual rate in the following 15 years according to a Credit Suisse's report. For 2016, the estimation for materials in the additive manufacturing market would be close to $1.4 billion (Figure 1.2) [21, 22].

The positive market estimates insight the imminent high demand for new, innovative and high-tech materials The development of materials that diminish the weakening effect due to the raster orientation would enormously simplify the design process, reducing the importance of the slicing stage and the orientation of fabrication.

While the growth of AM is inevitable, there are several issues which must be overcome. Here, the intent is to solve a problem observed in every AM technology [1-18].

In order for AM to reach its full potential, a method to defeat mechanical property anisotropy must be realized.

The work proposed here seeks to limit the mechanical property anisotropy through the development of new polymer matrix composites and polymer blends. When completed, this effort will answer the following research questions:

1. Can new materials be developed which will exhibit a lower mechanical sensitivity to build orientation.

2. What specific material aspects have the greatest effect in the resulting anisotropy?

3. What processing parameters are critical in the creation of new polymeric matrix composites and polymer blends?

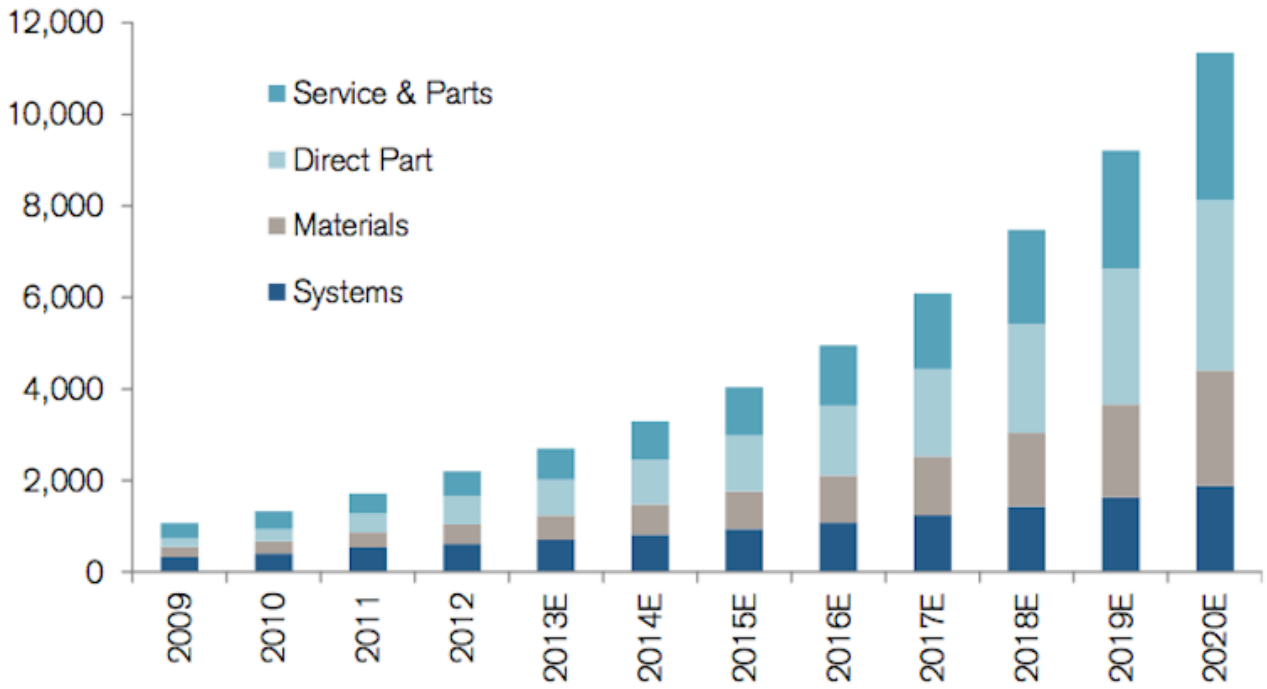

Figure 1.2: Primary global AM Market. US$ in millions. Credit Suisse estimates [21].

Preliminary work and proposed future work are discussed in the following sections. Success of this project could allow AM to reach its full potential as the manufacturing method of choice for society.

1.2. Background

Additive manufacturing, now more commonly known as 3D printing, represents a number of techniques where a digital three-dimensional model is processed into a physical part. The part is fabricated by the addition of material in subsequent layers with different shapes until the desired 3D object is realized. The novelty of this manufacturing process relies in adding material to compose the part, as opposed to the traditional subtractive manufacturing methodologies [20, 23]. Other technologies are detailed in Table 1.1.

Table 1.1: Additive Manufacturing: Most Common processes [24]

Classification	Technology	Description	Materials	Developers (Country)
Binder Jetting	3D Printing Ink-jetting S-Print M-Print	Creates objects by depositing a binding agent to join powdered material.	Metal, Polymer, Ceramic	ExOne (US) VoxelJet (Germany) 3D Systems (US)
Direct Energy Deposition	Direct Metal Deposition Laser Deposition Laser Consolidation Electron Beam Direct Melting	Builds parts by using focused thermal energy to fuse materials as they are deposited on a substrate.	Metal: Powder and wire	DM3D (US) NRC-IMI (Canada) Irepa Laser (France) Trumpf (Germany) Sciaky (US)
Material Extrusion	Fused Deposition Modeling	Creates objects by dispensing material through a nozzle to build layers.	Polymer	Stratasys (US) Delta Micro Factory (China) 3D Systems (US) RepRap Projects
Material Jetting	Polyjet Ink-jetting Thermojet	Builds parts by depositing small droplets of build material, which are then cured by exposure to light.	Photopolymer, Wax	Stratasys (US) LUXeXcel (Netherlands) 3D Systems (US)
Powder Bed Fusion	Direct Metal Laser Sintering Selective Lase Melting Electron Beam Melting Selective Laser Sintering	Creates objects by using thermal energy to fuse regions of a powder bed.	Metal, Polymer, Ceramic	EOS (Germany) Renishaw (UK) Phenyx Systems (France) Matsuura Machinery (Japan) ARCAM (Sweden) 3D Systems (US)
Sheet Lamination	Ultrasonic Consolidation Laminated Object Manufacture	Builds a part by trimming sheets of material and binding them together in layers.	Hybrids, Metallic, Ceramic	Fabrisonic (US) CAM-LEM (US)
VAT Photopolymerisation	Stereolithography Digital Light Processing	Builds parts by using light to selectively cure layers of material in a vat of photopolymer	Photopolymer, Ceramic	3D Systems (US) EnvisionTEC (Germany) DWS Srl (Italy) Lithoz (Austria)

1.2.1. Material extrusion additive manufacturing

Material extrusion or extrusion-based additive manufacturing is an additive manufacturing technique in which the material is selectively dispensed through a nozzle. This technique was developed in 1989 by S. Scott Crump, co-founder of Stratasys, Ltd. Crump patented the technology under the name fused deposition modeling® (FDM®) [25]. Fused filament fabrication (FFF) is another more generic, common way to denote this technique, first coined by the members of the Reprap project.

Acrylonitrile butadiene styrene (ABS) and polylactic acid (PLA) are the two thermoplastics most commonly used with these techniques. Other available thermoplastics for special applications are polycarbonate (PC), polyphenylsulfone (PPSF) and ULTEM, but these materials present some difficulties because they require higher extrusion temperatures and lower melting flow indexes (MFI), and advanced

techniques to overcome the warping effects. The use of low melting point metal alloys has been tried in the past, [26] and other laternative materials such as low and high density polyethylene (LDPE and HDPE) have been mentioned to be used without much practical demonstration of it. [27-30] Nevertheless, the use of various nylon grades is currently increasing. [31-33] The printer is usually characterized by two vertical extruders and a platform. The extruders have the ability of moving in the two horizontal directions but rarely in the vertical (Z) direction. One extruder will be loaded with the primary material for the part, and the other one with the material that will be used as support; in some cases both extruders will be loaded with primary materials to produce multi-material parts. The platform will usually be responsible of the vertical movement of the part, though other printer systems exist with static platforms and XYZ positional be extruders, such as delta printers. [34, 35]

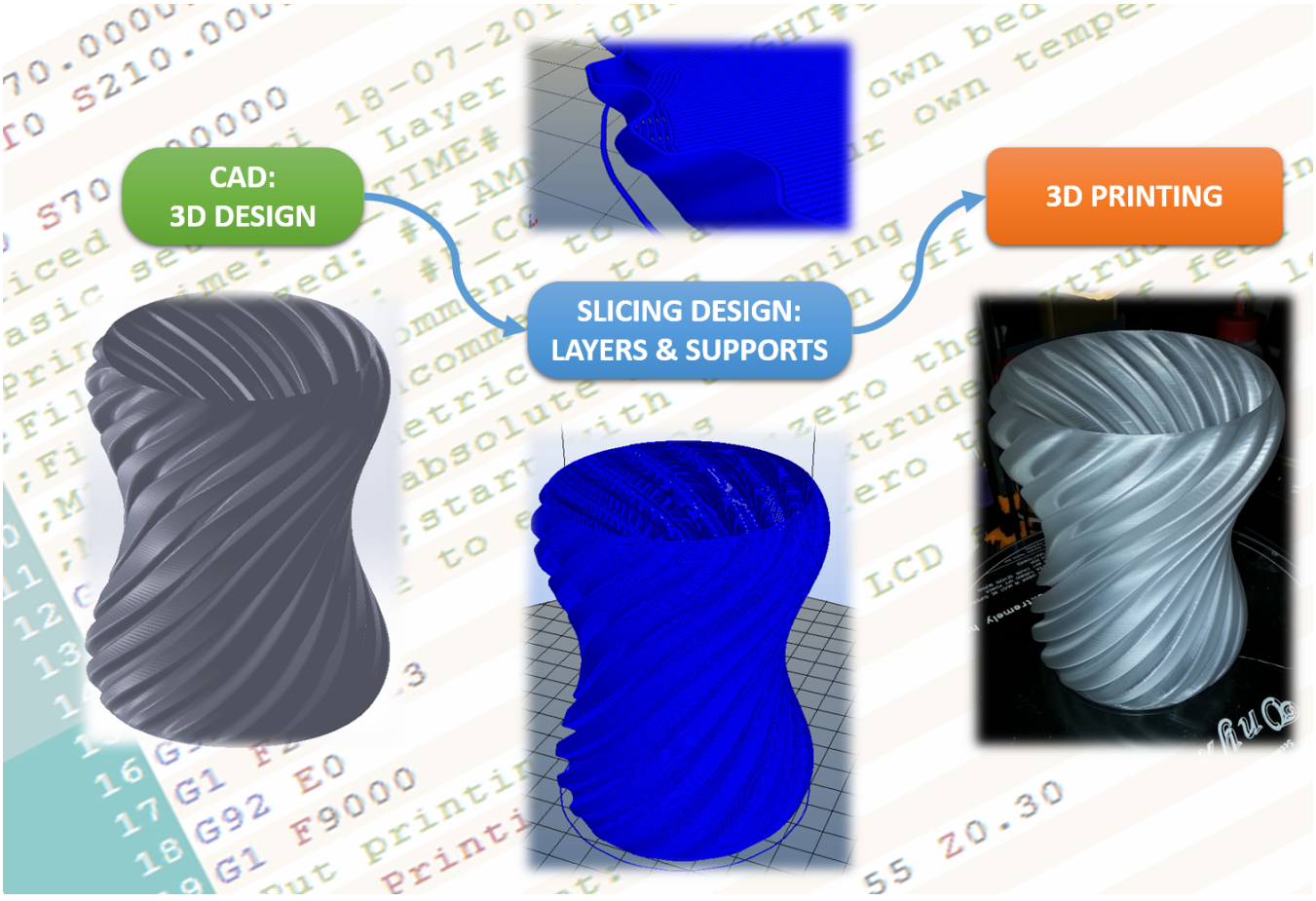

Figure 1.3: The steps in 3D printing: Scripted vases. Design by Håkan Langemark [36]

The part is design first with computer-aided design (CAD) software to generate a stereolithography file format (STL) file. This file will be processed again with a computer-aided manufacturing (CAM) tool that will generate the file with the information to govern the extruders and the platform. It is in this step where we will usually be prompted to select all the parameters that will determine the characteristics of the final part. The part is usually not fabricated completely solid. The printer will fabricate the part by depositing layer after layer. The shape of each layer will be drawn first, to be later filled with the chosen pattern, and the process is repeated until the part is completely finished. In some cases it is possible to choose the density of the part, meaning the filling percentage of material with which the part will be fabricated. In this case, the inner layers of the part will be drawn with a pattern that fulfills the chosen density ratio; this structure is completely surrounded by a continuous shell of material. It is reasonable to expect some kind of anisotropy in the parts produced with this technology due to the process that has been described. A schematic view of the process for a vase can be seen in Figure 1.3 [20, 23].

The most common applications for ME3DP are rapid prototyping and rapid manufacturing when they overcome the limitations related to the cost, that is, low number of units to be fabricated and very complex shapes that are not practical in other traditional methodologies for some low number fabrication runs Figure 1.4.

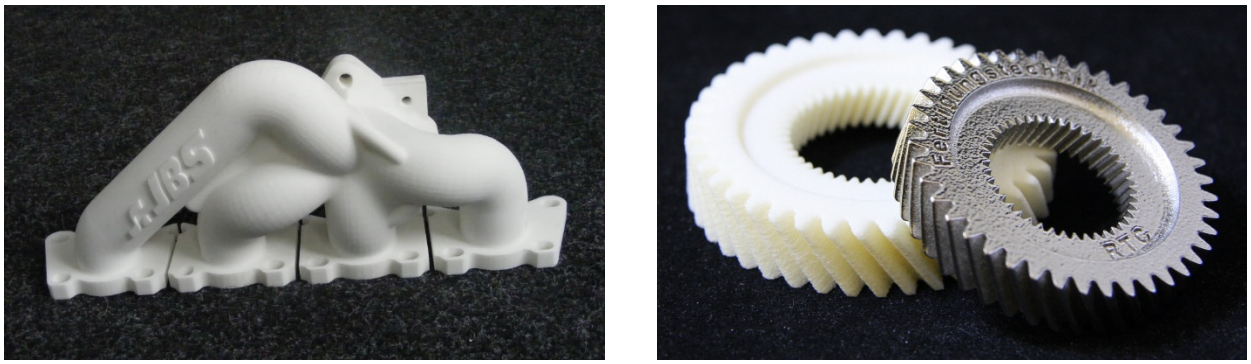

Figure 1.4: Rapid prototyping and rapid manufacturing examples [37, 38]

1.2.2. Slicing a part

The decisions taken during the slicing process of the 3D model are crucial in the final properties of the part [1-9]. The parameters available to the designer will depend of the machine being used. Some high end machines provide proprietary software that gives little margin of configuration to the operator,

but the final result is very good. It is usually the open-source 3D printing software the one that provides the user with more options, in part because a much longer and tedious set-up process is needed, but as well due to the diversity of machines that this software generally supports. It is necessary to highlight Skeinforge, Slic3r, Cura or Kisslicer among the most powerful slicing engines currently available for ME3DP. The parameters can significantly differ depending on the logic that each of them uses to decode the three-dimensional design, but in the end the output code will be very similar for all the tools. In any case, even the least configurable machines share some basic parameters that need to be defined prior to generate the file that will govern the 3D printer, although the material profiles can be already predefined.

Nozzle and filament diameter: It is necessary to define the nozzle size you are using and the filament diameter. It is possible to define a slightly smaller or bigger nozzle size than the actual installed nozzle. This will affect the slicing and the thickness of printed threads. This technique is usually referred to as over or underextrusion printing. The current standards for filament diameter are 1.75 and 3.00mm. A good quality tolerance is around ±0.05mm. A too think filament will jam the extruder while a too thin filament won't be stiff enough to be fed. The quality of the filament plays a very important role in the final quality of the part.

Extrusion and bed temperature: In some machines these values will be predefined by the material profile, but others will allow total flexibility. The color and the grade of the plastic can make a big difference in the printing parameters of the material, requiring variations of several tens of degrees. The printing speed plays an important role in the extrusion temperature required as well. This way, ABS is usually printed between 200 and 260°C and PLA between 170 and 240°C. The bed temperature helps the material to stick better on the platform as well as reducing the temperature gradient on the part, and therefore the warping. The temperature used in the bed is usually closed to, but below the glass transition temperature of the material (around 110°C for ABS and 70°C for PLA).

Envelope temperature: Some high end machines print in an enclosed envelope with a controlled temperature environment. In old machines is possible to control this temperature while in the new ones is usually given by the material profile being printed. This system helps to avoid warping effects due to temperature gradients in the parts.

Cooling fan: The printability of some materials or small parts can in general be improved by adding a small cooling fan that helps reducing the temperature of the fresh printed layers. Sometimes the part does not cool fast enough and deforms while trying to print successive layers. It is necessary that the part is kept hot enough to avoid a large difference of temperature with the material being extruded but cold enough to avoid it being dragged. This parameter needs to be adjusted depending on the size of the part being printed and the speed at which the process is being developed.

Layer thickness: The layer thickness is one of the most important parameters in ME3DP. It usually needs to be a value 60% or below the nozzle diameter size. The most common values are 0.4, 0.2 and 0.1mm. The layer thickness will affect the final properties of the parts as well as the surface finish.

Infill density, angle and patterns: One of the most interesting characteristics in ME3DP is the possibility of deciding the internal density of the part, that is, the plastic to air ratio. Any value is possible, from a completely empty part with only the external shell drawn, to a traditional 100% full part. Values between 35 and 100% are usually utilized. If the part is fabricated solid, the layers will use a rectilinear pattern in which parallel lines will be drawn and each layer pattern will usually be perpendicular to the previous layer. Some slicers allow to define the angle of rotation of the lines with each layer. When the infill is other than 100%, the process will be the same but the lines will be separated by a distance that will depend of the value selected. In some cases, other patterns will be available in this section such as honeycomb, Hilbert curve, archimedian chords or octagram spiral. Figure 1.5 shows some of these infill patterns varying with the infill density [39].

Vertical and horizontal shells: If the part is not going to be printed solid (100% infill), then these parameters define the minimum thickness of the solid walls in the external surface of the part, and usually can be set up independently for the lateral, and top and bottom surfaces. The perimeters will be drawn with a concentric pattern, independently of the infill pattern chosen.

Spiral vase: Some parts are meant to be printed with a single thread wall thickness. Some slicers have an option to spiralize the contour making the part from a single continuous thread instead of layers, smoothing the final look of the product.

Extrusion widths and overlapping: The width of the extruded threads is indirectly defined by the set nozzle size, but some slicers allow to define some corrections to these preset configurations. This way, we can define how much the threads will overlap, or ask the machine to over or under-extrude in some areas of the part (shells, perimeters, infill, thin walls, etc.).

Purging, skirts, brims, rafts and supports: During the purging stage, the machine gets rid of the plastic that remained in the nozzle and that is most likely corrupted due to excess of temperature. Each machine purges in a different way, either extruding some material on the air and brushing the nozzle afterwards, either extruding the corrupted material over the platform in an unused portion of it, or as an unused thread surrounding the part to be printed (skirt). In order to ensure adhesion to the platform. A brim or raft can be used.

Printing speeds: First and last layers, perimeters, infill, bridging.

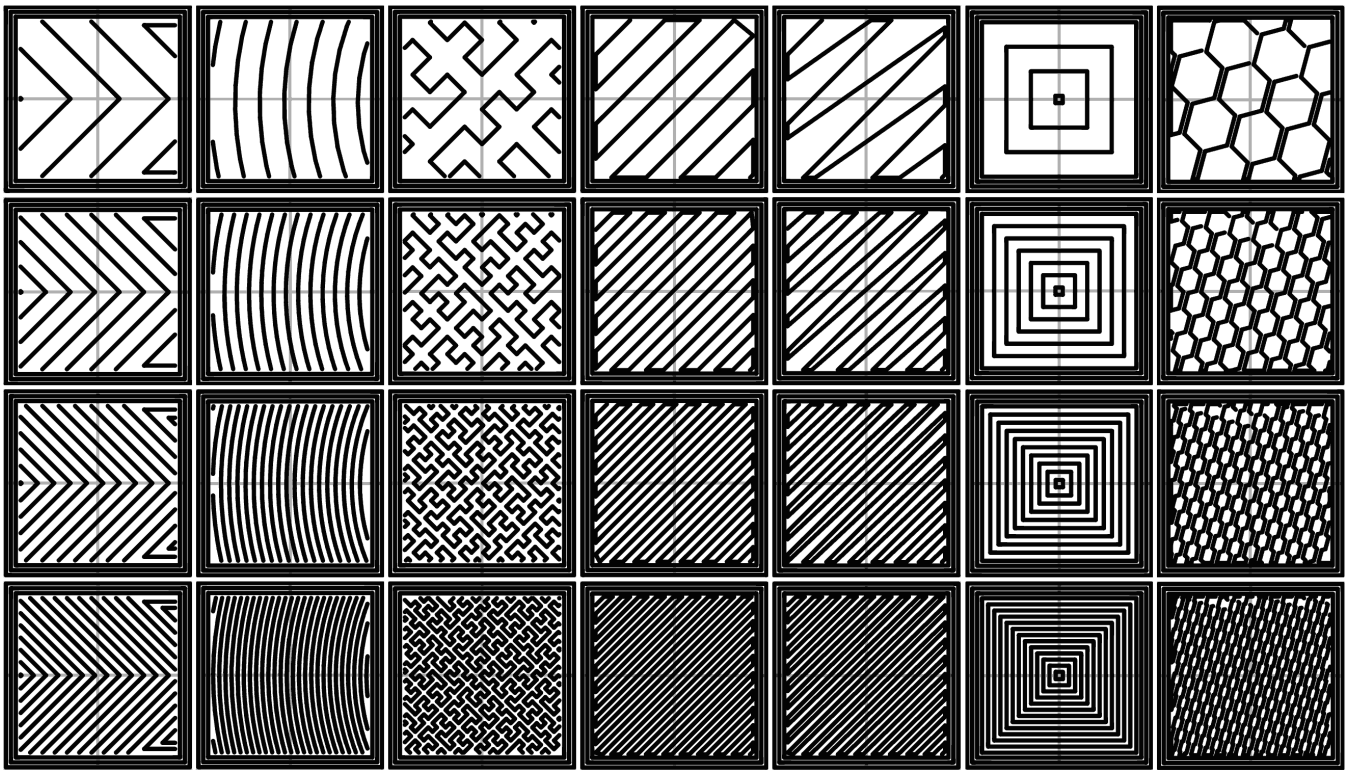

Figure 1.5: Infill patterns at varying densities. Top to bottom: 20%, 40%, and 60%. Left to Right: Honeycomb, Concentric, Line, Rectilinear, Hilbert Curve, Archimedean Chords, Octagram Spiral. Adapted from [39]

1.2.3. Composites in material extrusion additive manufacturing

The number of materials currently available for use in ME3DP are very limited when compared to other traditional manufacturing processes. This fact already points to the limitations for the practical applications of this technology, the application of end user parts fabricated from this technology, and the great need for new opportunities for novel printable material systems to be researched. The desirable properties for a printable material are: 1) a low glass transition temperature; 2) a moderately high melting flow index; and 3) a little tendency to shrinkage. There are not many materials that fulfill these requirements and, therefore, composition of materials looks like the logical path to follow in order to engineer their physical properties to optimize them to specific applications.

The composite can be based on a thermoplastic matrix that is already printable or for which the properties will be modified to make it printable. The chosen polymer is then loaded with different reinforcement agents. These reinforcement agents can be particles or fibers (polymeric composites), or other polymeric materials (polymeric blends or alloys). The addition of these agents will lead to changes on the mechanical properties such as ultimate tensile strength (UTS), the Young's modulus and fracture toughness; these properties have been linked to the loading ratio, the particle size or fiber length, and the surface adhesion between the materials [40,41]. The modification of other physical or chemical properties can be of special interest as well. Some examples of these properties are the thermal stability, the coefficient of thermal expansion, the decomposition temperature or ignition resistance, radiation penetration, biocompatibility, or wear resistance. Most often, the addition of alien substances to polymer will result in a weakened mixture with worse properties than the initial material. These effects can in some cases be palliated or completely reversed with the use of compatibilizers.

1.3. Plastics

A plastic material is a synthetic or semi-synthetic organic moldable solid. They are essentially petroleum based but some of them are partially obtained from natural sources. They are mostly based on organic polymers, large molecules composed by a repeated monomeric unit. These monomers are usually based on hydrocarbon chains linked to oxygen, chlorine, fluorine and/or nitrogen. Other different molecular groups confer specific properties to the plastic. Plastics are usually classified into thermoplastics and thermosets. [42]

1.3.1. Thermosets

Thermosets cure over a given temperature through a chemical reaction, not being possible to reshape them again. The strong cross-linkage created during the curing process confers high mechanical properties to the plastic but at the same time they tend to be more brittle. Reheating a thermoset usually leads to their decomposition, complicating the recycling process, if possible at all. Sometimes, thermosets are grounded to be used as reinforcement agents with other plastics. They can stand higher temperatures than thermoplastics, being ideal for high temperature applications, or as glues or varnishes [43-45].

1.3.2. Thermoplastics

Thermoplastics can be heated to be reshaped several times without altering their chemical composition. This is the reason why they are usually produced as pellets to be used later in extrusion, injection molding or 3D printing. Thermoplastics are more easily recycled and have a wider range of uses [43-45]. They conform the vast majority of the plastic produced, covering a percentage of the total as high as 80%.

Thermoplastic materials drastically change their mechanical properties according to the temperature. We can define three different ranges of temperature that are defined by the glass transition temperature, (T_g,) and the melting temperature ($T_{m)}$. Below the glass-liquid transition temperature T_g, thermoplastics exhibit a completely amorphous, glassy structure, becoming hard and brittle materials. The material experiences a pronounced decrease in the viscosity when the T_g is reached and it usually becomes rubbery due to a mix of rigid crystalline and elastic amorphous regions. Thermoplastics are therefore divided into amorphous and crystalline depending on the ratio of crystallization. Very few plastics are completely amorphous or crystalline and they are rather classified in this categories depending more on their actual properties. When the melting temperature T_m is reached, the thermoplastic becomes a liquid and acquires a completely disordered structure again, but in this case, with a high tendency to flow (Figure 1.6) [46, 47].

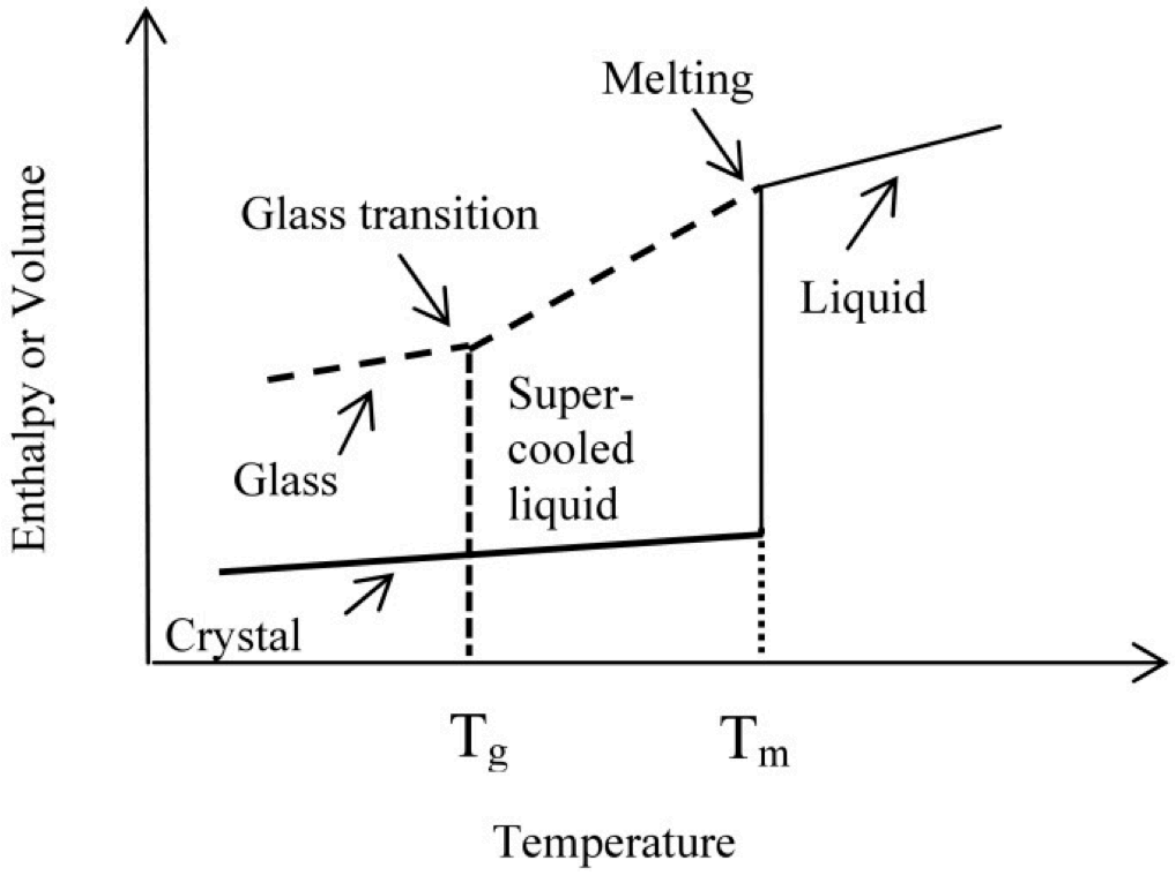

Figure 1.6: Behavior of thermoplastics [47]

Polyamide

Polyamide is a chain of a repeated unit linked by amide bonds. R-nE(O)$_x$NR'$_2$ where R and R' refer to a H or an organic group, and E to another element, usually C, S or P. They can be found naturally or be produced artificially. Polyamides are classified into *aliphatic polyamides*, *polyphthalamides* and *aramides*. Examples of polyamides are nylon, kevlar and nomex among many others, and some of their types are naturally present in wood or silk.

The aliphatic polyamides are commonly known as nylon in general. Their general properties can be found in Table 1.2. The most common types of nylon are nylon-6 (Figure 1.7 and Table 1.3), nylon-6,6 (Figure 1.8 and Table 1.4), nylon-6,9, nylon-6,10, nylon-6,12, nylon-11, nylon-12 and nylon-4,6.

Table 1.2: Nylon: General properties [48]

Density	1.15 g/cm^3
Melting point	463-624 ^oC

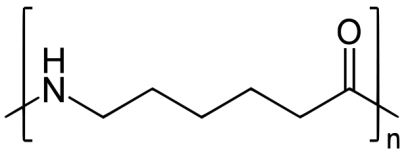

Figure 1.7: Nylon-6

Table 1.3: Nylon-6 [48]

Generic name	Nylon-6
IUPAC name	poly(hexano-6-lactam)
Molecular formula	$(C_6H_{11}NO)_n$
Density	1.084 g/cm^3
Melting point	583-613 K
Glass transition	413 K
Tensile Strength	90-100 MPa
Young's Modulus	3.2 GPa
Elongation break	9 %
Izod Impact Strength	30-250 J/m

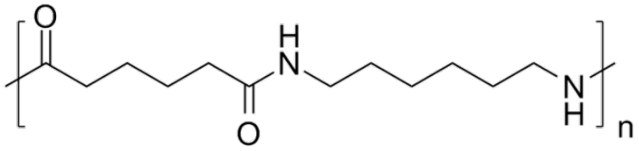

Figure 1.8: Nylon-6,6

Table 1.4: Nylon-6,6 [48]

Generic name	Nylon-6,6
IUPAC name	Poly[imino(1,6-dioxohexamethylene)imnohexamethylene
Molecular formula	$(C_{12}H_{22}N_2O_2)_n$
Density	1.15-1.24 g/cm^3
Melting point	537 K
Tensile Strength	78 MPa
Young's Modulus	1.7-3.3 GPa
Elongation break	30-60 %
Izod Impact Strength	53-133 J/m

Polyethylene (PE)

Polyethylenes (PE) are a family of polyolefins based on long hydrocarbon chains based on the ethylene monomer, usually with $(C_2H_4)_nH_2$ as chemical formula (Figure 1.9). Their general properties can be found in Table 1.6.

They have very good chemical resistance in most cases. The glass transition is very difficult to identify in many cases but it usually goes from -130 to -80 ºC. Polyethylenes are usually highly crystalline as well. Polyethylenes are usually classified by their molecular weight, branching and crystallinity (Table 1.5): HDPE (High Density Polyethylene, Table 1.7) is a material with more linear molecule with very few side brasssnches. LDPE (Low Density Polyethylene, Table 1.8) has much shorter molecules but they are branched, decreasing the compactness ability and therefore the density. LLDPE (Linear Low Density Polyethylene) is similar to LDPE but the molecules have shorter branches. HMWPE (High Molecular Weight Polyethylene) and UHMWPE (Ultra High Molecular Weight Polyethylene) has higher molecular weight molecules than HDPE which translates into higher toughness, wear and abrasion resistance and impact strength, but a more difficult injectability.

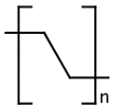

Figure 1.9: Polyethylene

Table 1.5: Polyethylene: Classification

UHMWPE	Ultra-high-molecular-weight polyethylene
HMWPE	High-molecular-weight polyethylene
HDXLPE	High-density cross-linked polyethylene
HDPE	High-density polyethylene
PEX or XLPE	Cross-linked polyethylene
MDPE	Medium-density polyethylene
LLDPE	Linear low-density polyethylene
LDPE	Low-density polyethylene
ULMWPE or PE-WAX	Ultra-low-molecular-weight polyethylene
VLDPE	Very-low-density polyethylene
CPE	Chlorinated polyethylene

Table 1.6: Polyethylene: General properties

IUPAC name	Polyethene or Poly(methylene)
Density	0.880-0.940 g/cm^3
Melting point	378-403 ^oC
Glass transition	143-193 K
Crystallinity	60-80 %

Table 1.7: HDPE [48]

Generic name	HDPE
IUPAC name	High-density polyethylene
Density	0.996 g/cm^3
Melting point	391-419 K
Tensile Strength	10-60 MPa
Young's Modulus	0.06-0.3 GPa
Elongation break	400-1800 %
Izod Impact Strength	30-200 J/m

Table 1.8: LDPE [48]

Generic name	LDPE
IUPAC name	Low-density polyethylene
Density	0.910-0.935 g/cm^3
Melting point	378-388 K
Tensile Strength	9-15 MPa
Young's Modulus	0.1-0.3 GPa
Elongation break	100-800 %
Izod Impact Strength	No break

Polypropylene (PP)

Polypropylene (PP) is a polymer based on the repetition of the propene monomer (Figure 1.10). It is a technical plastic that competes with plastics as ABS due to its strength, toughness, flexibility and good resistance to fatigue and chemical abrasion [48]. Its general properties can be found in Table 1.9.

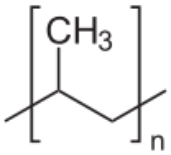

Figure 1.10: Polypropylene

Table 1.9: Polypropylene: General properties [48]

Generic name	Polypropylene
IUPAC name	Poly(propene)
Molecular formula	$(C_3H_6)_n$
Density	0.855 g/cm^3 (amorphous)
	0.946 g/cm^3 (crystalline)
Melting point	398-459 K
Glass transition	283-293 K
Tensile Strength	25-35 MPa
Young's Modulus	0.5 GPa
Elongation break	150-300 %
Izod Impact Strength	20-100 J/m

Acrylonitrile butadiene styrene (ABS)

Acrylonitrile butadiene styrene (ABS, Figure 1.11) is a complex polymer based on the combination of the three monomers composing its name. These monomers are combined in different proportions to confer specific properties to the final material. These proportions can vary from 15 to 35% acrylonitrile, 5 to 30% butadiene and 40 to 60% styrene. The acrylonitrile group is responsible of forming polar bondings between the chains, producing a stronger material. The butadiene is a rubbery substance,

providing better resilience. The styrene produces a shiny, glossy finish [49]. ABS is an absolutely amorphous plastic, therefore has no true melting [50]. The general properties are gathered in Table 1.10.

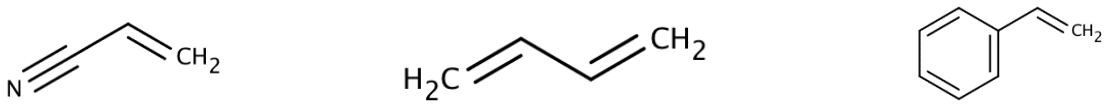

Figure 1.11: ABS (a) Acrylonitrile (b) Butadiene (c) Styrene

Table 1.10: ABS. General properties [50]

Generic name	Acrylonitrile butadiene styrene
Molecular formula	$(C_8H_8)_x$Â·$(C_4H_6)_y$Â·$(C_3H_3N)_z$
Density	1.04 g/cm^3
Melting point	Undetermined
Glass transition	378 K
Tensile Strength	40-60 MPa
Young's Modulus	2.3 GPa
Elongation break	55-125 %

Polylactic Acid (PLA)

Polylactic acid (PLA, Figure 1.12) is a biodegradable, biocompatible and recyclable thermoplastic aliphatic polyester, extensively researched and utilized. PLA's properties has shown potential to be easily tailored within a wide range of values. These properties in conjunction with the easiness and low-consuming processability make PLA a polymer very well suited for packaging, consumer and biomedical applications. On the other hand, PLA suffers from having poor toughness when compared with traditional petrochemical-based polymers. PLA is chemically unstable, therefore degrades over time at a rate that depends on its specific chemical composition [48, 51, 52]. PLA has a high number of possible polymerizations, being two of the most common types poly-L-lactide (PLLA) and poly-D-lactide (PLDA), or a combination of both. The chemical and physical properties can differ substantially depending on the specific microcomposition [53]. PLA is of extensive use by hobbyist for 3D printing due to its high printability and low extrusion temperature. Its properties are located at Table 1.11.

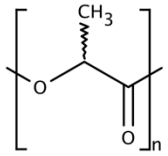

Figure 1.12: Polylactic Acid

Table 1.11: Polylactic Acid. General properties [48]

Generic name	Polylactic acid
Molecular formula	$(C_3H_4O_2)_n$
Density	1.25-1.29 g/cm^3
Melting point	418-459K
Glass transition	323-337K
Tensile Strength	28-50 MPa
Young's Modulus	1.2-3.0 GPa
Elongation break	2-6 %

Thermoplastic Polyurethane (TPU)

Thermoplastic polyurethane (TPU) is a variant inside the family of polyurethanes, characterized for being a linear elastomer. It is due to this characteristic that TPU has thermoplastic properties. TPUs are the third most widely used thermoplastic elastomer, covering 15% of the total market. Among their many benefits we can highlight their high elasticity, transparency, chemical stability and resistance to abrasion. Based on their chemical origin the main classed of TPUs are polyester TPUs, polyether TPUs and polycaprolactone TPUs, all of them with differences in their final properties and applications [48, 55-56].

Polycarbonate (PC)

Polycarbonate is the name that receives a group of polymers based on carbonate groups on their structures (Figure 1.13). The most common of these polymers is synthesized based on bisphenol A (BPA) and phosgene COCL2. Polycarbonate is a very strong and impact resistant plastic, with high transparency, but is easy to scratch and highly hygroscopic. It can be cold-processed, as it can be largely deformed without cracking [54]. The most common commercial names are LEXAN® (Sabic), MAKROLON®

(Bayer) or CALIBRE® (Styron) among others. The properties of PC based on BPA can be found in Table 1.12.

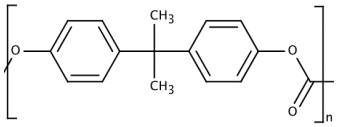

Figure 1.13: Polycarbonate

Table 1.12: Polycarbonate based on BPA [48]

Generic name	Polycarbonate
Density	1.20 - 1.22 g/cm^3
Melting point	428 K
Glass transition	423 K
Tensile Strength	55-75 MPa
Young's Modulus	2.0-2.4 GPa
Elongation break	110 %

Polyetherimide (PEI)

Polyetherimide (Figure 1.14) is an amorphous thermoplastic with an amber-transparent color, commonly known as ULTEM® (Sabic) is a thermoplastic with outstanding resistance to heat and flames, very high strength and modulus and easy to process by traditional molding processes. Therefore, its applications usually involve high temperature environments and composition with other reinforcing agents [48, 54, 54]. The properties of PEI can be found in Table 1.13.

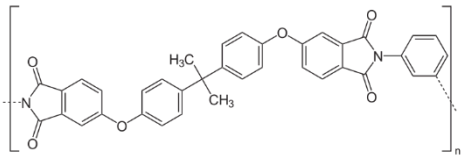

Figure 1.14: PEI

Table 1.13: Polyetherimide [48]

Generic name	Polyetherimide
Molecular formula	$(C_{37}H_{24}O_6N_2)_n$
Density	1.27 g/cm^3
Melting point	477-505 K
Glass transition	489 K
Tensile Strength	83-179 MPa
Young's Modulus	3.0 GPa
Elongation break	50-70 %

Polyetheretherketone (PEEK)

Polyetheretherketone (Figure 1.15) is a semicrystalline thermoplastic with very good mechanical properties and thermal stability, and abrasion and chemical resistance. Suitable for high temperature applications. It is commonly known as KETRON® (Cope) or KETASPIRE® (Solvay). It is used as a replacement to metals in certain applications [54-57]. Its properties are collected in Table 1.14.

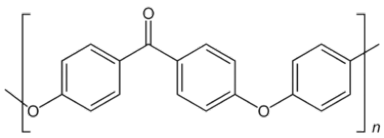

Figure 1.15: PEEK

Table 1.14: Polyetheretherketone [50, 57]

Generic name	Polyetheretherketone
Molecular formula	$(CH_2O)_n$
Density	1.32 g/cm^3
Melting point	616 K
Glass transition	416 K
Tensile Strength	90-100 MPa
Young's Modulus	3.7 GPa
Elongation break	50 %

1.3.3. Compatibilizers

Silanes

Silanes are inorganic compounds with chemical formula SiH_4. Among many other applications, the interest on silanes rely on their uses as coupling agents or adhesion promoters to help adhere fibers or particles to polymeric matrices. Silanes chemically functionalize the external surface of the particles creating a coating that will interact in a better manner with the polymer, facilitating the bonding and avoiding the delamination [58, 59]. Silanes might be the solution to anisotropy in 3D printing, helping to produce a better adhesion in the deposition of the new layers. The selection of the silane compound depends on the specific polymeric matrix [60-62]. The most common silanes can be found in Tables 1.15, 1.16, 1.17, 1.18, 1.19, 1.2, 1.21 and 1.22.

Table 1.15: Amino silanes [62]

Amino silane	Acrylic, Epoxy, Melamine, Nitrile, Nylon, Phenolic, PVC, Urethane
	gamma-Aminopropyltriethoxysilane
	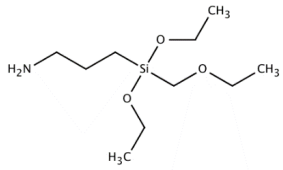

Table 1.16: Chloropropyl [62]

Chloropropyl	ABS, Elastomer, Epoxy, Polyolefin, Urethane
	3-Chloropropyltriethoxysilane
	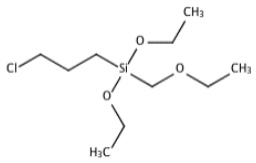

Table 1.17: Epoxide [62]

Epoxide	Acrylic, Epoxy, Polyester, Polysulfide, Urethane
	gamma-Glycidoxypropyltrimethoxysilane
	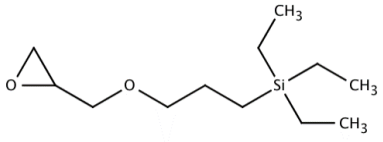

Table 1.18: Other [62]

Other	Elastomers
	3-Thiocyanatopropyltriethoxysilane 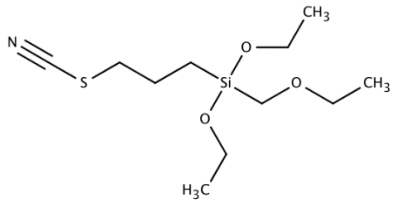

Table 1.19: Mercapto [62]

Mercapto	Elastomers
	3-Mercaptopropyltriethoxysilane 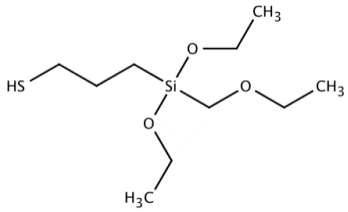

Table 1.20: Sulfides [62]

Sulfides	Elastomers
	Bis(3-Triethoxysilylpropyl)tetrasulfide 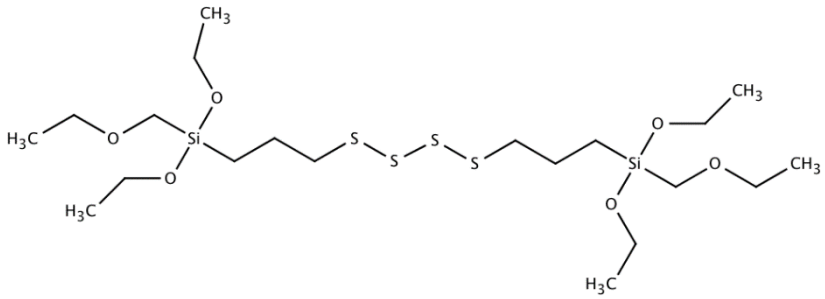 Bis(3-Triethoxysilylpropyl)disulfide 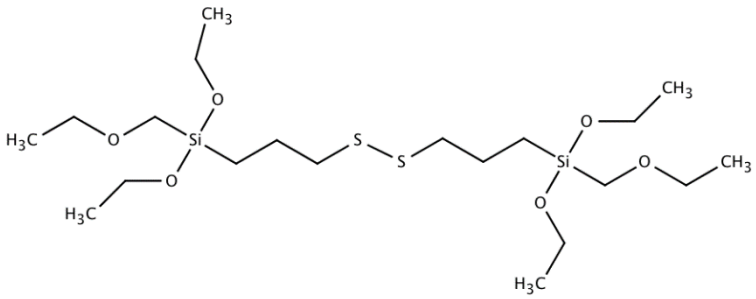

Table 1.21: Methacryloxy [62]

Methacryloxy	Acrylic, EVA, Polyester, Polyolefin
	gamma-Methacryloxypropyltrimethoxysilane
	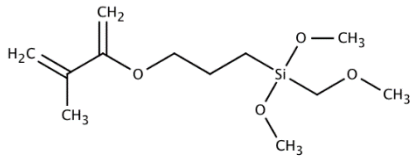

Table 1.22: Vinyl [62]

Vinyl	Polyester Resin, Thermoplastic Olefin
	Vinyltrimethoxysilane
	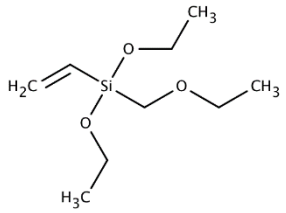
	Tris(methoxyethoxy)ethenylsilane
	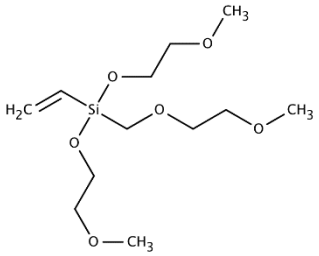

Maleic Anhydride

Maleic anhydride (MA) is an organic compound with chemical formula C2H2(CO)2O (Figure 1.16) extensively used as compatibilizer in different ways. Some of this compatibilization processes can be achieved by means of a coating for filler elements, copolymerizing to form new polymeric chains or directly grafting on polymeric surfaces.

The MA groups could potentially be used to produce blends of incompatible polymers such as ABS and polyethylenes by grafting with the molecules of the polymers increasing the linkage between the plastics involved. [63-67]

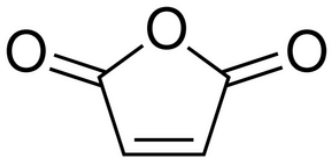

Figure 1.16: Maleic Anhydride

1.4. Extrusion of thermoplastics

Extrusion is a continuous process in which the material is pushed through a die to create objects with a constant cross sectional profile. Extrusion can be used with a wide number of material types, such as metal, ceramics, food and of course, plastic [68, 69].

Extrusion of thermoplastics begins with the material in the form of pellets or powder. This material is heated and pushed by the screw or screws through a die that provides the specific shape desired. The raw materials for material extrusion additive manufacturing are thermoplastic filaments with a circular section, usually 1.75 or 3.00mm of diameter, that are provided in spools by weight.

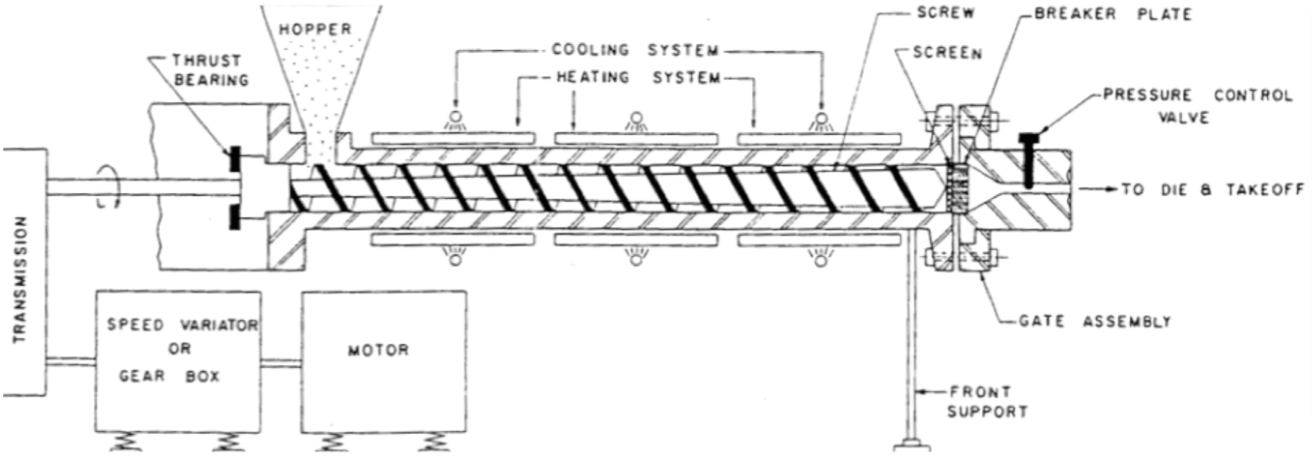

Figure 1.17: Components of an Extruder. Adapted from [69]

The extruders are usually comprised of three parts: The hopper, the barrel/screw assembly, and the die. The hopper is an opening at the beginning of the barrel through which the material is delivered; it can be as simple as metallic sheet enclosure in which the material is deposited, to a more sophisticated device that ensures the flow of material provided is constant. The screw is the more complicated part of the extruder and it is usually designed specifically for the plastic that is going to be most often processed, or

designed with a universal shape if the extruder is going to be used with different kind of plastics; some applications use a twin screw configuration to help the material to flow better. The die is the part in charge of giving the final shape to the plastic, in our case a circular shape. Figure 1.17 shows a schematic of the different parts in an extruder.

The Polymer Extrusion laboratory is equipped with a Dr. Collin Twin Screw Extruder/Compounder Model ZK 25T (Dr. Collin Gmbh, Ebersberg, Germany) seen in Figure 1.18 from is equipped with a co-rotating, intermeshing twin screw system showed in Figure 1.19. The mix of raw materials intended to be extruded is deposited in the hopper. This machine is equipped with a special dual screw hopper to ensure that the flow provided to the barrel is constant and homogeneously mixed. Once in the barrel, the material is slowly pushed by another dual screw system that conducts the material through six heating steps towards the die, gradually increasing its temperature and ensuring the best dispersion of the reinforcement agents into the base plastic or blend. Figure 1.19 shows the universal screw set chosen for this machine. This extruder includes an additional part called melting pump which purpose is to ensure constant pressure at the die section, guaranteeing a constant flow, and minimizing the diameter variations of the produced filament. It is as well conFigured with a 3mm die that will pre-shape the filament to a circular section. The material leaves the extruder with a filament form to enter the water bath where it will be gradually cooled down to room temperature and the diameter frozen to the final diameter. The filament will see a final deformation during this cooling section where the circular section is decreased. This deformation is very precisely controlled through the selection of the speed in a dual belt system that pulls the material towards the spooler, which will gather the final product.

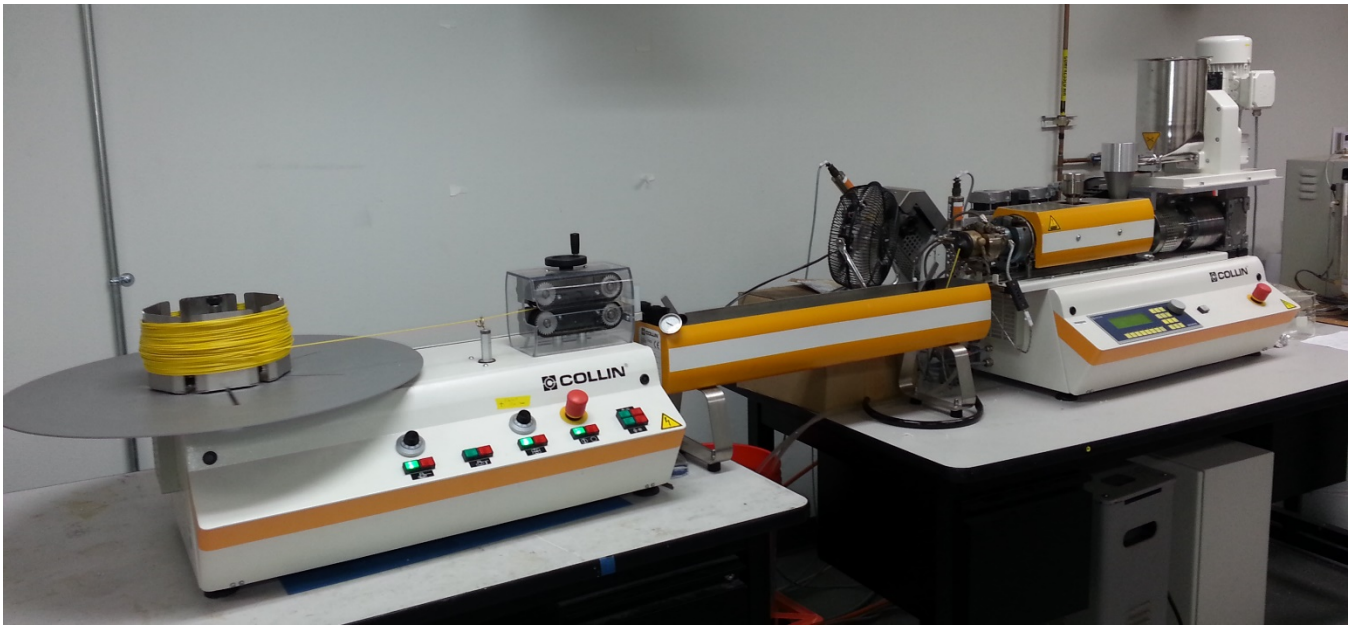

Figure 1.18: Dr. Collin Twin Screw Extruder/Compounder Model ZK 25T

The extrusion process is complicated and the parameters have to be carefully selected to deliver a quality product. The parameters that can be controlled in this machine are enumerated below:

Hopper screws speed: This parameter will control the flow of the material delivered to the machine.

Main screws speed: This parameter will control the flow of the material delivered to the die, and indirectly the pressure inside the barrel.

Temperatures: Six different temperatures can be set up in different sections of the extruder. These include five sections on the barrel and the temperature on the melting pump.

Other sensors on the extruder:

Power: The load percentage, or current consumed in the motor, to drag the material with the screws inside the barrel.

Pressure: The actual pressure on the final section of the barrel.

Temperatures: On each of the sections and another one directly inside the barrel that monitors the material temperature.

Heating or cooling rates: Indicates the percentage out of the total capacity that the machine is employing in keeping the temperature in each section to reach the temperatures that have been set up.

If the melt pump is connected and activated, the hopper and main screws speeds will be automatically control to satisfy these other parameters:

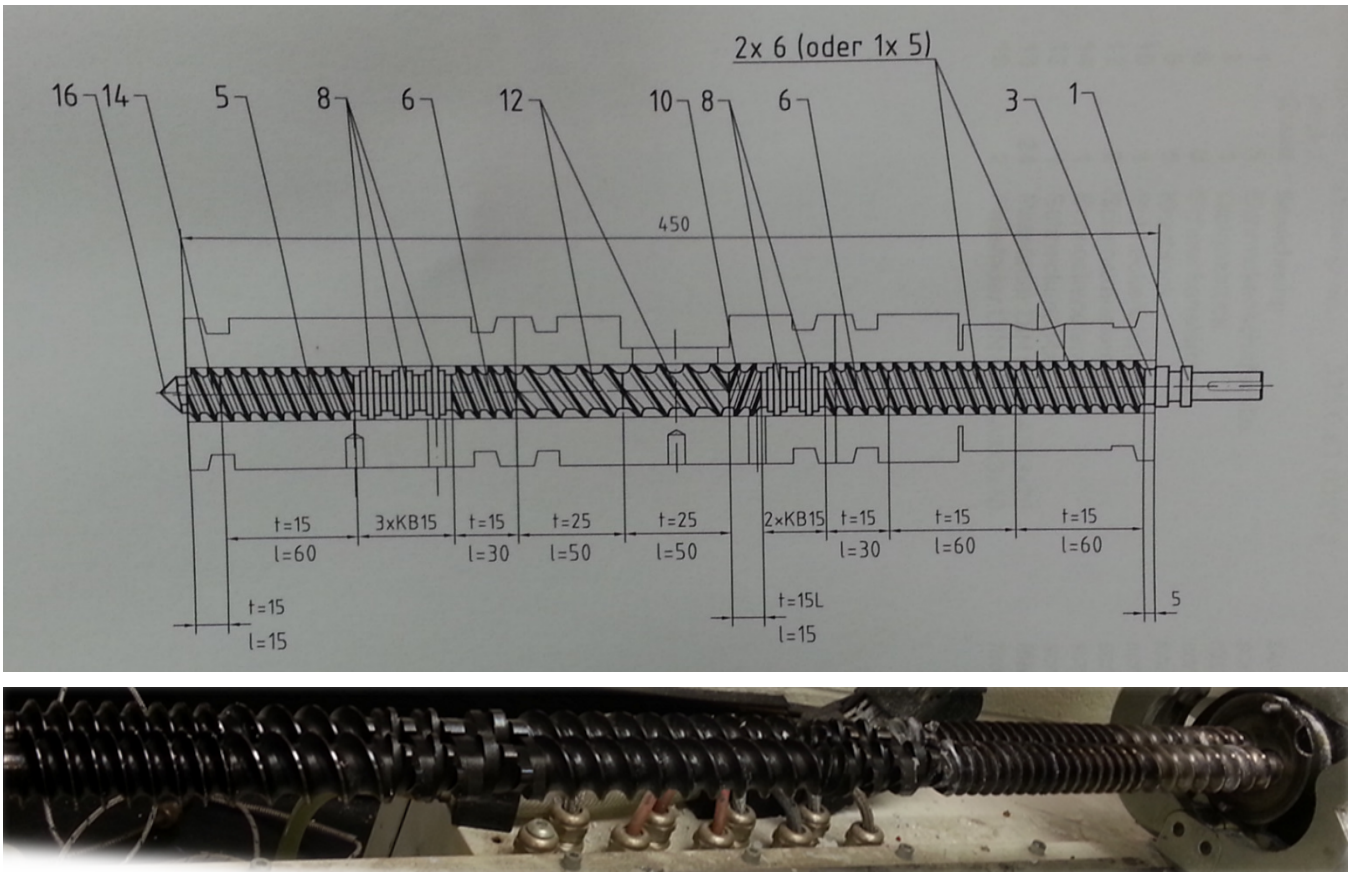

Figure 1.19: Screw

Melt pump speed: The speed on the melting pump that will control the flow of the material coming out through the die.

Melting pump pressure: The pressure that we want to keep on the melting pump.

1.4.1. Extrusion defects

The extrusion process is a complex tasks in which the outcome depends on a combination of a lot of factors that at the same interact between them. The most common defects that we can encounter during the extrusion process of thermoplastics are collected in this section. Below are listed the most common problems, the root cause and how to solve them within the capability of the machine being used.

Diameter deviation.

The final diameter is regulated by the system of opposite pulleys at the end of the extruding group. The speed of this system has be adjusted in order to get the proper diameter depending this speed on the actual flow of material from the extruder. Variations on the diameter can be caused by many factors:

The material itself: Sometimes it is the material itself the one that generates the problems. Some materials need of very specific equipment to be processed, if possible at all. This is for instance the case of UHMWPE.

The screws: We will find as well that different materials flow differently inside the extruder. For some specific materials will be better to choose a different configuration of geometry and number of screws. Any additive to a polymeric matrix will affect as well the way the material flows inside the machine. The speed of the system has to be adjusted until the material inside the machine is completely homogeneous.

The hopper configuration: The number and shape of the screws set on the hopper will affect the flow of material being delivered to the barrel. If the selection of screws is not adequate, the material will struggle to be fed, and the flow will be irregular, affecting the diameter stabilization.

The temperature: The temperature affects the viscosity of the material, and therefore the easiness of the material to flow inside the extruder. Excess of temperature will produce the material to flow excessively and thus to deform so much at the exit of the die, producing a thinner diameter than the target one. A lack of temperature won't allow the material to deform fast enough, causing the material to break or to keep residual stresses (this might in some cases be beneficial).

The cooling rate: The temperature and the height of the water in the bath will affect when the diameter freezes. The temperature of the water will keep raising due to heat transferred from the

filament and it will keep evaporating. These effects will modify the cooling rate and therefore the diameter of the final filament.

Ovality.

The filament is never perfectly round and the aspect ratio between the larger and the smaller diameter of the filament will affect the way the material will feed in the printer. Therefore this parameter must be closely watched. The rollers in the water bath are meant to redirect the filament through the water and then again towards the spooler. The rollers will therefore apply a certain force to the filament, that will deform if has not been properly cooled. Again, many parameters will affect the ovality:

The material: Some materials have a very low range of temperatures between the glass transition temperature and the melting point, complicating their processability. This is the case of PC whose viscosity varies a lot in a temperature range of 8ºC.

The temperature: Excess of the temperature will usually lead to ovality because the material will not be able to decrease the temperature enough before reaching the rollers.

The water: The temperature and the height of the water will determine the deformability of the filament when it reaches the roller.

The roller: The diameter of the roller as well as the angle that the filament will form due to the roller will determine the forces applied to the filament. Lower angles and bigger diameters will reduce the ovality.

Distance between die and roller: This distance will determine the drop of the temperature before reaching the roller. The filament will be first cooled by air, and then by water. It is better to keep the roller as submerged as possible, and try to improve the cooling rate in the air section.

The flow: The faster the filament moves through the more it will take to cool down, increasing the possibilities to reach the rollers at higher temperatures.

Void core and bubbles.

Some filaments present internal bubbles or void cores when closely examined after their processing. Some of the factors that affect the creation of this defect are listed below:

The material: Some materials and additives, like ABS and PC, are very hygroscopic producing bubbles on the material if they are not properly treated and dried prior to the extrusion process. In some cases the material can generate fumes that are trapped inside the filament.

The cooling process: If the difference of temperature between the material and the water bath is very high, it can cause that the filament cools much faster in the surfaces than in the core. In some situations the core will not be able to deform fast enough to accommodate the stresses produced by this gradient of temperatures, internally breaking and generating an internal void in the filament. This can be solved by decreasing the temperature of the process when possible, or increasing the temperature of the water in the bath.

The flow: If the material flows very fast, the drop of temperature in the air section will be lower, and the difference of temperatures between the water and the filament will be bigger, increasing the possibilities of the defects.

1.4.2. Post-processing

ABS surface smoothing with acetone

ABS parts produced with material extrusion additive manufacturing can be smoothed by brushing or evaporating acetone over the surface (Figure 1.20). This provides a shiny and smooth finish on the part by fusing the layer surfaces together, eliminating any trail of layer built and providing a finish similar to injection molding.

A more refined technique consists in placing the part into a glass vessel or a similar container in with a small layer of acetone on the bottom. The vessel is then placed into a heating surface that forces the acetone to evaporate and solves the material on the surface [70, 71].

Although, Horn *et al*. presented a preliminary study about the effects that acetone produce on the mechanical properties of 3DP parts [72], there is not a lot of research about how this smoothing process affects to the mechanical properties of the parts produced, and it might benefit the interlayer bonding in the Z direction, diminishing the isotropy of the final part.

Figure 1.20: Acetone smoothing: From left to right, a) Acetone smoothing finish, b) 0.1mm layer thickness finish, c) 0.27mm layer thickness finish [70, 71]

Friction welding

It is possible to weld parts together through a process called friction welding. The process consists in keeping the parts together while rotating a filament of the same or another material (usually one that softens at a lower temperature than the one you want to weld) at the border of the surfaces to be weld [73].

1.5. Anisotropy in material extrusion 3D printing

The intrinsic anisotropy presented by the different additive manufacture techniques is not a new topic. It has been extensively researched and discussed [1-11], although always centered more in the influence of the printing process (raster directions, gaps and others…) and generally based in ABS as the main printing material.

Ahn *et al*. [1] among others demonstrated something that everybody was already sensing: The importance of the slicing parameters on the anisotropy. They based their experiment in variations of several parameters, and gave some general building recommendations to help optimize the output properties. They concluded that the best properties derived from parts built with a negative air gap (or with interference between the rasters) and intertwined rasters between the layers, in which the rasters changed direction by 90º for each new layer, in comparison to those parts in which the rasters were all oriented in one same direction. They indirectly remarked the importance of the shell rasters as well, although they didn't provide much data about it.

Bagsik *et al.* [8] conducted a more detailed work based on ULTEM and an already optimized way of slicing the final part. They centered their study in the influence of parameters like the gap or overlap between the rasters, the thickness of the rasters, the angle between the raster and the perimeter, or just the build direction -but always with a perpendicular raster direction between layers, no matter what the direction of the raster was for the first layer- and demonstrated that they may induce big variances on the final strength (Figure 1.21 b). Specimens fabricated in different directions showed an important difference in their strength as showed by Figure 1.22. Specimens fabricated in positions XZY exhibited the biggest strength values (81MPa in the best case), followed by those in positions XYZ (64MPa) (Figure 1.21 a). As you may have already guessed, the specimens fabricated in the ZXY position showed the lowest strength values (43MPa). Therefore, the anisotropy demonstrated for ULTEM was of roughly 2:1 between the XZY and the ZXY directions.

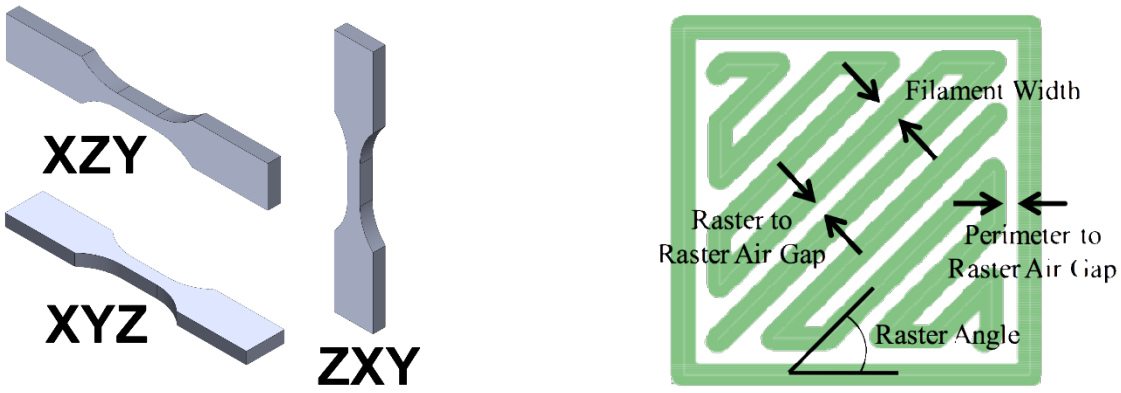

Figure 1.21: Directions and rasters (a) Directions based in [8] (b) Parameters in material extrusion [8]

The truth is that although anisotropy has been explored in literature, there is little cohesion between the research performed and it only provides an insight of small portions of the total picture. More work is needed in order to put all the pieces together and provide a better perspective of what are the mechanisms playing a role in the final properties of a 3D printed part.

		X STRESS thin	X STRESS thick	X STRAIN thin	X STRAIN thick	Y STRESS thin	Y STRESS thick	Y STRAIN thin	Y STRAIN thick	Z STRESS thin	Z STRESS thick	Z STRAIN thin	Z STRAIN thick
NORMAL	0	58	53	4.4	3.7	68	80	4.8	6.8	39	39	2.6	2.6
NORMAL	30	50	43	4.5	3.7	70	74	5.5	5.5	36	42	2.4	2.6
NORMAL	45	49	45	5.2	4.7	62	76	6.2	6.2	41	40	2.4	2.4
NEGATIVE	0	68	64	5	4.6	71	81	6	7.8	40	42	2.6	2.4
NEGATIVE	30	53	52	5.5	4.2	78	67	6.5	4	43	43	2.5	2.5
NEGATIVE	45	53	52	6.2	5.2	78	69	6.5	4.8	40	43	2.4	2.5
POSITVE	0	50	50	4.5	3.5	60	73	4	6.8	32	35	2.3	2.4
POSITVE	30	40	50	4.7	3.5	57	67	4	4.2	35	40	2.4	2.4
POSITVE	45	41	42	5.5	5	69	76	7	7	34	32	2.2	2.3
AVERAGE		51	50	5	4	68	74	6	6	38	40	2	2
ST. DEV.		8.5	6.6	0.6	0.7	7.4	5.2	1.1	1.3	3.7	3.8	0.1	0.1
MAX		68	64	6	5	78	81	7	8	43	43	3	3
MIN		40.0	42.0	4.4	3.5	57.0	67.0	4.0	4.0	32.0	32.0	2.2	2.3

Figure 1.22: Influence of the parameters in the strength and the strain of Ultem® Parts.
On the left: normal, negative or positive air gap combined with 0, 30 or 45° angle.
On top: resulting stress and strain depending on the direction in MPa.Based on data from [8]

1.6. References

[1] Ahn, S. H., Montero, M., Odell, D., Roundy, S., & Wright, P. K. "Anisotropic material properties of fused deposition modeling ABS." *Rapid Prototyping Journal, Vol 8, No 4, p248-257, 2002*

[2] Ziemian, Constance, Mala Sharma, and Sophia Ziemian. "Anisotropic mechanical properties of ABS parts fabricated by fused deposition modelling." *Mechanical Engineering. Intech, p159-180, 2012*

[3] Montero, M., Roundy, S., Odell, D., Ahn, S. H., & Wright, P. K. "Material characterization of fused deposition modeling (FDM) ABS by designed experiments." *Proceedings of Rapid Prototyping and Manufacturing Conference, SME, 2001*

[4] Hague*, R., S. Mansour, and N. Saleh. "Material and design considerations for rapid manufacturing." *International Journal of Production Research, No 42, Vol 22, p4691-4708, 2004*

[5] Bellini, Anna, and Selçuk Güçeri. "Mechanical characterization of parts fabricated using fused deposition modeling." *Rapid Prototyping Journal, Vol 9, No 4, p252-264, 2003*

[6] Es-Said, O. S., Foyos, J., Noorani, R., Mendelson, M., Marloth, R., & Pregger, B. A. "Effect of layer orientation on mechanical properties of rapid prototyped samples." *Materials and Manufacturing Processes, Vol 15, No 1, p107-122, 2000.*

[7] Lee, C. S., Kim, S. G., Kim, H. J., & Ahn, S. H. "Measurement of anisotropic compressive strength of rapid prototyping parts." *Journal of materials processing technology, Vol 187, p627-630, 2007*

[8] Agnes Bagsik, V. S., "Mechanical properties of fused deposition modeling parts manufactured with ultem*9085", *ANTEC 2011, Boston*, 2011.

[9] El-Gizawy, A. Sherif, Shan Corl, and Brian Graybill. "Process-induced Properties of FDM Products."

[10] Rodríguez, J. F., Thomas, J. P., & Renaud, J. E. "Design of fused-deposition ABS components for stiffness and strength." *Journal of Mechanical Design, Vol. 125, No 3, p545-551, 2003*

[11] Shaffer, S., Yang, K., Vargas, J., Di Prima, M. A., & Voit, W. "On reducing anisotropy in 3D printed polymers via ionizing radiation." Polymer, 2014.

[12] Hague, R., Mansour, S., Saleh, N., & Harris, R. "Materials analysis of stereolithography resins for use in rapid manufacturing". *Journal of materials science, Vol. 39, No 7, p2457-2464, 2004*

[13] Vega, V., Clements, J., Lam, T., Abad, A., Fritz, B., Ula, N., & Es-Said, O. S. "The effect of layer orientation on the mechanical properties and microstructure of a polymer". *Journal of materials engineering and performance, Vol. 20, No 6, p 978-988, 2011*

[14] Caulfield, B., McHugh, P. E., & Lohfeld, S. "Dependence of mechanical properties of polyamide components on build parameters in the SLS process" *Journal of Materials Processing Technology, Vol. 182, No 1, p477-488, 2007*

[15] Murr, L. E., Quinones, S. A., Gaytan, S. M., Lopez, M. I., Rodela, A., Martinez, E. Y., … & Wicker, R. B. "Microstructure and mechanical behavior of Ti–6Al–4V produced by rapid-layer manufacturing, for biomedical applications." *Journal of the mechanical behavior of biomedical materials, Vol. 2, No 1, p20-32, 2009*

[16] Takaichi, A., Nakamoto, T., Joko, N., Nomura, N., Tsutsumi, Y., Migita, S., ... & Hanawa, T. "Microstructures and mechanical properties of Co–29Cr–6Mo alloy fabricated by selective laser melting process for dental applications." *Journal of the mechanical behavior of biomedical materials, Vol. 21, p67-76, 2013*

[17] Murr, L. E., Amato, K. N., Li, S. J., Tian, Y. X., Cheng, X. Y., Gaytan, S. M., E. Martinez, Shindo, P. W., Medina, F., and Wicker, R. B., *"Microstructure and mechanical properties of open-cellular biomaterials prototypes for total knee replacement implants fabricated by electron beam melting, Journal of the mechanical behavior of biomedical materials" Vol. 4, No 7, p1396-1411, 2011*

[18] Griffith, M. L., Keicher, D. M., Atwood, C. L., Romero, J. A., Smugeresky, J. E., Harwell, L. D., & Greene, D. L. *"Free form fabrication of metallic components using laser engineered net shaping (LENS)." En Proceedings of the Solid Freeform Fabrication Symposium. University of Texas at Austin,. p. 125-131, 1996*

[19] "Standard terminology for additive manufacturing technologies," ASTM International, *F2792-12a*, 2013.

[20] Ludmila Novakova-Marcincinova "Application of Fused Deposition Modeling Technology in 3D Printing Rapid Prototyping Area" *Manuf. and Ind. Eng., Vol 11, No 4, 2012*

[21] "CREDIT SUISSE: 3D Printing Is Going To Be Way Bigger Than What The 3D Printing Companies Are Saying" *http://www.businessinsider.com/the-3-d-printing-market-will-be-huge-2013-9,* 7/14/2014

[22] "CREDIT SUISSE: The 3-D Printing Market Is Going To Be 357% Bigger Than We Initially Though" *http://www.businessinsider.com/credit-suisse-on-3d-printing-2014-1,* 7/14/2014

[23] Wong, Kaufui V., and Aldo Hernandez. "A review of additive manufacturing." *ISRN Mechanical Engineering, Vol 2012, 2012*

[24] "Layer-by-Layer: Opportunities in 3D printing", *http://www.marsdd.com/mars-library/layer-by-layer-opportunities-in-3d-printing/* 1/17/2014.

[25] Chee Kai Chua; Kah Fai Leong, Chu Sing Lim "Rapid Prototyping: Principles and Applications" World Scientific. p. 124, 2003.

[26] Mireles, J., Espalin, D., Roberson, D., Zinniel, B., Medina, F., & Wicker, R. "Fused deposition modeling of metals.", 2013m

[27] Pearce, J. M., Blair, C. M., Laciak, K. J., Andrews, R., Nosrat, A., & Zelenika-Zovko, I. "3-D printing of open source appropriate technologies for self-directed sustainable development". *Journal of Sustainable Development, 2010, 3(4), p17.*

[28] Leong, K. F., Cheah, C. M., & Chua, C. K. "Solid freeform fabrication of three-dimensional scaffolds for engineering replacement tissues and organs". *Biomaterials, 2003, 24(13), 2363-2378.*

[29] Wittbrodt, B. T., Glover, A. G., Laureto, J., Anzalone, G. C., Oppliger, D., Irwin, J. L., & Pearce, J. M. "Life-cycle economic analysis of distributed manufacturing with open-source 3-D printers". *Mechatronics, 2013, 23(6), 713-726.*

[30] Kreiger, M. A., Mulder, M. L., Glover, A. G., & Pearce, J. M. "Life cycle analysis of distributed recycling of post-consumer high density polyethylene for 3-D printing filament". *Journal of Cleaner Production, 2014, 70, 90-96.*

[31] "Polyamide" http://reprap.org/wiki/Polyamide

[32] Taylor, "Printing with Nylon" *https://www.matterhackers.com/articles/printing-with-nylon*

[33] "FDM Nylon 12" *http://www.stratasys.com/materials/fdm/nylon*

[34] Bell, C. "Getting a 3D Printer. In Maintaining and Troubleshooting Your 3D Printer" *Apress. 2014, 53-84*

[35] Horvath, J. "The Desktop 3D Printer. In Mastering 3D Printing", *Apress, 2014, 11-20*

[36] Håkan Langemark "Scripted vases" *https://www.thingiverse.com/thing:104694/#files*, 5/12/2014

[37] "Rapid Prototyping", *http://www.iwf-duisburg.de/werkzeuglose-fertigung/rapid-prototyping.html*, 7/10/2014.

[38] "NEW JBS Garrett GT28 Cast and Tubular Manifolds", *http://www.ttforum.co.uk/forum/viewtopic.php?f=28&t=123736*, 7/10/2014.

[39] "Slic3r Manual: Infill Patterns and Density" *http://manual.slic3r.org/expert-mode/infill* 7/16/2014.

[40] Shao-Yun Fua, Xi-Qiao Feng, Bernd Lauke, Yiu-Wing Mai "Effects of particle size, particle/matrix interface adhesion and particle loading on mechanical properties of particulate–polymer composites", *Composites: Part B, Vol 39, p 933–961*, 2008.

[41] S. Tjong, "Structural and mechanical properties of polymer nanocomposites," *Materials Science and Engineering, Vol 53, p 73–197*, 2006.

[42] "Lifecycle of a plastic product", *http://plastics.americanchemistry.com/Life-Cycle*, 11/03/2013.

[43] Charles A. Edward M. Petrie, "Plastics materials and processes. A concise encyclopedia". Willey-Interscience, 2003.

[44] Ebewele, Robert O."Polymer science and technology". *CRC press, 2000*.

[45] Rosato, Donald V., Marlene G. Rosato, and Dominick V. Rosato. "Concise encyclopedia of plastics". *Springer, 2000*.

[46] "The glass transition", *http://www.pslc.ws/macrog/tg.htm*, 12/01/2013.

[47] Kelly A. Ross, Susan D. Arntfield and Stefan Cenkowski "A Polymer Science Approach to Physico-Chemical Characterization and Processing of Pulse Seeds" DOI: 10.5772/46145

[48] Galanty, P. G., and J. E. Mark. "Polymer Data Handbook." *JE Mark, Oxford University Press, Oxford, 1999*

[49] Carraher's Carraher Jr, Charles E. "Carraher's polymer chemistry". *CRC Press, p 254, 2013*.

[50] "Prospector: Find raw materials faster." *http://plastics.ides.com/,* 05/12/2014.

[51] Södergård, Anders, and Mikael Stolt. "Properties of lactic acid based polymers and their correlation with composition" *Progress in polymer science, Vol 27, No.6, p1123-1163, 2002*

[52] Rasal, Rahul M., Amol V. Janorkar, and Douglas E. Hirt. "Poly (lactic acid) modifications" *Progress in polymer science, Vol 35, No 3, p338-356, 2010*

[53] Quynh, T. M., Mitomo, H., Nagasawa, N., Wada, Y., Yoshii, F., & Tamada, M.. "Properties of crosslinked polylactides (PLLA & PDLA) by radiation and its biodegradability" *European polymer journal, Vol 43, No 5, p1779-1785, 2007*

[54] ADCOMP Partners "Thermoplastic Composites: Best Practice Guide" 2009

[55] "A guide to thermoplastic polyurethanes (TPU)" *Huntsman Corp*. *http://www.huntsman.com/portal/page/portal/polyurethanes/Media%20Library/global/files/guide_tpu.pdf*

[56] *Harper, Charles A*. "Handbook of Plastics, Elastomers, and Composites" *McGraw-Hill Inc*. 1996."

[57] Parvaiz, M. R., Mohanty, S., Nayak, S. K., & Mahanwar, P. A.. "Polyetheretherketone (PEEK) composites reinforced with fly ash and mica." *Journal of Minerals and Materials Characterization and Engineering, Vol 9, No 01, p25, 2010*

[58] Kim, H. J., Jung, D. H., Jung, I. H., Cifuentes, J. I., Rhee, K. Y., & Hui, D "Enhancement of mechanical properties of aluminium/epoxy composites with silane functionalization of aluminium powder." *Composites Part B: Engineering, Vol 43, No 4, p1743-1748, 2012*

[59] Ma, Peng Cheng, Jang-Kyo Kim, and Ben Zhong Tang. "Functionalization of carbon nanotubes using a silane coupling agent" *Carbon Vol 44, No 15 p3232-3238, p2006*

[60] Samuel Sterman, James G. Marsden “Silane coupling agents”, *Reinforced Plastic Symposium, Vol 58, No 3, 1966*

[61] “Silane Coupling Agents: Connecting Across Boundaries” Gelest, Inc. 2006 Catalog *http://www.gelest.com/goods/pdf/couplingagents.pdf,* 04/05/2014.

[62] “Silane Coupling Agents Brochure” Struktol, 2008 Catalog *http://www.struktol.com/pdfs/TEB0009%20-%20Silane%20Coupling%20Agents%20-%202008.pdf*

[63] Ha, C. S., Park, H. D., Kim, Y., Kwon, S. K., & Cho, W. J. “Compatibilizer in polymer blends for the recycling of plastics waste I: preliminary studies on 50/50 wt% virgin polyblends”. *Polymers for Advanced Technologies, 1996, 7(5-6), 483-492*.

[64] Borggreve, R. J. M., & Gaymans, R. J. “Impact behaviour of nylon-rubber blends: 4. Effect of the coupling agent, maleic anhydride. Polymer”, *1989, 30(1), 63-70*.

[65] Araújo, E. M., Hage Jr, E., & Carvalho, A. J. F. “Morphological, mechanical and rheological properties of nylon 6/acrylonitrile-butadiene-styrene blends compatibilized with MMA/MA copolymers”. *Journal of materials science, 2003, 38(17), 3515-3520*.

[66] Wilkinson, A. N., Clemens, M. L., & Harding, V. M. “The effects of SEBS-g-maleic anhydride reaction on the morphology and properties of polypropylene/PA6/SEBS ternary blends”. *Polymer, 2004, 45(15), 5239-5249*.

[67] Rzayev, Z. M. “Graft copolymers of maleic anhydride and its isostructural analogues: High performance engineering materials”. *arXiv preprint arXiv:1105.1260. 2011*

[68] Giles Jr, Harold F., Eldridge M. Mount III, and John R. Wagner Jr. “Extrusion: the definitive processing guide and handbook” William Andrew, 2004

[69] “Extrusion Principles”, *Product Application & Research Centre Mumbai,* 03/24/2013 http://www.ril.com/downloads/pdf/extrusion%20principles.pdf

[70] “Smooth surfaces of ABS 3D printed parts with acetone vapor”, *http://www.3ders.org/articles/20130226-smooth-surfaces-of-abs-3d-printed-parts-with-acetone-vapor.html,* 11/03/2013.

[71] Ben Chapman, Shivam Desai, Mark Muraoka, Teodora Vidolova “Investigating Methods of Prototyping with ABS”

[72] T. Horn, R. Aman, O. Harrysson, H. West, C. Keough, J. Brennan, D. Davis “Effect of Acetone Vapor Polishing Parameters for on the Properties of 3D Printed ABS Components” *25th Annual International Solid Freeform Fabrication Symposium, 2014 Aug 4-6, Austin, TX*

[73] Dawes, C. J., Murch, M. G., Needham, J. C., Nicholas, E. D., Temple-Smith, P., & Thomas, W. M. "Friction welding." *U.S. Patent No. 5,460,317. 24 Oct. 1995*.

CHAPTER 2: RESEARCH OBJECTIVES AND PRESENTED PUBLISHED PAPERS

2.1. Research objectives

The first chapter has covered the complexity of the whole ME3DP universe, from the very first stages in the processing of the material, to the parameters used during the printing process. The objective of this chapter is to give an insight of the complexities and the high number of parameters that can have an impact into the quality and the properties of the final part.

The main goal of this research is to further understand the mechanisms that will lead to a decrease in build orientation anisotropy, leaving aside the influence of all the mechanical parameters that can be controlled (since this has been broadly covered in the literature), and focusing more on what materials have to offer. This document intends to give clues about:

- How the processing of the materials affects the mechanical properties of the final parts.
- How the layers are bonded with each other in ME3DP, and how to improve the interlayer bonding of this process
- How to help reduce anisotropy in commonly used materials in ME3DP.
- How to improve the blending of materials that are incompatible due to their opposed polarity on their main polymeric chains.

Overall, the goal is to characterize the development of a material system that will exhibit a lower sensitivity to mechanical property anisotropy. The learnings made here can then be applied to other AM platforms and improve the technology of additive manufacturing as a whole.

Extrusion-based additive manufacturing is a very complex process that is still in its very early infancy stage. The present document has provided insights about the high amount of factors influencing the process, and how much it is still in the need of research. 3DP has traditionally borrowed materials from other applications that resulted suitable for it, but few materials have been specifically engineered for ME3DP. The process usually leads to a specific building direction for each design, but this position might not lead to the most desirable properties due to the resulting anisotropy. A solution for this anisotropy is therefore desirable, whether it is given by composition of different materials or a modification in the process.

2.2. Published works

The next two chapters are composed by published works that served as the foundation for the research developed in the last chapters. The lines below introduce the abstracts of those works and the role that they played in the subsequent investigation.

Chapter 3

The material in Chapter 3 explores the fracture surface of four different material systems and was the leading force into the anisotropy world. It was published in Journal of Failure Analysis and Prevention cited as follows:

Torrado, A. R., Roberson, D. A., & Wicker, R. B. (2014). "Fracture surface analysis of 3D-printed tensile specimens of novel ABS-based materials". *Journal of Failure Analysis and Prevention, 14(3), 343-353*.

Permission to use the article cited above in this dissertation has been granted by the publisher as documented in Appendix 5.

Abstract

One of the most common materials utilized by material extrusion 3D printing is acrylonitrile butadiene styrene (ABS). The work presented in this research explored the effect of the addition of reinforcing materials on the mechanical properties of ABS in an effort to create materials with enhanced physical properties. A comparison was made between pure ABS, two ABS matrix composites, and one ABS/elastomer blend with the purpose of characterizing the effect of additives on the mechanical properties. Tensile test results of specimens built in different orientations showed that ABS reinforced with 5% by weight TiO_2 exhibited the highest ultimate tensile strength for specimens built in both horizontal and vertical directions with 32.2 and 18.4MPa, respectively. The compounding of an elastomeric material with ABS improved the surface finish of parts as they were visibly smoother compared to those printed from the ABS baseline material, though there was an observable decrease in the ductility of tensile specimens. Analysis was performed on the fracture surface of the tensile specimens through the use of scanning electron microscopy. Fractography revealed different modes of failure related to the different additives. The effects of additives on the anisotropy associated with the mechanical properties of 3D-printed parts were also analyzed.

Chapter 4

The material in Chapter 4 continues the work started by the previous article, broadening the number of systems and being the first showing a substantial decrease of the anisotropy in one of them. The following chapters continue the investigation reflected in this work. It has been published in the journal of Additive Manufacturing under the following citation:

Torrado, A. R., Shemelya, C. M., English, J. D., Lin, Y., Wicker, R. B., & Roberson, D. A. (2015). "Characterizing the Effect of Additives to ABS on the Mechanical Property Anisotropy of Specimens Fabricated by Material Extrusion 3D Printing". *Additive Manufacturing. Accepted 6 February 2015*

Permission to use the article cited above in this dissertation has been granted by the publisher as documented in Appendix B.

Abstract

Material extrusion 3D printing (ME3DP), based on Fused Deposition Modeling (FDM) technology is currently the most widely available 3D printing platform. As is the case with other 3D printing methods, parts fabricated from ME3DP will exhibit physical property anisotropy where build direction has an effect on the mechanical properties of a given part. The work presented in this paper analyzes the effect of physical property-altering additives to acrylonitrile butadiene styrene (ABS) on mechanical property anisotropy. A total of six ABS-based polymer matrix composites and four polymer blends were created and evaluated. Tensile test specimens were printed in two build orientations and the difference in ultimate tensile strength and % elongation at break was compared between the two test sample versions. Fracture surface analysis was performed via scanning electron microscopy (SEM) which gave insight to the failure modes and rheology of the novel material systems as compared to specimens fabricated from the same ABS base resin. Here it was found that a ternary blend of ABS combined with styrene ethylene butylene styrene (SEBS) and ultra high molecular weight polyethylene (UHMWPE) lowered the mechanical property anisotropy in terms of relative UTS to a difference of 22 ±2.07 % as compared to 47 ±7.23% for samples printed from ABS. The work here demonstrates the mitigation of a problem associated with 3D printing as a whole through novel materials development, and analyzes the effects of adding a wide variety of materials on the physical properties of a thermoplastic base resin.

CHAPTER 3: FRACTURE SURFACE ANALYSIS OF 3D-PRINTED TENSILE SPECIMENS OF NOVEL ABS-BASED MATERIALS

3.1. Introduction

Additive manufacturing, now more commonly referred to as 3D printing (3DP), has gained acceptance and popularity in manufacturing, educational, and home-use settings [1, 2]. Material extrusion 3D printers similar in function to the trademarked fused deposition modeling (FDM) process are the most common type of equipment used in 3DP and rely on a process by which a polymeric filament is extruded and deposited in a layer-by-layer manner until a 3D object is created. Parts are fabricated from a thermoplastic polymer that has rubbery, tacky phase above the glass transition temperature and facilitates fusion between subsequent layers. Currently, the number of polymers compatible with material extrusion 3DP platforms is very limited due to the particular properties needed for a successful print such as a relatively low glass transition temperature (T_g), melting point (T_m), and a low tendency to shrink upon solidification. The T_g will have an effect on how easily the material will be extruded, how the parts will shrink during the cooling process (therefore, affecting the warping, but not being the only one) and the thermostability of the final part. The T_m can provide some clues about the extrusion temperature (T_e), but the final T_e will depend greatly on the configuration of the feeding system in the machine. Most of the 3D printers nowadays are able to work at temperatures of less than 300 °C. Two of the most widely used materials for material extrusion 3DP are acrylonitrile butadiene styrene (ABS, T_g = 110 °C, not a true melting point) and polylactic acid (PLA, T_g = 60 °C, T_m = 175 °C) because of their dimensional stability and low T_g. Other printable polymers are polycarbonate (PC, T_g = 145 °C, T_m = 230–260 °C), polyvinyl alcohol (PVA, T_g = 85 °C, T_m = 170 °C), and polythermide (Ultem, T_g = 185–216 °C, T_m = 350–400 °C), but the use of such materials presents some limitations. These materials require higher extrusion temperatures, over 300 °C. Other specific requirements in order to decrease warpage (due to the higher gradients of temperature to be cooled) are temperature-controlled build envelopes, preheated platforms and vacuum platforms, or the use of adhesive materials.

Since the number of usable polymer types is limited, the number of applications that can benefit from material extrusion 3DP is as well limited. A strategy for increasing the applicability of material

extrusion 3DP is the development of new material systems with a wider range of physical properties. A logical path to engineering the physical properties of materials used in 3DP is the development of composites where the matrix material is a printable polymer to maintain compatibility with material extrusion 3D printers. There are multiple examples of successful implementation of such material modifications for use in FDM™ [3-7].

The development of polymer matrix composites (PMC) is an obvious path to developing better materials for use in material extrusion 3D printers due to the ease of material blending and compounding, combined with the generally low prices of the matrix materials (less than a dollar per pound for ABS). Moreover, the ability to make a composite monofilament compatible with material extrusion 3D printers through conventional screw extrusion equipment offers rapid data turns in novel materials development. The augmenting of polymeric materials can be done in many ways, one being the compounding of particulate or fiber-reinforcing additives in the creation of PMC, or through the compounding with other polymeric materials in the creation of polymer blends. Particles give the flexibility to tailor the characteristics of the resulting composite to fill a variety of applications based on many different factors. Parameters such as the particle size, the particle loading percentage, or the interfacial adhesion can affect the mechanical properties such as the ultimate tensile strength (UTS), the Young's modulus or the fracture toughness, and other properties including the thermostability, the coefficient of thermal expansion, decomposition temperature, or even flame-retardant characteristics [8, 9].

As new composite material systems are developed for use in material extrusion 3D printers, understanding the effect of additives on the mechanical behavior of the polymeric matrix is paramount. An important aspect of composite materials development is the characterization of the influence of reinforcing agents on the mechanical properties (in comparison with the material alone) and their relation with the fracture morphology of the failed components, namely, the characterization of the effect of reinforcing agents on the mechanical properties (compared with the matrix material alone) and a correlation of changes to the fracture morphology of the failed components are important aspects to consider. The objective of the work performed in this paper is to explore the effect of additives on tensile testing data and fracture surface morphology for two ABS matrix-printable composites and one

ABS/elastomer blend subjected to tensile testing. The effect of build orientation on the mechanical properties and fracture surface was also analyzed, as one of the major flaws of additive manufacturing is the anisotropy on the 3D-printed items. Three different additives were chosen for this investigation: (1) TiO_2 for a particle-loaded composite; (2) jute fiber for short fiber reinforcement based on its green manufacturing composition [10]; and (3) a thermoplastic elastomer (TPE) to explore the rubber-toughening effect when blended with ABS [11].

3.2. Experimental Procedure

Monofilaments were produced using a Dr. Collin Twin Screw Extruder/Compounder Model ZK 25T (Dr. Collin GmbH, Ebersberg, Germany) with co-rotating, intermeshing screws. Two composite types were produced utilizing ABS as a matrix material: ABS (Cyclolac®, GE ABS resin) loaded with 5 wt. % jute fiber, and ABS loaded with 5 wt. % TiO_2. In addition, a polymeric blend was obtained by mixing ABS with 5 wt. % of a TPE. The filament was produced to be compatible with the MakerBot Replicator (MakerBot Industries, Brooklyn, NY USA) material extrusion 3D Printer and possessed a diameter of 1.77 mm. The three ABS-based materials were compared with the ABS filament provided by MakerBot Industries. The compounded materials were produced with the same extrusion parameters, as represented in table 3.1. Micrographs were taken of the additives before the processing using a Hitachi TM-1000 scanning electron microscope (SEM) (Hitachi High-Technologies Europe GmbH, Germany) operating at 15 kV. Images are shown in Figure 3.4.

The specimens were printed following the Type V dimensions described by the American Society for Testing and Materials (ASTM) D638 standard [12] and verified to fulfill the tolerance requirements. All specimens were created in the same area on the machine's platform to minimize variability due to possible temperature gradients inside the build envelope. The fabrication orientation on the machine as well as the print raster path (also known as fill pattern) can play an important role on the mechanical properties of the fabricated part due to the anisotropic nature of this fabrication technique [13-15] For this reason, two sets of specimens were produced for each material type, one printed in the XYZ direction and another set printed in the ZXY direction as seen in Figures 3.1 and 3.2. The testing samples produced from the four material types were fabricated with the same parameters on the machine, which were previously

iterated to get the optimum filling on the specimen without leading to dragging of the part due to an excess of material deposited to obtain, a part with the lower amount of air gaps in between the deposited threads (Figure 3.3). Table 3.2 shows the values for the parameters utilized in the 3D printer. Figure 3.4 shows the SEM micrographs of the raw additives before the processing.

Table 3.1: Parameters of extrusion for ABS composite filaments

Temperature Zone 1 (ºC):	160
Temperature Zone 2 (ºC):	205
Temperature Zone 3 (ºC):	225
Temperature Zone 4 (ºC):	230
Temperature Zone 5 (ºC):	230
Speed on main screws (rpm):	35
Speed on feeding screws (%):	8
Pressure on main screws (bar):	25
Load (%):	63

Table 3.2: Extrusion parameters used with MakerBot replicator

Object infill (%):	100
Layer Height (mm):	0.27
Number of Shells:	1
Feedrate (mm/s):	40
Travel Feedrate (mm/s):	55
Print Temperature (◦C):	230
Filament Diameter (mm):	1.9
Nozzle Diameter (mm):	0.4
Raft material	No

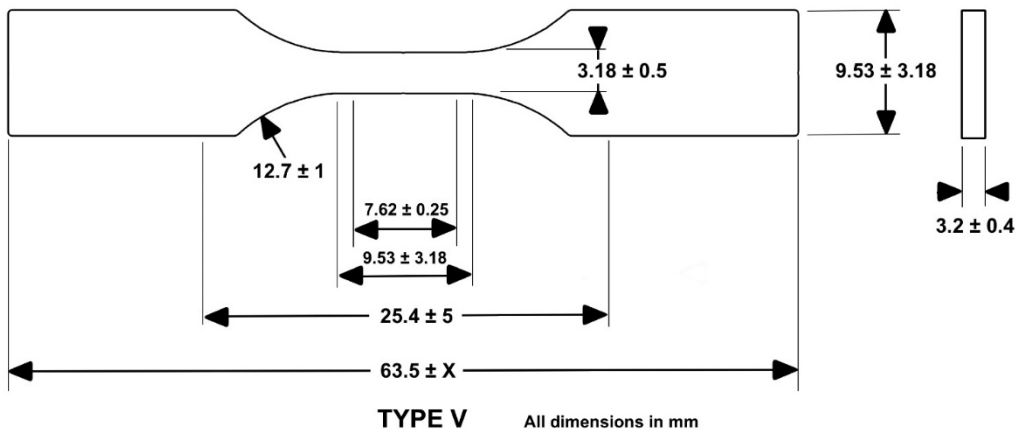

Figure 3.1: ASTM 638, type V: dimensions

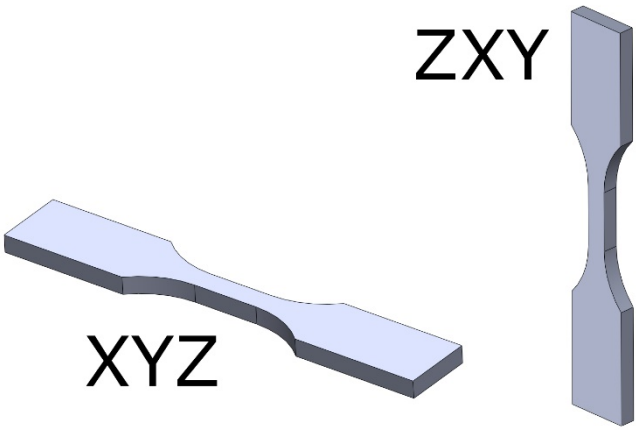

Figure 3.2: Printing directions

An Instron® 5866 (Instron, Norwood, MA, USA) tensile testing machine equipped with a 10 kN load cell was utilized to perform the tensile testing. The specimens were tested at a speed of 10 mm/min and a temperature of 23 °C. An Instron® 2663-821 advanced video extensometer (AVE) was used to determine the instant strain at every moment, allowing for the plotting of the entire stress–strain curve and the automatic calculation of the modulus and the % elongation to break. The distance between the marks of 7.6 was used for the AVE. Figures 3.5 and 3.6 show the stress–strain curves results for the four material types produced. The stress–strain curves were plotted based on the average results from a sample size of five specimens. The data extracted from the AVE and the load cell were processed with a program developed in Matlab® which homogenized the data in order to generate stress–strain curves. The program

allowed for the plotting of a single stress–strain curve for each sample set by calculating a composite of the stress–strain curves for all the specimens in a given sample pool. Figure 3.7 shows an example of the resulting curve for the ABS specimen sample set tested in this study. The fracture surfaces were analyzed via SEM.

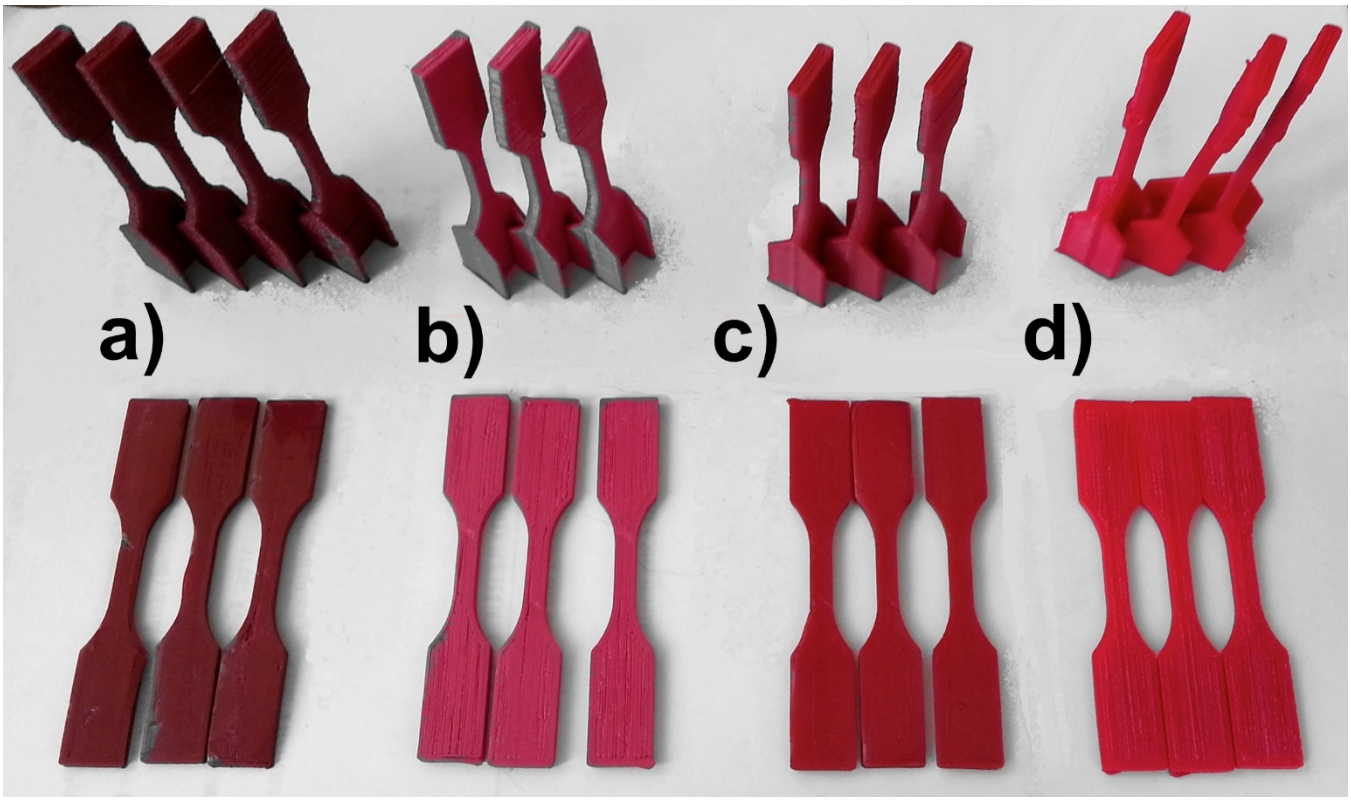

Figure 3.3: Samples (vertical above, horizontal below): (a) ABS and jute fiber, (b) ABS and TiO , (c) ABS with TPE, and (d) pure ABS

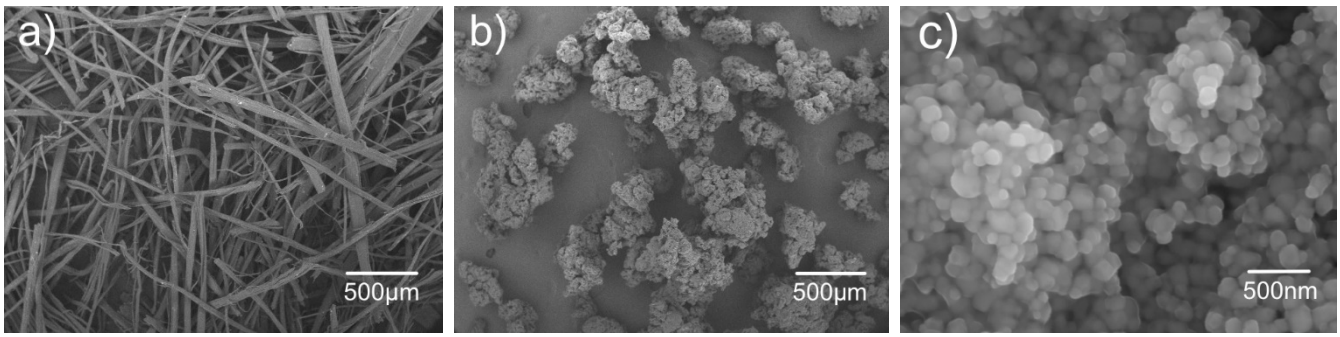

Figure 3.4: Additives: (a) jute fibers, (b) TPE, and (c) TiO_2

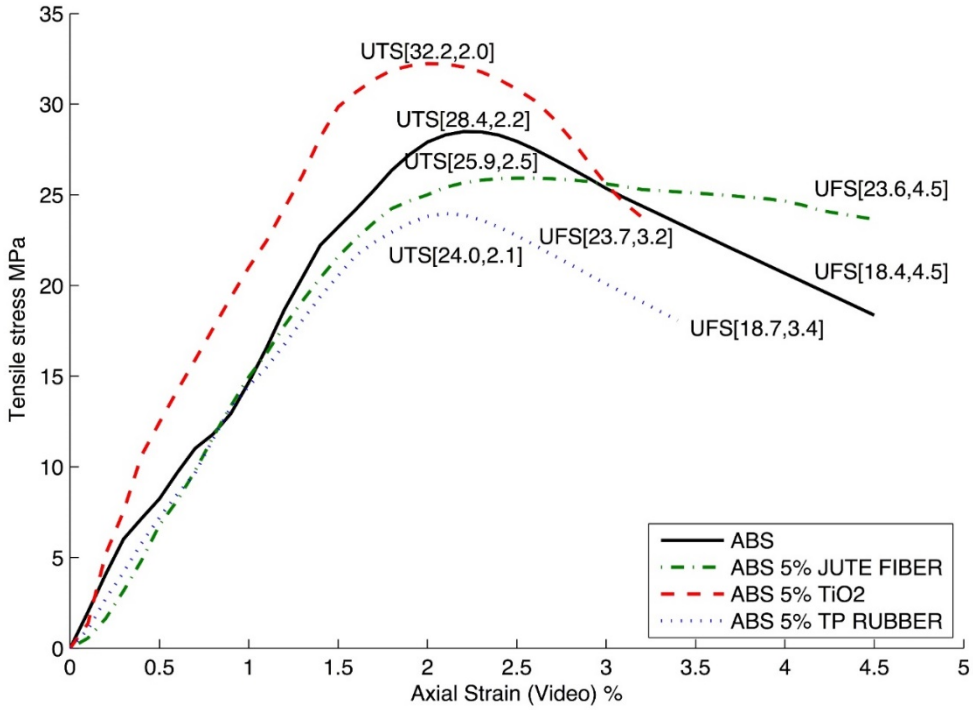

Figure 3.5: Stress–strain curves: XYZ direction

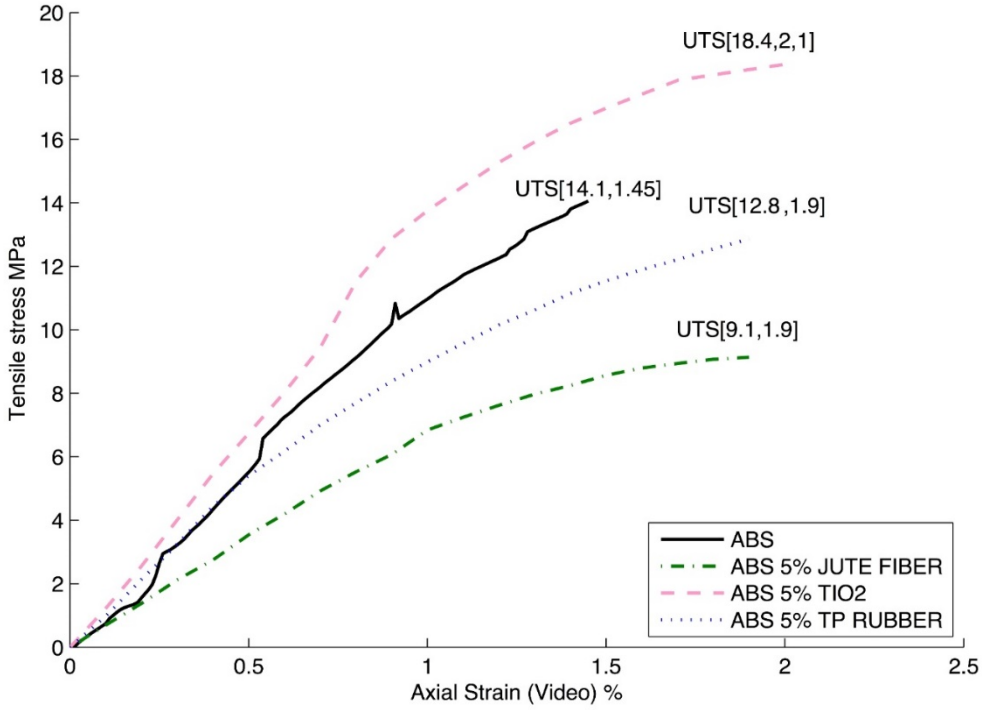

Figure 3.6: Stress–strain curves: ZXY direction

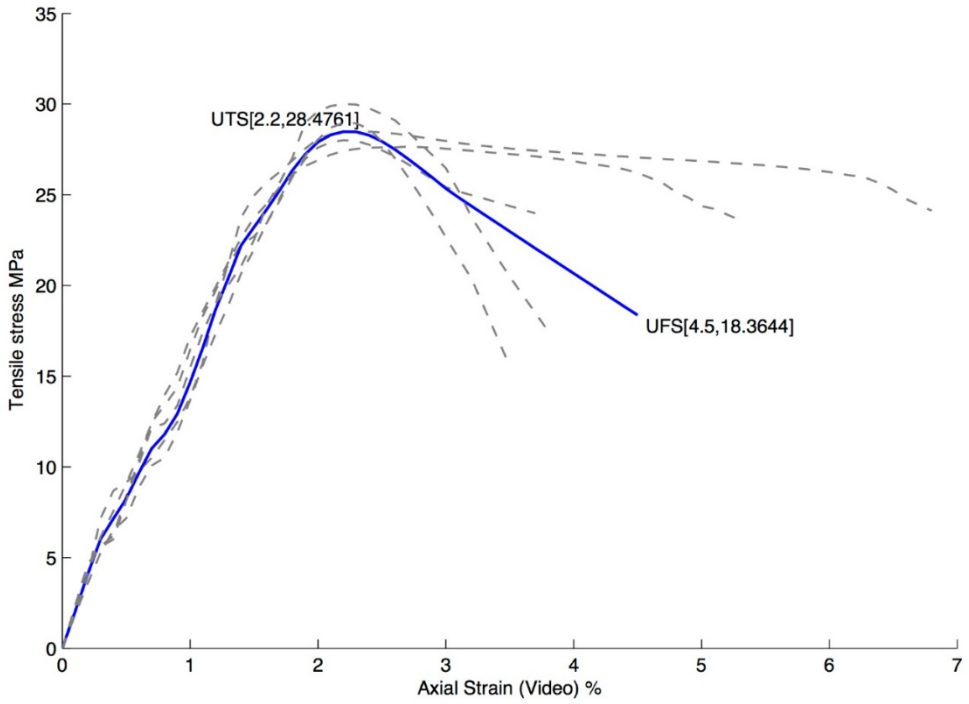

Figure 3.7: Stress–strain curve averaging with Matlab®

3.3. Tensile Test Results

3.3.1. ABS/TiO_2 Composite

The composite prepared from ABS in combination with TiO_2 was the only sample pool which demonstrated an improvement in UTS with an increase of 13.2% in comparison with the commercially available ABS. Moreover, the strength at fracture was on average 30% higher, while the strain at fracture was reduced by 29%. The UTS in the ZXY direction was improved by 30%, while the strain was increased by 45% compared with samples made from ABS filament. The parts produced from ABS/TiO_2 also exhibited a lower roughness than samples fabricated from pure ABS.

3.3.2. ABS/TPE Blend

The blending of ABS with TPE had the effect of reducing the UTS by 16% in the case of parts printed in XYZ direction and also reduced the UTS by 9% in the case of parts printed in the ZXY direction compared with baseline ABS samples. The percent elongation for ABS/TPE samples did not deviate compared with ABS for components printed in the XYZ direction, however parts printed in the ZXY

direction were able to withstand 31% more strain compared to those printed from pure ABS. The stress–strain curve indicated the modulus of the ABS/TPE blend was the same as the modulus observed for tensile testing of ABS printed in the XYZ direction, not modifying the behavior in the linear-elastic region; however, the UTS was reduced. Even though the mechanical properties were compromised, blending ABS with TPE resulted in an improvement on the final surface finish and a reduction in warping during the printing process.

3.3.3. ABS/Jute Fiber Composite

The compounding of jute fiber with ABS had the effect of reducing the UTS by 9% but improved the amount of plastic deformation increasing the strength at fracture by 28% in the case of samples printed in the XYZ direction.

For samples printed in the ZXY direction, the addition of jute fiber reduced the fracture strength by 35% and increased the fracture strain by 31%. Parts fabricated from the jute composite exhibited the highest roughness of the four compared materials. It was also observed that the addition of jute to ABS decreased the amount of warping, leading to greater dimensional stability.

The results of tensile testing are represented in tables 3.3 and 3.4. Overall, parts fabricated in the ZXY direction were able to withstand less plastic deformation than those fabricated in the XYZ direction. There is a precedent in the literature for the characterization of the effect of mechanical properties on build orientation for components fabricated from material extrusion 3DP [13-15].

Table 3.3: Values of UTS and UFS for XYZ specimens

Material	UTS Stress (MPa)	UFS Stress (MPa)	Young's Modulus (MPa)	
	@Strain (%)	@Strain (%)	Average	St. Dev.
ABS	28.4 @ 2.2	18.4 @ 4.5	1530	114
ABS 5% jute	25.9 @ 2.5	23.6 @ 4.5	1543	121
ABS 5% TiO_2	32.2 @ 2.0	23.7 @ 3.2	1708	121
ABS 5% TP rubber	24.0 @ 2.1	18.7 @ 3.4	1580	113

Table 3.4: Values of UTS and UFS for vertical specimens

Material	UTS/ UFS Stress (MPa)	Young's Modulus (MPa)	
	Strain (%)	Average	St. Dev.
ABS	14.1 @ 1.5	1190	166
ABS 5% jute	9.1 @ 1.9	871	234
ABS 5% TiO_2	18.4 @ 2.0	1355	244
ABS 5% TP rubber	12.8 @ 1.9	1101	300

3.4. Fractography

The breakage occurred in the gage section for the all the samples tested. Figure 3.8 shows a representative tested sample from each sample set. The fracture surfaces were analyzed for samples printed in both the horizontal XYZ and vertical ZXY directions in low magnification (Figures 3.9 and 3.11) and high magnification (Figures 3.10 and 3.12). Representative electron micrographs of the fracture surfaces for the four material systems studied in this paper demonstrated drastically different fracture behaviors. In most cases, the fracture of a thermoplastic component is ductile due to the reorientation and stretching of the thread-like macromolecules that allow for high deformation on the material. In contrast, the fracture surfaces of thermoset polymeric components typically do not exhibit a high amount of plastic deformation as their macromolecules possess a relatively high level cross-linkage between the polymeric chains. Elastomers tend to fracture after a high amount of elastic distortion, leaving a very slight residual deformation [16]. In our case, we were dealing with the examination of thermoplastics and a thermoplastic/elastomer blend, and so one would expect to see fracture characteristics typical of ductile fracture.

3.4.1. Fractography of Samples Printed in the XYZ Direction

Voids are commonly found in material extrusion 3DP between the deposited print rasters. However, a different level of filling was achieved depending on the unique characteristics of the molten composite.

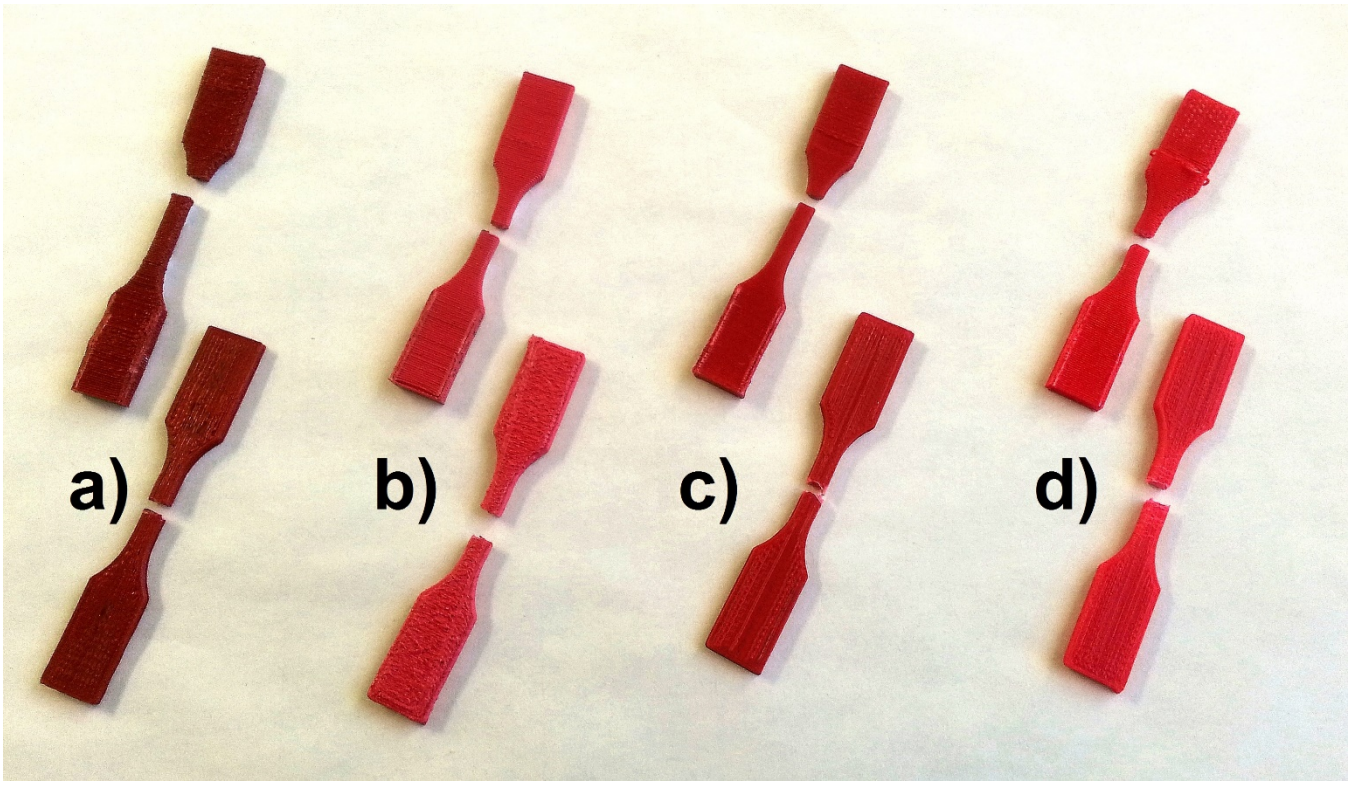

Figure 3.8: Broken specimens after tensile test (vertical above, horizontal below): (a) ABS and jute fiber, (b) ABS and TiO_2, and (c) ABS with TPE, (d) pure ABS

The fracture surface of the baseline sample fabricated from ABS is characteristic of ductile fracture observed in thermoplastic materials (Figures 3.9a and 3.10a). As can be seen in the micrographs, several opened-up crazes were generated by tear fractures during the deformation of the continuous threads. Figure 3.10a shows a V-shaped ramp characteristic of a tear fracture that is typically generated on the surface and then propagates inward [16].

Multiple craters and voids can be observed on the surface fracture of ABS loaded with jute fiber (Figures 3.9b and 3.10b). Jute fiber has been reported to undergo decomposition starting at temperatures of 180 °C [17]. The breakdown of the cellulose would lead to secondary byproducts within the mixture and the generation of combustion gases that would remain trapped within the filament during the extrusion process, depending on the time of exposure to the high temperatures. Even if the decomposition process was not completed during the compound of the monofilament through the twin-screw extrusion process, the process of material extrusion 3DP entails subjecting the monofilament to an extrusion process at temperatures above the decomposition temperature of jute. It can be observed in Figure 3.10b. that little

remains of the original morphology of the fibers, most likely due to the fact that mixing process inside the extruder exposes the fibers to shear forces that break down the fibers, and because of the decomposition process already mentioned. The voids inside the material provide an explanation for the decrease in UTS. The increase in strain observed in the plastic deformation region of the stress–strain curve plot may be due to the particles having a higher freedom to easily reallocate themselves inside the matrix [16] leading to an ability to sustain more plastic deformation than ABS alone.

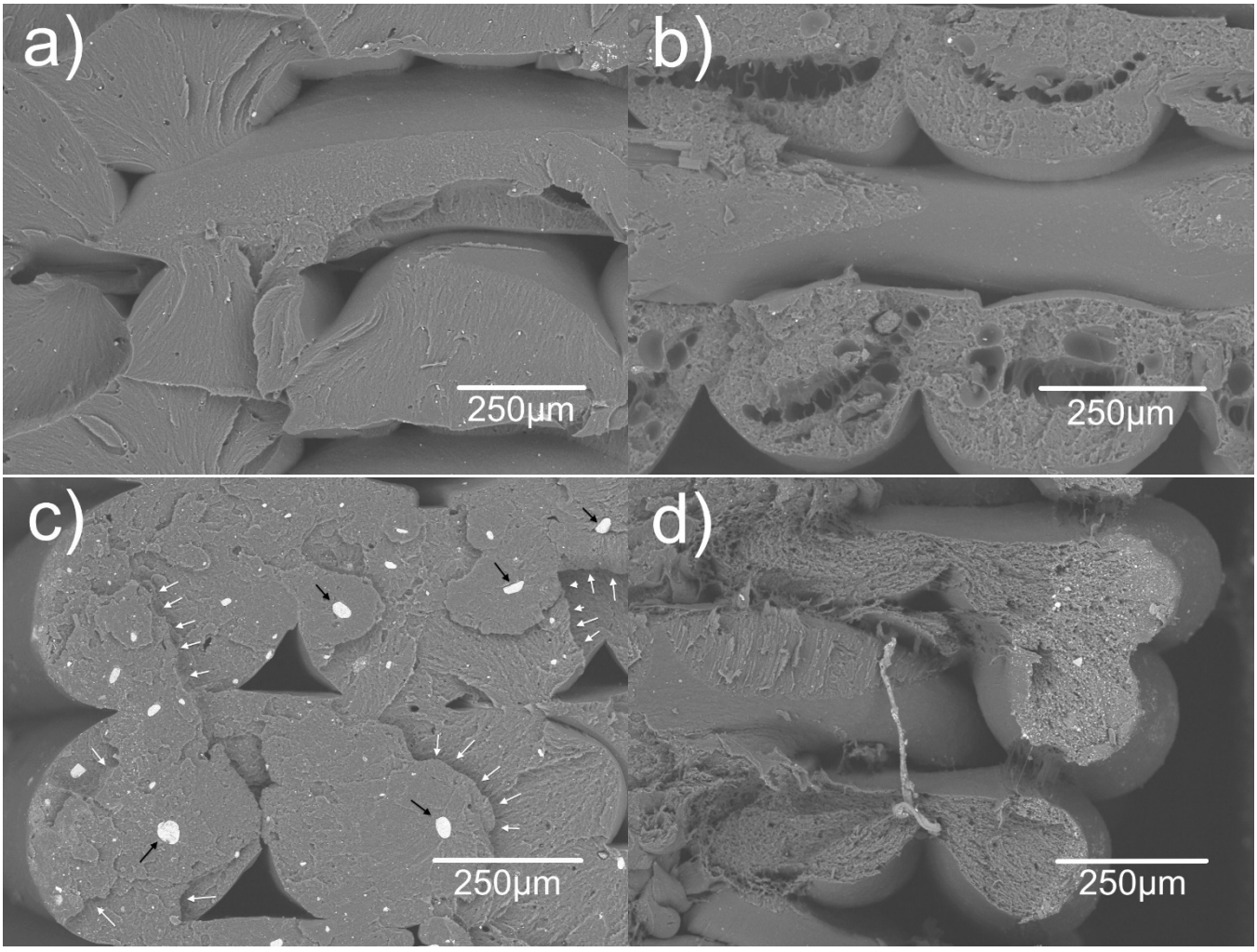

Figure 3.9: SEM images of the fractures of the XYZ samples: low magnification. (a) ABS, (b) ABS and jute fiber, (c) ABS and TiO_2, and (d) ABS and TPE

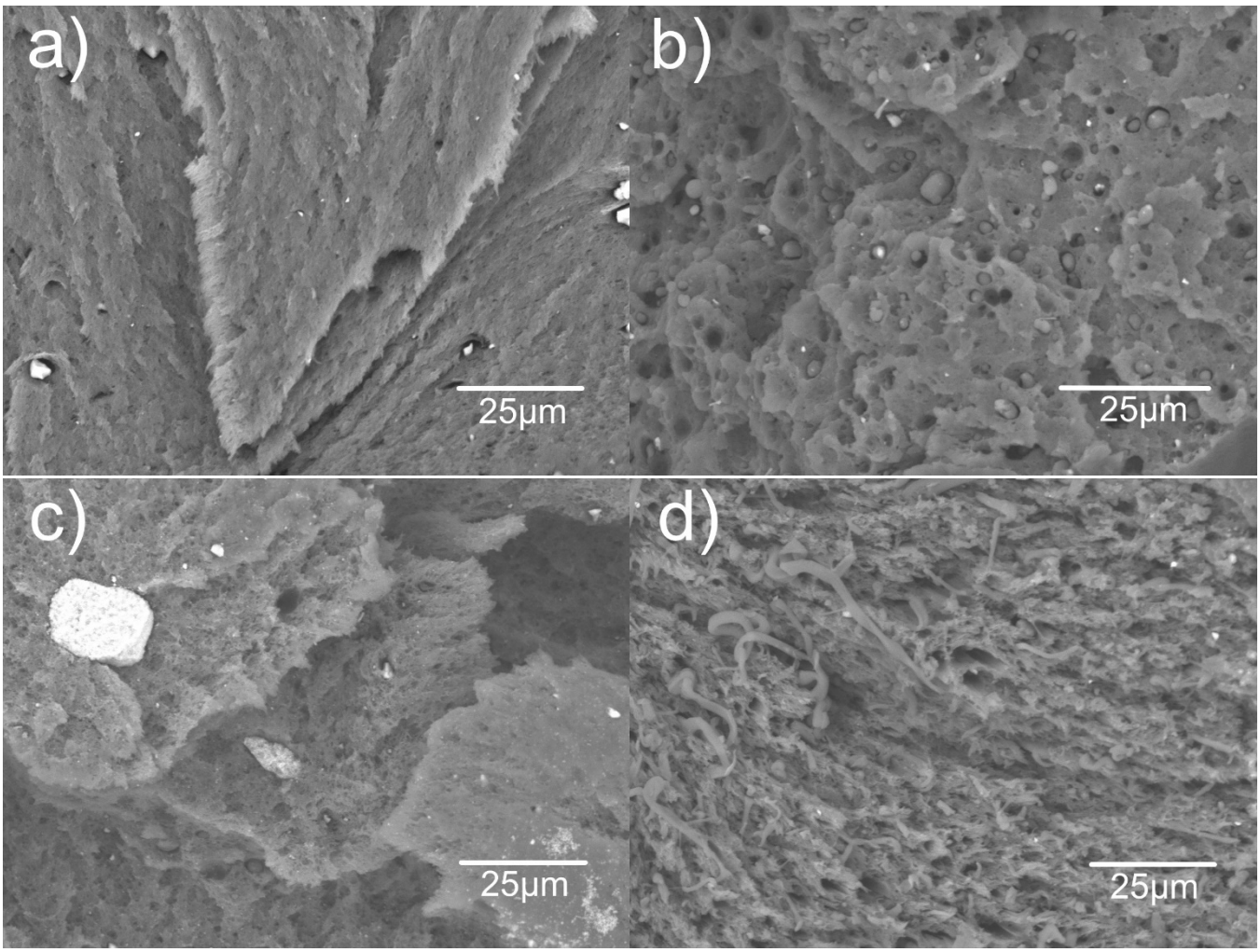

Figure 3.10: SEM images of the fractures of the XYZ samples: high magnification. (a) ABS, (b) ABS and jute fiber, (c) ABS and TiO_2, and (d) ABS and TPE

The presence of TiO_2 reduces the freedom of the plastic macromolecules to slide over one another, producing a fracture surface indicative of a brittle failure. When micrographs of the TiO_2 composites are compared with the other material types as observed in Figures 3.9c and 3.10c, it is notable that the fracture surface is nearly flat and without regions of deformation. No deformed fibrils are present. Abrupt steps and striations are observed as indicated with white arrows. The observed results are congruent to the reduction of the plastic region observed on the stress–strain curve plot for samples fabricated from the ABS/TiO_2 material system. Agglomerated TiO_2 powder with diameters up to 25μm can be seen in the micrographs indicated with black arrows, though initial characterization of the powder revealed the nominal particle diameter to be an order of magnitude smaller, on the order of 50nm, indicating a problem

with particle dispersion during the compound of the composite monofilament. The use of silanes has proven to be a successful avenue in improving the dispersion and adhesion of TiO_2 particles within a polymer matrix [18]. As mentioned before, the ABS/TiO_2 system exhibited the highest value for the Young's modulus. The variation of the Young's modulus for the other materials tested is negligible compared with ABS alone.

The ABS/TPE blend exhibited characteristics indicative of ductile fracture after undergoing the highest amount of plastic deformation of the four compositions (Figures 3.9d and 3.10d). Figure 3.10d shows one of the craze regions with multiple torn-off fibrils with diameters between 1 and 5μm coinciding with a normal stress zone, typical of elastomeric materials [16].

3.4.2. Fractography of Components Fabricated in the ZXY Direction

The fracture surfaces observed on tensile specimens fabricated from the four material types that were printed in the ZXY direction (Figures 3.11 and 3.12) present different characteristics compared to those fabricated in the XYZ direction. The fracture surfaces in the case of the ZXY direction-built specimens exhibit brittle characteristics and large cavities with the exception of the specimens loaded with jute fiber.

The fracture surfaces of the sample printed from ABS are shown in Figures 3.11a and 3.12a and exhibit brittle fracture surface characteristics in contrast to the ductile fracture characteristics observed on the fracture surface of XYZ direction. The formation of circular cavities with diameters from 5μm in the outer section of the fracture to larger diameters of up to 50μm on the inside of the fracture can be observed. Another notable feature of the fracture surface is the lack of the presence of fibrils (Figure 3.12a). A key characteristic of this fracture surface is a flake-like morphology indicative of an extended normal stress zone. The fracture surface of ABS/TiO_2 composite possesses similar characteristics to that of the ABS specimen (Figures 3.11c and 3.12c). However, the ABS/TiO_2 fracture surface exhibited a lower number of cavities with a more uniform diameter distribution along the surface. The fracture surface of the sample fabricated from the ABS/TPE blend showed similar brittle fracture characteristics to ABS and the ABS/TiO_2 composite (Figures 3.11d and 3.12d), but with fewer voids of smaller diameter on average. The increase in tensile strength and modulus at the expense of ductility is a common tradeoff in the fabrication

of composite materials. Moreover, the presence of TiO_2 particles acts as a stress concentrator. The particles act as barriers to the propagation of microfractures produced in the matrix during the plastic deformation of the sample. As the cracks are not able to progress when they reach a particle, the effective ductility is reduced. The accumulation of microfractures within a certain region will eventually lead to a brittle macrofracture when the rupture occurs.

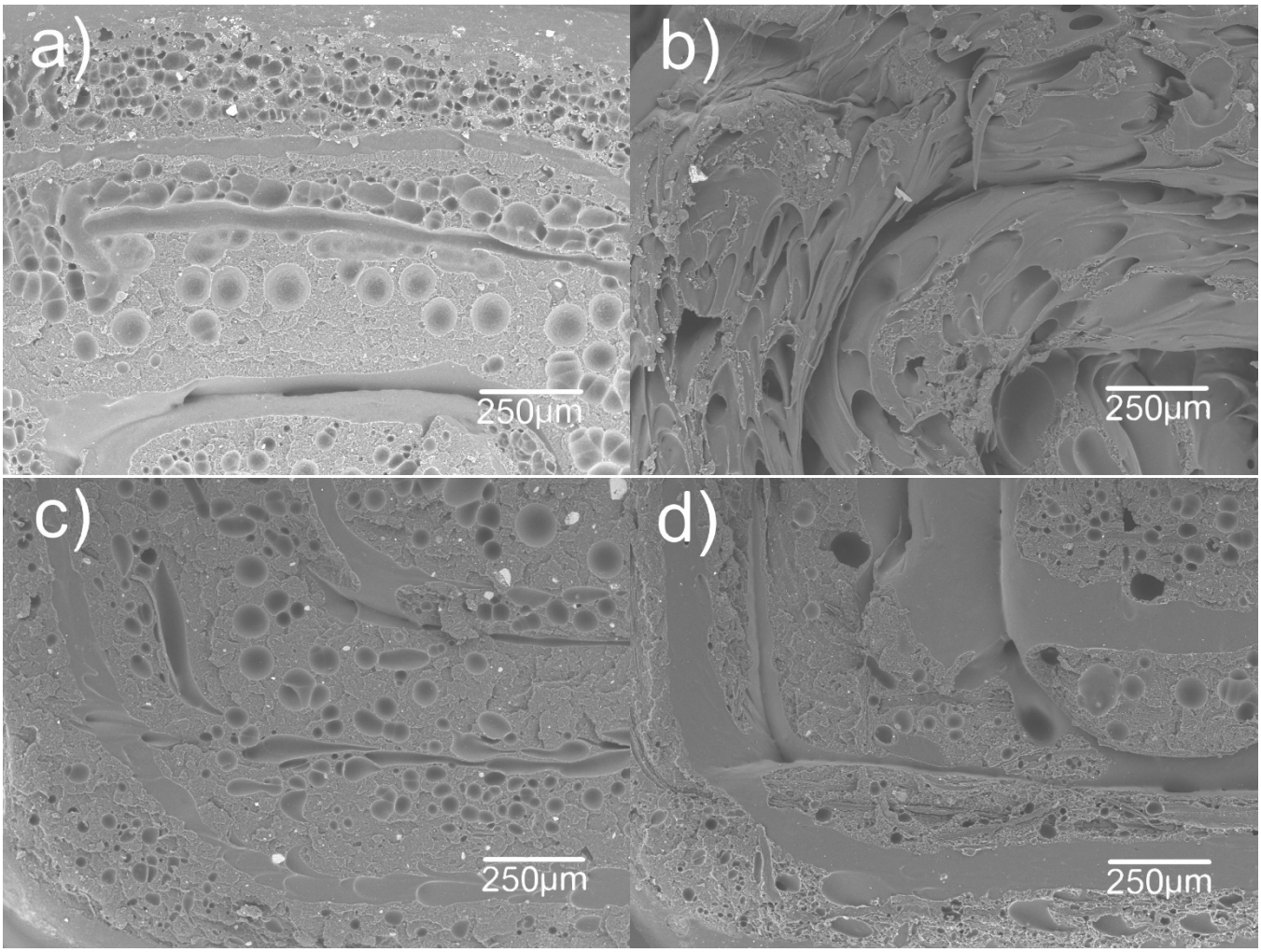

Figure 3.11: SEM images of the fractures of the ZXY samples: low magnification. (a) ABS, (b) ABS and jute fiber, (c) ABS and TiO_2, and (d) ABS and TPE

The fracture surface of the ABS/jute fiber composite was the only material type to exhibit ductile-like fracture characteristics (Figures 3.11b and 3.12b) among the sample types printed in the ZXY direction. The ductile-like morphology of the fracture surface is misleading as it was most likely

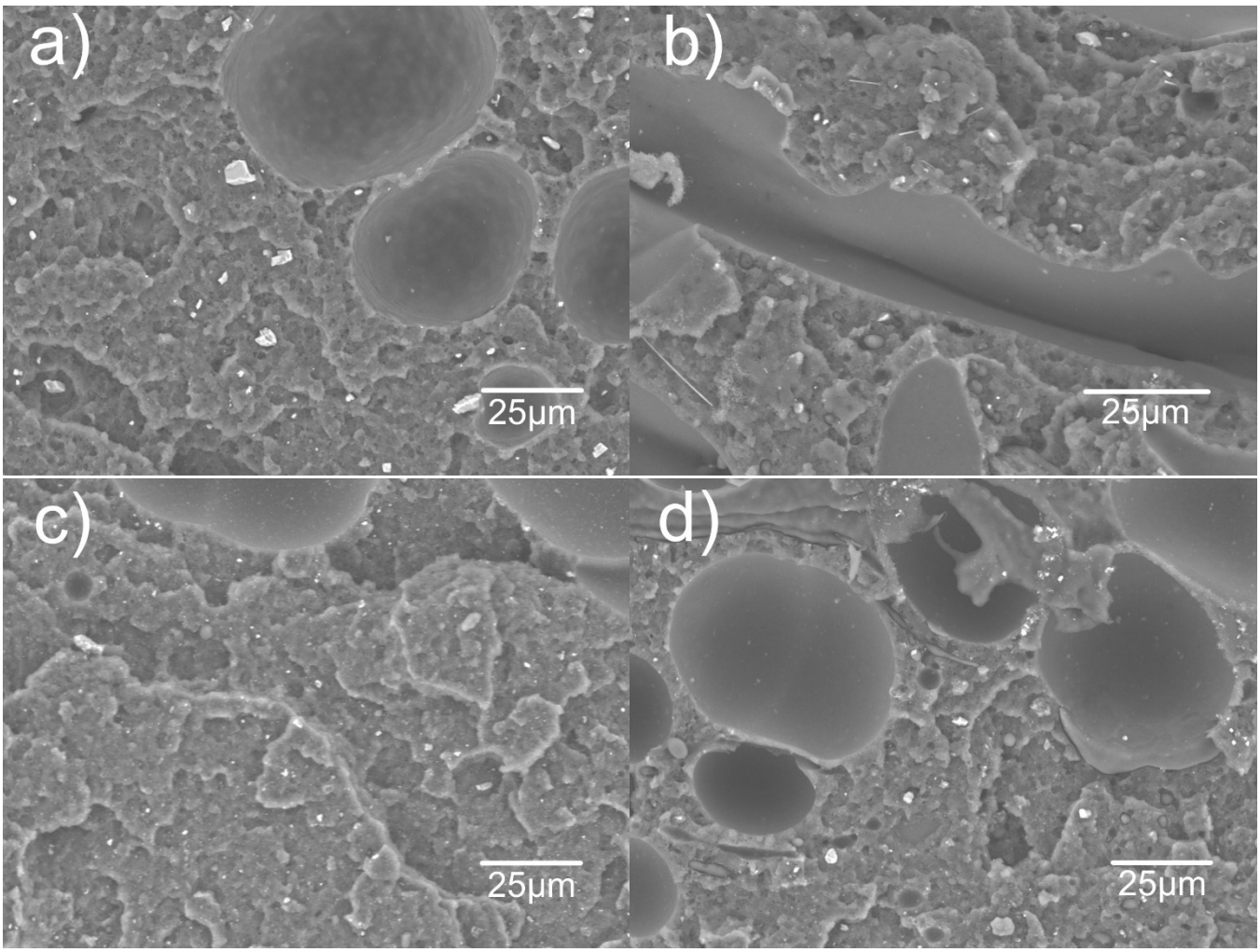

Figure 3.12: SEM images of the fractures of the ZXY samples: high magnification. (a) ABS, (b) ABS and jute fiber, (c) ABS andTiO_2, and (d) ABS and TPE

caused by the transverse rupture of the printed filament (Figure 3.13). The voids observed in the XYZ direction-built specimen were oriented perpendicular to the applied stress for samples printed in the ZXY direction. Though the morphology of the fracture surface resembles and therefore, suggests a torsional fracture, the deformation was produced during the fabrication of the test specimens and follows the direction of print deposition. The present vacancies were caused by the decomposition jute as discussed previously. During the fracture process, the voids deformed further, and crazes were generated from these voids. The normal stress region is reduced with respect the other materials tested, but still no fibrils were observed indicating the fracture was brittle in nature. The addition of jute fiber provokes the lowest Young's modulus of all the materials, which correlates with the higher deformation. For samples

fabricated in the ZXY direction, there are two failure modes present: (1) the failure of the inter-layer bond between printed rasters as observed in the ABS, ABS/TiO_2, and ABS/TPE blend; and (2) transfilament rupture caused by the voids present in the ABS/Jute fiber composite.

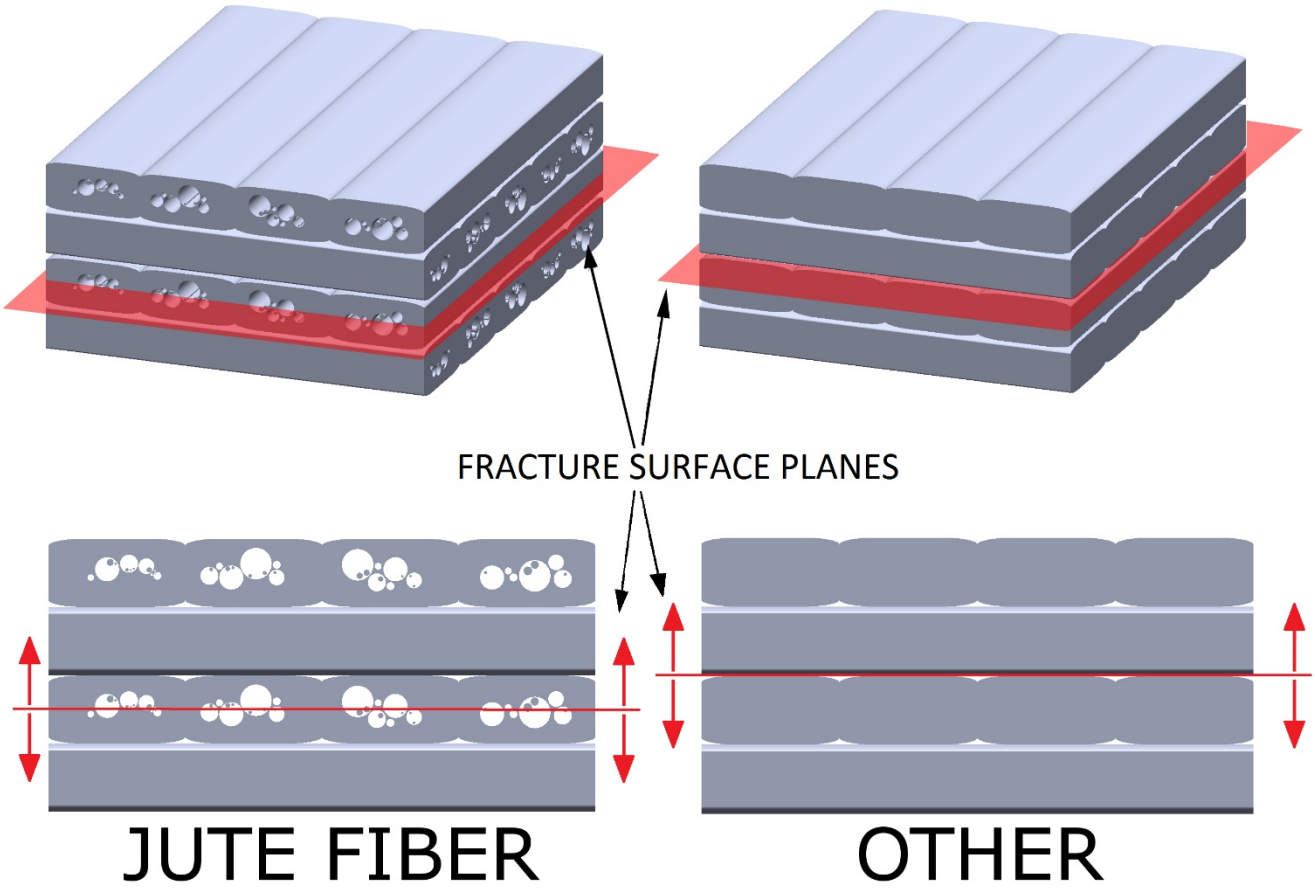

Figure 3.13: Schematic of fracture plains for jute fiber compared with other composites

The data plots represented in Figure 3.14 summarize the results for the UTS, modulus, and elongation to break for all the material systems tested for samples manufactured in both the vertical and horizontal printing directions. Figure 3.14a shows that only the addition of TiO_2 particles leads to an improvement in UTS compared with the other experiments; however, of notable interest is the reduction in the difference between vertical and horizontal UTS values for the ABS/ TPE blend, indicating a decrease in mechanical property anisotropy for components printed from this material system. The addition of TiO_2 had the effect of increasing the modulus as can be seen in Figure 3.14b. Figure 3.14c also

indicates reduction in the difference of the elongation to break between the vertical and the horizontal samples for both the materials with the addition of TiO_2 and TPE.

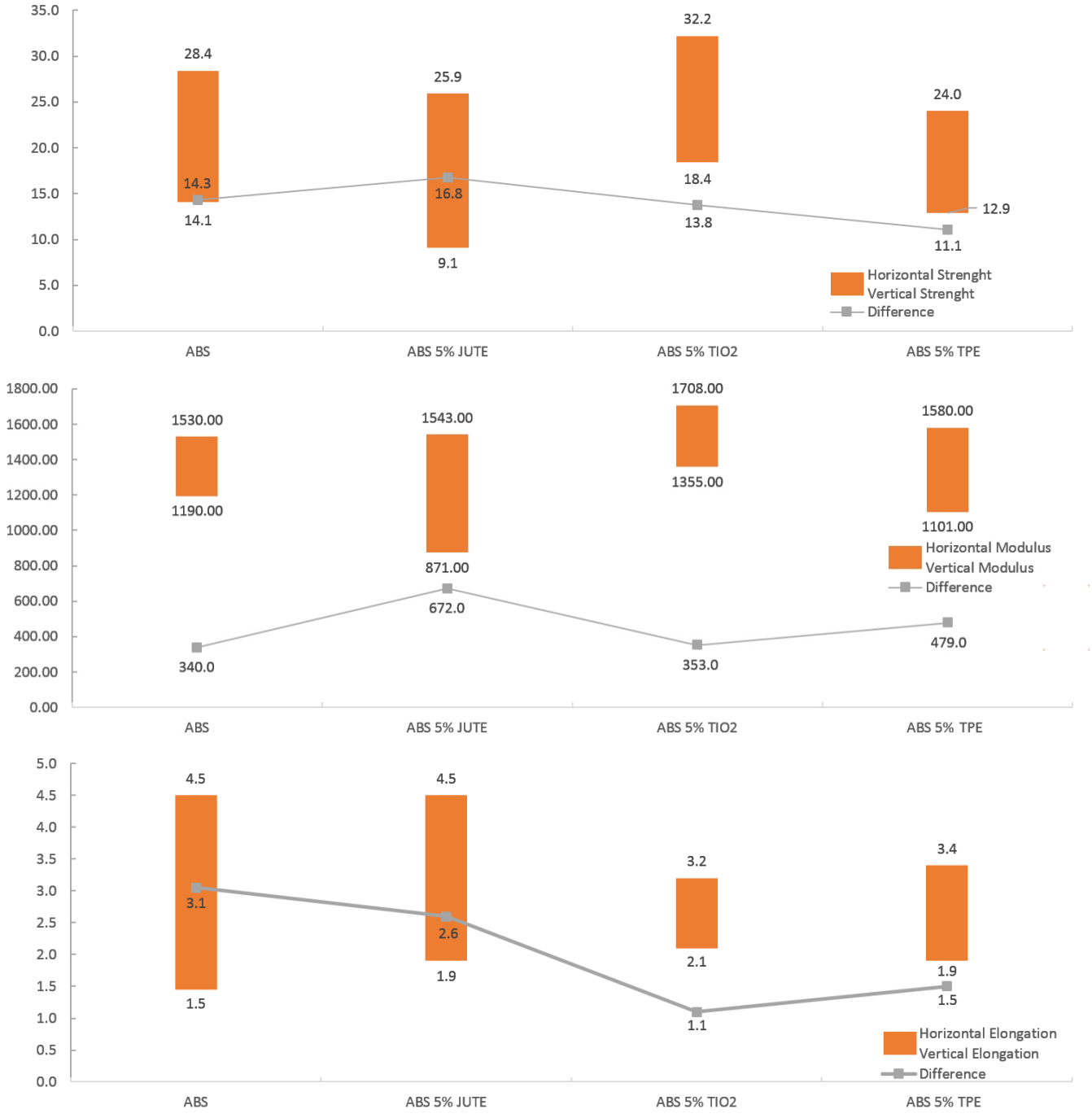

Figure 3.14: Differences in the results of XYZ and ZXY samples for: (a) UTS, (b) modulus, and (c) elongation to break

3.5. Conclusions

The addition of reinforcing agents to ABS PMC has an effect on the mechanical properties and fracture surface characteristics of tensile specimens compared with pure ABS. Instead of the expected ductile fracture behavior, the addition of additives led to fracture surfaces that exhibited brittle characteristics. These systems were ABS with 5 wt. % jute fiber, ABS with 5 wt. % TiO_2, and ABS with 5 wt. % TPE. The ABS/TiO_2 system displayed higher UTS compared with pure ABS and the other composite systems studied in this paper, but the fracture characteristics of this material system indicated brittle fracture. The present study gives an indication of the manipulation of mechanical failure characteristics of components fabricated from 3D-printable composites and polymeric blends.

The fracture surfaces for parts fabricated in the two build orientations exhibited different morphological characteristics, most notably, the presence of cavities, which was more abundant for parts built in the ZXY direction, most likely due to a failure of the interface between printed layers. It is known that the mechanical strength for parts fabricated in the ZXY direction is lower as opposed to parts fabricated in the XYZ direction [14, 15]. Here, the same behavior was observed; however, the results of the ABS/TPE system suggest a pathway toward reducing the characteristic anisotropy of components fabricated form material extrusion 3DP.

3.6. References

[1] B. Berman, 3-D printing: the new industrial revolution. Business Horiz. 55(2), 155–162 (2012)

[2] J.L. Chulilla-Cano, The cambrian explosion of popular 3D printing. IJIMAI 1(4), 30–32 (2011)

[3] S. Masood, W. Song, Development of new metal/polymer materials for rapid tooling using fused deposition modeling. Mater. Des. 25(7), 587–594 (2004)

[4] M. Nikzad, S.H. Masood, I. Sbarski, Thermo-mechanical properties of a highly filled polymeric composites for fused deposition modeling. Mater. Des. 32(6), 3448–3456 (2011)

[5] A. Safari, E.K. Akdogan, Rapid prototyping of novel piezoelectric composites. Ferroelectrics 331(1), 153–179 (2006)

[6] M.L. Shofner, K. Lozano, F.J. Rodríguez-Macías, E.V. Barrera, Nanofiber-reinforced polymers prepared by fused deposition modeling. J. Appl. Polym. Sci. 89(11), 3081–3090 (2003)

[7] M.L. Shofner, F.J. Rodríguez-Macías, R. Vaidyanathan, E.V. Barrera, Single wall nanotube and vapor grown carbon fiber reinforced polymers processed by extrusion freeform fabrication. Composites 34(12), 1207–1217 (2003)

[8] S.-Y. Fu, X.-Q. Feng, B. Lauke, Y.-W. Mai, Effects of particle size, particle/matrix interface adhesion and particle loading on mechanical properties effects of particle size, particle/matrix interface adhesion and particle loading on mechanical properties of particulate–polymer composites. Composites 39, 933–961 (2008)

[9] S. Tjong, Structural and mechanical properties of polymer nanocomposites. Mater. Sci. Eng. 53, 73–197 (2006)

[10] T. Huq, A. Khan, T. Akter, N. Noor, K. Dey, B. Sarker, M. Saha, R.A. Khan, Thermo-mechanical, degradation, and interfacial properties of jute fiber-reinforced PET-based composite. J. Thermoplast. Compos. Mater. 24(6), 889–898 (2011)

[11] S. Wu, Phase structure and adhesion in polymer blends: a criterion for rubber toughening. Polymer 26(12), 1855–1863 (1985)

[12] ASTM Standard D6110, Standard Test Method for Tensile Properties of Plastics, (ASTM International, West Conshohocken, 2010)

[13] S.-H. Ahn, M. Montero, D. Odell, S. Roundy, P.K. Wright, Anisotropic material properties of fused deposition modeling abs. Rapid Prototyping 8(4), 248–257 (2002)

[14] A. Bellini, S. Gu¨c¸eri, Mechanical characterization of parts fabricated using fused deposition modeling. Rapid Prototyping J. 9(4), 252–264 (2003)

[15] O.S. Es-Saida, J. Foyosa, R. Noorania, M. Mendelsona, Effect of layer orientation on mechanical properties of rapid prototyped samples. Mater. Manuf. Process. 15(1), 107–122 (2000)

[16] L. Engel, H. Klingele, G.W. Ehrenstein, H. Schaper, An Atlas of Polymer Damage: Surface Examination by Scanning Electron Microscope (Prentice-Hall, Inc., Englewood Cliffs, 1981)

[17] J. Gassan, A.K. Bledzki, Thermal degradation of flax and jute fibers. J. Appl. Polym. Sci. 82(6), 1417–1422 (2001)

[18] M. Altan, H. Yildirim, A. Uysal, Tensile properties of polypropylene/metal oxide nano composites. Online J. Sci. Technol. 1(1), 25–29 (2011)

CHAPTER 4: CHARACTERIZING THE EFFECT OF ADDITIVES TO ABS ON THE MECHANICAL PROPERTY ANISOTROPY OF SPECIMENS FABRICATED BY MATERIAL EXTRUSION 3D PRINTING

4.1. Introduction

Additive manufacturing (AM) has gained acceptance in many fabrication arenas due to the advantages of this technology over conventional manufacturing methods, such as the ability to fabricate complex geometries, rapid design to fabrication cycle times, and a lower amount of waste material generated, among others. While the advantages of AM are well known, the disadvantages are not widely addressed. Mechanical property anisotropy is an undesirable trait observed in components fabricated from material extrusion 3D printing (ME3DP) —more traditionally referred to by the trademarked moniker, fused deposition modeling (FDM)— as well as nearly every other AM technology such as electron beam melting (EBM), selected laser melting (SLM), selected laser sintering (SLS), stereolithography (SLA), and laser engineered net shaping (LENS) [1-14]. In most cases, the mechanical property anisotropy is observed through the analysis of ultimate tensile strength (UTS) or impact resistance for parts fabricated in various directions, where Z-direction-built parts typically display lower tensile strength and impact resistance [1-10, 13, 14] values with the exception of parts fabricated via EBM [12]. While machine parameters such as raster direction, layer thickness, and air gap (depending on the given 3DP technology) play a role in the mechanical properties [1, 15] and to some degree, the level of anisotropy, there is no clear cut strategy for the mitigation of differences in mechanical properties based on build orientation. A potential path towards the limitation of build orientation-based mechanical property differences is the development of new material systems which are compatible with 3D printing platforms that are designed to exhibit a lower level of mechanical property anisotropy.

While there are many AM platforms to choose from in the battle to defeat anisotropy, material extrusion 3D printing is currently the most common; and relatively simple as compared to other AM platforms. Therefore, we chose this technology as an arena to develop material systems and evaluate the performance of these materials in terms of build orientation-based differences in mechanical properties. There are several examples in literature of the development of polymer matrix composites for use in FDM using fillers ranging from plant fibers and metal particles to piezoelectric ceramics [1, 16-20]. These

examples demonstrate the strategy of increasing the applicability of FDM-type platforms through the development of application-specific feedstock.

Another strategy which can be executed in the development of new 3D printable material systems for FDM-type processes is the creation of new polymeric blends where one or more polymers are combined in the creation of a new material. Here, in the case of ME3DP, our strategy was to use a known printable material such as ABS as the primary constituent in the blend with the theory that the resulting material system would retain compatibility with existing 3D printer platforms. There have been several cases where ABS has been blended with other polymers such as Nylon-6 and polyphenelyne sulfide (PPS) [21-24] however, there is not a large body of research which has been devoted to the development of new polymer blends for material extrusion 3D printing— though Rocha *et al*. [25] has explored the development of ABS-based blends for ME3DP technologies.

The work presented here evaluates the effect of additives on the anisotropy observed in the mechanical properties of tensile test specimens printed from ABS-based material systems. Initially, the additives were chosen based on different goals, such as the manipulation of the electromagnetic properties where metal oxides were added to ABS or examination of the solubility of other polymeric materials within an ABS matrix in the case of binary and ternary blends as discussed in Rocha *et al*. [25]. The evaluation here is to explore unexpected benefits related to the addition of additives to ABS, namely the effect on mechanical property anisotropy. A total of six ABS-based polymer matrix composites and four ABS-based polymer blends were compared with ABS to evaluate the performance of these new 3D printable materials from the point of view of anisotropic mechanical behavior. The metric used to assess this difference was mechanical testing data from tensile test specimens printed in two orientations. Although some materials may show decreased mechanical strength along with decreased anisotropy, this work examines the print quality and fracture behavior in order to determine if any particular additive alters specific properties which in turn decrease anisotropy. The knowledge gleaned from this work can then be applied in the development of future 3D printable material systems with a lower propensity to produce parts exhibiting mechanical property anisotropy without a compromise to mechanical strength.

4.2. Experimental procedure

Experiments performed in this work involved several polymer matrix composites (PMC)s and polymer blends where the base material was a CYCOLAC™ ABS grade MG37CR resin (GE, now Sabic, Pittsfield, MA, USA) combined with various additives such as plant fibers, metal oxides, and other polymers (Table 4.1). Jute plant fiber derived from rope purchased at a hardware store (Home Depot), MayaCrom® Blue (Mayan Pigments, Inc., El Paso, TX, USA), titanium dioxide (TiO_2 Reagent Plus®, Sigma-Aldrich), zinc oxide (ZnO) nanorods, strontium titanate ($SrTiO_3$, 5μm, Sigma-Aldrich) and alumina (Al_2O_3 0.5μm, Metallurgical Supply Co, Houston, TX, USA), were compounded with ABS in the creation of polymer matrix composites. The ZnO nanorods were synthesized according to the process described by Lin *et al*. [26] where a two-step process was used starting with the synthesis of ZnO nanoparticles through the dissolution of zinc acetate dihydrate in ethanol with a subsequent dilution in a sodium hydroxide (NaOH) solution. The synthesized nanoparticles were then subjected to the second step of the nanorod synthesis process where the ZnO nanoparticles were added to a mixture of zinc nitrate hydrate and hexamethylenetetramine (HMTA) where the nanorod growth occurred. Finally, the grown nanorods were rinsed in deionized water and then dried. Images of the raw additives are shown in Figure 4.1.

In the case of the four polymeric blends tested here, ABS was blended with styrene ethylene butylene styrene (SEBS) supplied by Kraton (A1536 HU SEBS, Kraton, Houston, TX, USA) to create binary ABS/SEBS blends. Two additional ternary polymeric blends were tested in this study where ABS was blended with ultra high molecular weight polyethylene (UHMWPE) supplied by Celeanese (GUR® 1020 UHMWPE, Celeanese, Irving, TX, USA) along with SEBS. The compositions of the polymeric blends tested in this study are also listed in Table 1 and are indicated by relative weight ratio.

Compounding of the PMCs and polymer blends was carried out through the use of a Dr. Collin twin screw extruder/compounder (Model ZK 25T Dr. Collin GmbH, Ebersberg, Germany) equipped with a dual co-rotating, intermeshing screw system. The filaments were produced targeting a diameter of 1.75 ±0.05mm, which is the standard for most FDM-type 3D printing platforms. Due to the difference in material properties between the material systems tested here, different machine parameters were needed

to facilitate extrusion of a monofilament compatible with our material extrusion 3D printer. The main extrusion parameters utilized for each system are presented in Table 4.2

Table 4.1: Material systems evaluated in this study.

	ABS (wt%)	Additive (wt%)	
"ABS Matrix Composites"	100	-	-
	95	Jute	5
	98	MayaCrom® Blue	2
	95	TiO_2	5
	98	ZnO	2
	95	$SrTiO_3$	5
	95	Al_2O_3	5
ABS Blends (Weight Ratio)	ABS:SEBS		
	95:5		
	80:20		
	ABS:UHMWPE:SEBS		
	75:25:10		
	90:10:10		

Table 4.2: Extrusion processing parameters for each material created in this study.

Material	T Zone 1 (ºC)	T Zone 2 (ºC)	T Zone 3 (ºC)	T Zone 4 (ºC)	T Zone 5 (ºC)	Main Screw Speed (RPM)	Feed Screw Speed (% Main)	P Main Screw (bar)	Load (%)
ABS	170	182	187	187	187	35	100	100	72
ABS 5% JUTE FIBER	170	182	187	187	187	35	100	100	72
ABS 2% MayaCrom® Blue	170	175	175	175	175	50	53	53	63
ABS 5% TiO_2	170	182	187	187	187	35	100	100	72
ABS 2% ZiO	180	185	185	185	185	50	40	40	60
ABS 5% $SrTiO_3$	170	175	175	175	175	50	47	47	61
ABS 5% Al_2O_3	170	175	180	180	180	50	52	52	61
ABS:SEBS									
95:5	170	182	187	187	187	35	6	100	72
80:20	170	182	190	190	190	35	6	92	72
ABS:UHMWPE:SEBS									
75:25:10	155	185	185	185	185	40	6	80	62
90:10:10	155	195	195	195	190	40	6	72	60

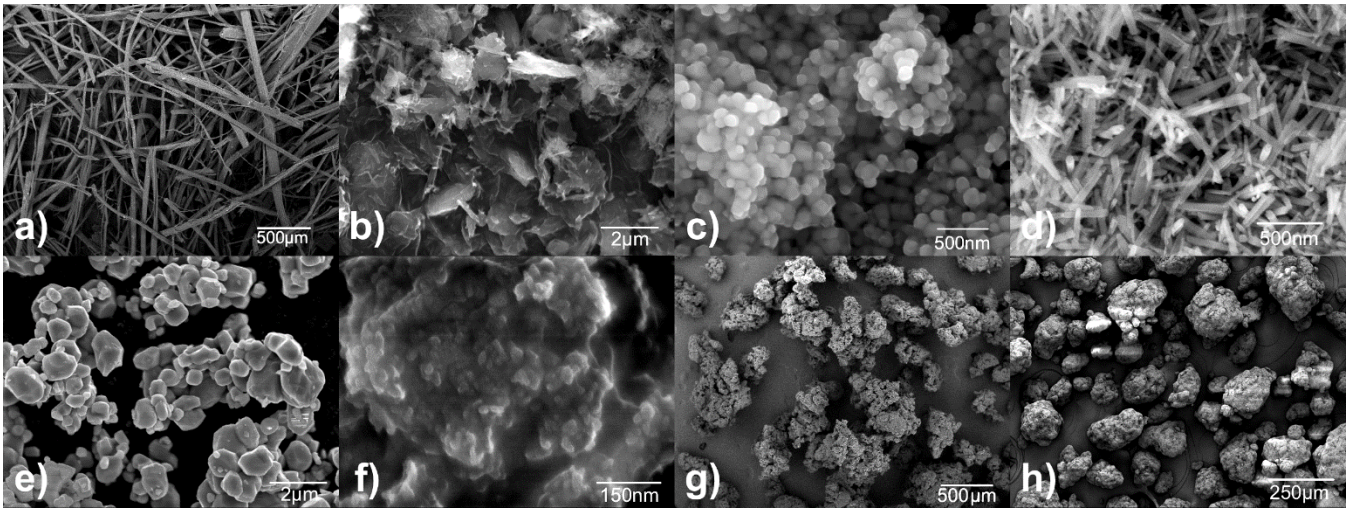

Figure 4.1: SEM micrographs of the materials which were added to ABS in the compounding of polymer matrix composites and polymer blends a) Jute fiber, [1] b) MayaCrom® Blue, c) TiO_2, [1] d) ZnO, e) $SrTiO_3$, f) $Al2O_3$, g) SEBS, [1] h) UHMWPE.

Printing of the tensile test specimens was performed with a MakerBot Replicator (MakerBot Industries, Brooklyn, NY USA) following the ASTM Standard D638-10 according to the Type V dimensions [27] in XYZ (or horizontal) and ZXY (or vertical) directions. For each material system in in the case of both build orientations, five specimens were printed (sample size n = 5 for all experiments). As was the case in the extrusion of the monofilaments, print parameters differed between the material systems. The print parameters for the different material systems tested here are listed in Table 4.3. In the case of the ABS/UHMWPE/SEBS blends, we found it necessary to use a print nozzle with a physical diameter of 0.8mm to facilitate printing, but the printer was run with a raster width machine parameter of 0.6mm. The specimens were printed with a rectangular fill pattern oriented at an angle of 0º, in which the rasters change direction by 90º every layer. Figure 4.2 shows the build orientations the specimens were printed in and the directions of the raster patterns on the faces (hash marks). The parameters were tuned with the goal of minimizing the air gap between the rasters (with the goal of 100% infill), for a more solid final specimen. It should be noted that the work presented here examines the anisotropy by comparing samples fabricated in one build orientation to another build orientation, while keeping the material constant. The ratio between mechanical properties for specimens printed in the XYZ vs. the ZXY direction should be independent of print conditions, even if the printing parameters or print nozzle changes from one material to the next.

Table 4.3: MakerBot print parameters used for the materials tested in this study.

Material	Object Infill (%)	Layer Height (mm)	Number of Shells	Feedrate (mm/s)	Travel Feedrate (mm/s)	Print Temperature (°C)	Filament Diameter (mm)	G-code Nozzle Diameter (mm)	Actual Nozzle Diameter (mm)	Raft
ABS	100	0.27	1	40	55	230	1.8	0.4	0.4	No
ABS 5% JUTE FIBER	100	0.27	1	40	55	230	1.8	0.4	0.4	No
ABS 2% MayaCrom® Blue	100	0.27	1	40	55	230	1.8	0.4	0.4	No
ABS 5% TiO_2	100	0.27	1	40	55	230	1.8	0.4	0.4	No
ABS 2% ZnO	100	0.27	1	40	55	230	1.8	0.4	0.4	No
ABS 5% $SrTiO_3$	100	0.27	1	40	55	230	1.8	0.4	0.4	No
ABS 5% Al_2O_3	100	0.27	1	40	55	230	1.8	0.4	0.4	No
ABS:SEBS										
95:5	100	0.27	1	40	55	240	1.8	0.4	0.4	No
80:20	100	0.27	1	40	55	240	1.8	0.6	0.8	No
ABS:UHMWPE:SEBS										
75:25:10	100	0.27	1	40	55	230	1.8	0.6	0.8	No
90:10:10	100	0.27	1	40	55	230	1.8	0.6	0.8	No

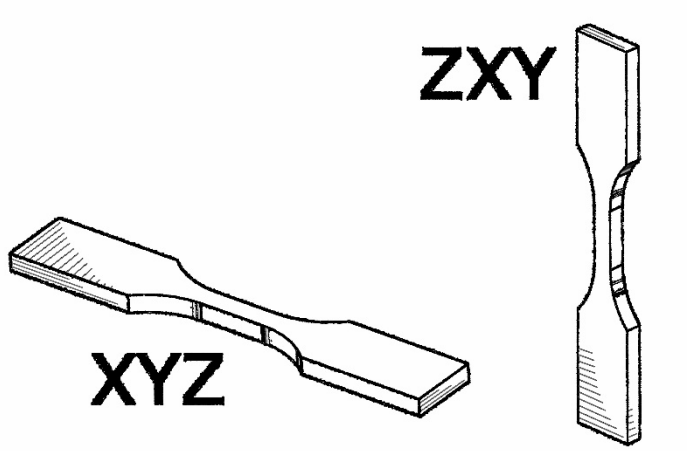

Figure 4.2: Representation of XYZ and ZXY printing directions and actual raster orientations after printing (hash marks.)

An Instron® 5866 (Instron, Norwood, MA) tensile testing machine equipped with a 10kN load cell was utilized to perform the tensile testing. The specimens were tested at a strain rate of 10mm/min at room temperature. The tensile test apparatus relied on the Instron® 2663-821 advanced video extensometer (AVE) to measure % elongation (%EL). The fracture surfaces were analyzed via scanning electron microscopy (SEM) with a Hitachi TM-1000 (Hitachi High-Technologies Europe GmbH, Germany)

operating at a 15kV accelerating potential and equipped with a backscatter electron (BSE) detector. Prior to analysis, samples were sputter coated with a gold/palladium alloy using a Gatan Model 682 Precision Etching Coating System (Gatan, Inc., Pleasanton, CA, USA) in order to eliminate charging effects on the surface.

4.3. Results and Discussion

Tensile test results for each of the PMCs and polymer blends were compared with baseline data obtained from samples printed from the same ABS base resin. Figures 4.3 4.4 offer a graphical representation of the data. The ultimate tensile strength (UTS) and the elongation to break (%EL) was compared between specimens printed in the XYZ (horizontal) and ZXY (vertical) directions. Tables 4.4 and 4.5 show the mean and standard deviation (σ) values of UTS and %EL for the material systems evaluated here. The absolute difference in mechanical test values between the printed directions, and the percent difference (the difference in UTS values relative to the horizontally printed samples) of those values in the ZXY direction with respect the XYZ direction are also tabularized on Tables 4.4 and 4.5. The percent difference for UTS and %EL between print orientations was calculated following the equations:

$$\Delta(\%)_{UTS} = \frac{UTS_{XYZ} - UTS_{ZXY}}{UTS_{XYZ}} \quad (1)$$

and

$$\Delta(\%)_{\%\mathrm{EL}} = \frac{\%\mathrm{EL}_{XYZ} - \%\mathrm{EL}_{ZXY}}{\%EL_{XYZ}} \quad (2)$$

It should be noted that while each material can be compared to each other's performance, in general this is not applicable as each system has differing volumetric loadings. However, rheological changes provide a much greater effect on anisotropy (as will be discussed in greater detail), and if print parameters remain constant between orientations (for the same material), sufficient conclusions can be drawn as to the effects on anisotropy. As such, this work examines the relationship between material properties

(complex viscosity, mechanical strengthening) and the corresponding anisotropy in order to find trends which can be used to defeat anisotropy in the development of future composites.

Table 4.4: UTS values along with relative and absolute difference between print orientations.

Material	UTS_{XYZ}		UTS_{ZXY}		Δ			
	Mean*	σ	Mean*	σ	Absolute	σ	Relative†	σ
	MPa	MPa	MPa	MPa	MPa	Mpa	%	%
ABS	33.96	1.74	17.73	2.52	16.23	3.07	47.79%	7.23%
ABS 5% JUTE FIBER	24.25	2.34	8.63	3.59	15.62	4.29	64.43%	27.55%
ABS 2% MayaCrom® Blue	17.31	0.52	7.79	2.61	9.52	2.66	54.98%	18.46%
ABS 5% TiO_2	32.90	1.43	16.67	3.23	16.22	3.53	49.32%	9.78%
ABS 2% ZnO	20.70	0.55	7.41	2.38	13.29	2.44	64.19%	20.69%
ABS 5% $SrTiO_3$	21.60	0.63	5.95	2.32	15.65	2.40	72.46%	28.28%
ABS 5% Al_2O_3	28.80	2.62	12.14	4.82	16.67	5.49	57.86%	23.59%
ABS:SEBS								
95:5	25.51	2.02	11.30	0.91	14.21	2.22	55.70%	6.30%
80:20	25.20	1.65	8.41	0.50	16.79	1.72	66.63%	5.89%
ABS:UHMWPE:SEBS								
90:10:10	23.07	0.78	10.24	3.83	12.83	3.90	55.60%	20.85%
75:25:10	14.70	0.63	11.47	0.96	3.24	1.15	22.02%	2.07%

* Sample size n = 5
†Calculated from Equation (1)

Table 4.5: %EL values and relative and absolute differences between print orientations.

Material	$\%EL_{XYZ}$		$\%EL_{ZXY}$		Δ			
	Mean*	σ	Mean*	σ	Absolute	σ	Relative†	σ
	%	%	%	%	%	%	%	%
ABS	8.64	3.35	2.08	0.55	6.56	3.39	75.92%	35.62%
ABS 5% JUTE FIBER	4.25	1.14	1.55	0.70	2.70	1.34	63.48%	33.43%
ABS 2% MayaCrom® Blue	8.86	1.40	2.02	0.51	6.84	1.49	77.17%	23.11%
ABS 5% TiO_2	3.77	1.93	1.61	0.60	2.16	2.02	57.25%	36.31%
ABS 2% ZnO	6.32	1.53	1.07	0.24	5.25	1.55	83.13%	27.68%
ABS 5% $SrTiO_3$	5.56	0.61	1.06	0.47	4.50	0.76	81.01%	36.84%
ABS 5% Al_2O_3	2.94	0.73	1.60	0.24	1.34	0.77	45.68%	13.30%
ABS:SEBS								
95:5	3.56	0.59	1.92	0.47	1.64	0.75	46.07%	13.51%
80:20	11.90	1.90	2.00	0.44	9.90	1.95	83.00%	22.56%
ABS:UHMWPE:SEBS								
90:10:10	8.40	0.94	2.41	0.99	5.99	1.36	71.31%	30.26%
75:25:10	5.68	0.65	2.26	0.59	3.42	0.88	60.21%	17.12%

*Sample size n = 5
†Calculated from Equation (2)

Fractography was performed on the fracture surfaces from representative samples of tensile specimens from each material type with the aid of scanning electron microscopy (SEM). Analysis of the

composites composed of ABS compounded with jute, TiO_2, and the polymer blend of 95:5 ABS:SEBS was performed by Torrado *et al*. [1] and is included here as a comparison. Key aspects of notable interest are the distinct effect of additives on the morphology of fracture surfaces of the ABS-based material systems. While it is difficult to generalize the fracture behavior observed among the material systems here, the fracture for samples printed in the ZXY direction are, for the most part, dominated by the rupture within the interlayer interface between print rasters

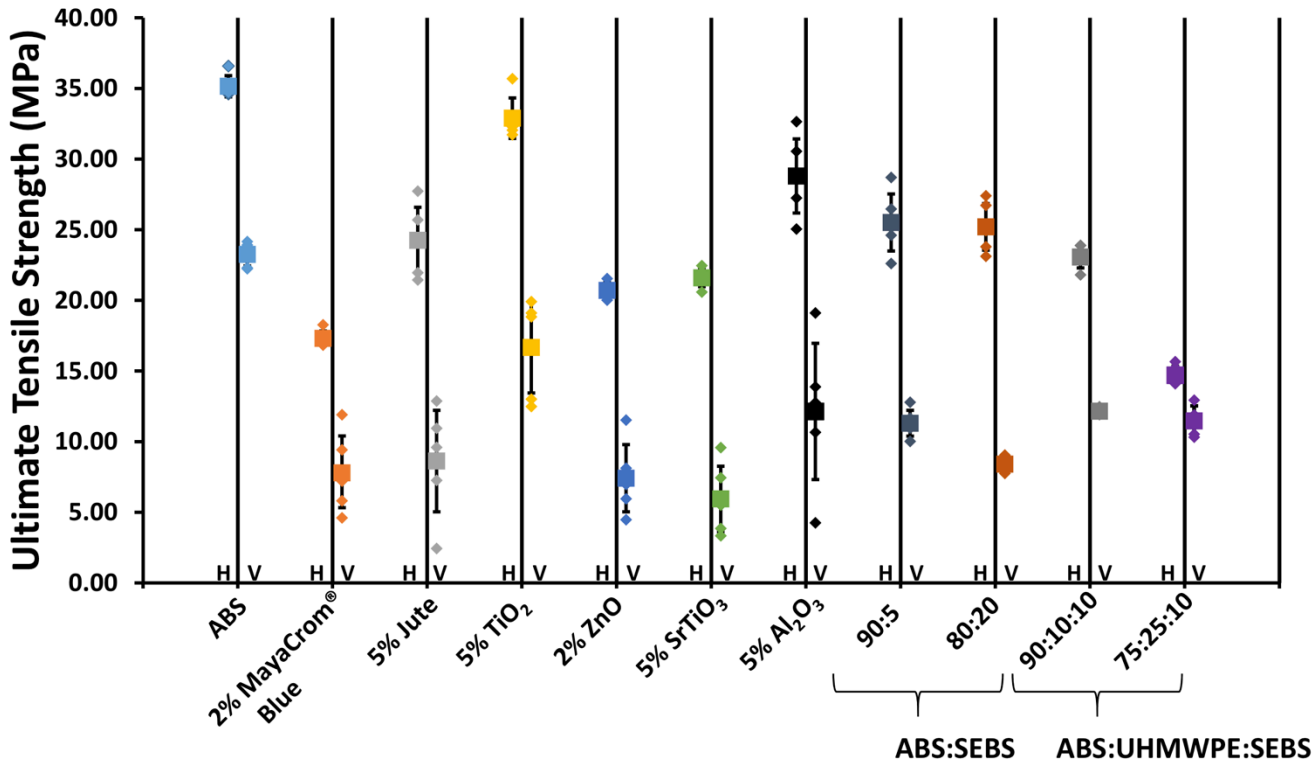

Figure 4.3: Graphical representation of the anisotropy of UTS values for the materials tested in this study. Here H corresponds to horizontal (XYZ) build orientation and V corresponds to vertical (ZXY) build orientation. The large square represents the mean of each sample pool.

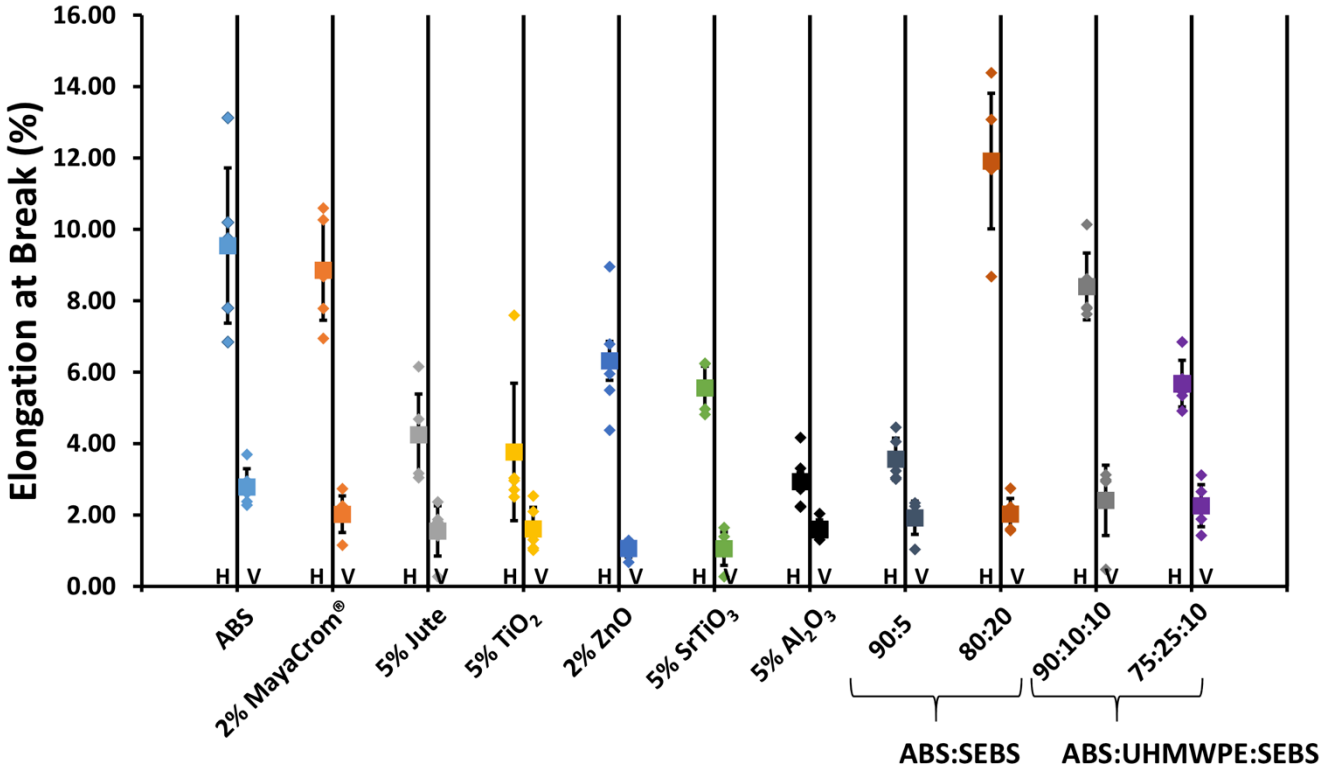

Figure 4.4: Graphical representation of the anisotropy of %EL values for the materials tested in this study. Here H corresponds to horizontal (XYZ) build orientation and V corresponds to vertical (ZXY) build orientation. The large square represents the mean of each sample pool.

4.3.1. ABS

Electron micrographs taken from the fracture surfaces of representative mechanical testing specimens printed in both the horizontal (XYZ) and vertical (ZXY) directions are presented for comparison in Figure 4.5. As discussed in Torrado *et al*. [1], ABS exhibits a completely ductile fracture mode indicated by a large amount of plastic deformation on the fracture surface resulting in the manifestation of sharp ridges, which are characteristic of craze cracking. The large amount of deformation indicates that there was material flow prior to rupture.

It can be observed from the micrograph of an ABS tensile sample printed in the ZXY direction seen in Figure 4.5 that a robust adhesion between print raster layers was achieved as indicated by the large fracture surface area that manifested upon failure in comparison with the void volumes (sparsity) between rasters. The formation of cusps ranging in diameter from 5 to 50μm manifested during the fracture process and are characteristic of rupture occurring within the interlayer bond between print rasters which is a

different mode of failure as compared to samples printed in the XYZ direction where rupture occurred within the bulk material.

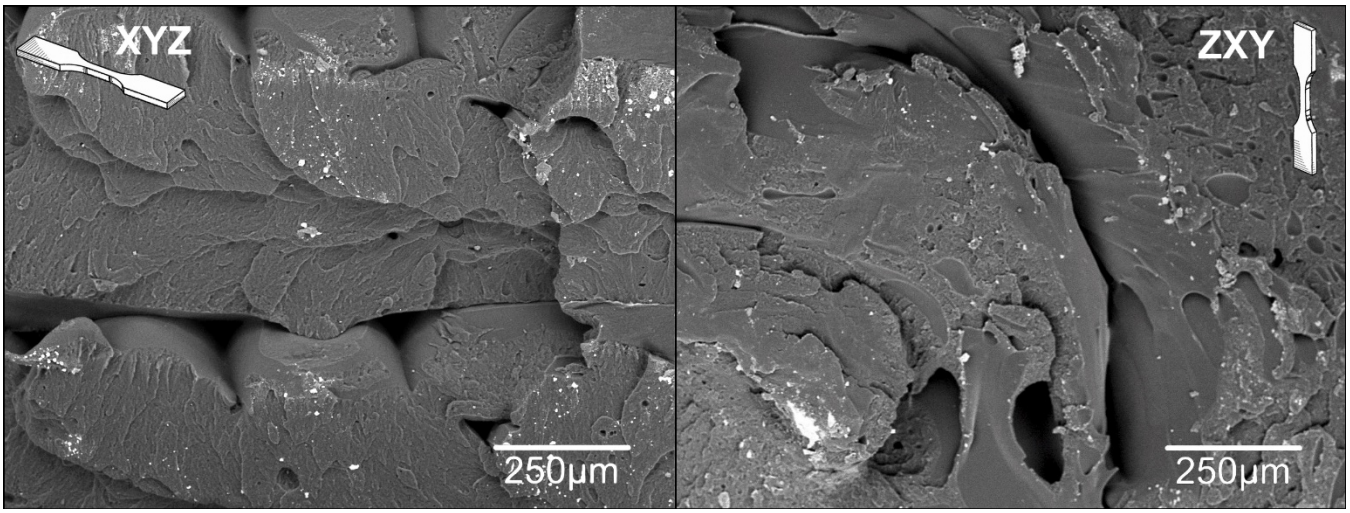

Figure 4.5: Fracture surfaces of ABS specimens in the XYZ print orientation sample and ZXY print orientation

4.3.2. ABS/Jute Composite

Tensile specimens printed in the XYZ build orientation (Figure 4.6) from the ABS/jute composite presented a brittle fracture mode in which the filament possessed a high number of voids in the cross-section. As has been explained elsewhere [1], the high temperatures during both extrusion processes (filament processing and extrusion deposition during printing) caused the decomposition of the jute fiber. The gases generated during the decomposition process remained trapped inside the filament leading to the formation of voids, which remained after the printing process was complete, reducing the effective cross-section of the specimens and diminishing the ultimate tensile strength of the material. In addition to lowering the effective cross-sectional area, the discontinuities acted as stress concentrators, which aided in the failure of the specimens.

As mentioned previously, the voids observed on the fracture surfaces of the ABS/jute composite printed in the XYZ direction manifested as a result of combustion process due to the high temperatures endured by jute plant fiber within the composite. In the case of the ZXY (Figure 4.6) printed samples, this process led to a unique failure mode in which the rupture of the specimen occurred within the individual

print raster meaning that the bulk material was weaker than the interlayer adhesion between the printed layers. The fracture surface is essentially the longitudinal cross section of a print raster which was riddled with voids as has been explained by Torrado *et al*. [1]. In addition to creating a unique fracture surface morphology, the UTS of the ABS/Jute composite was also compromised by the voids and led to values of 8.63 ±3.59 MPa as compared to 17.73 ±2.52 MPa for ABS samples printed in the same orientation.

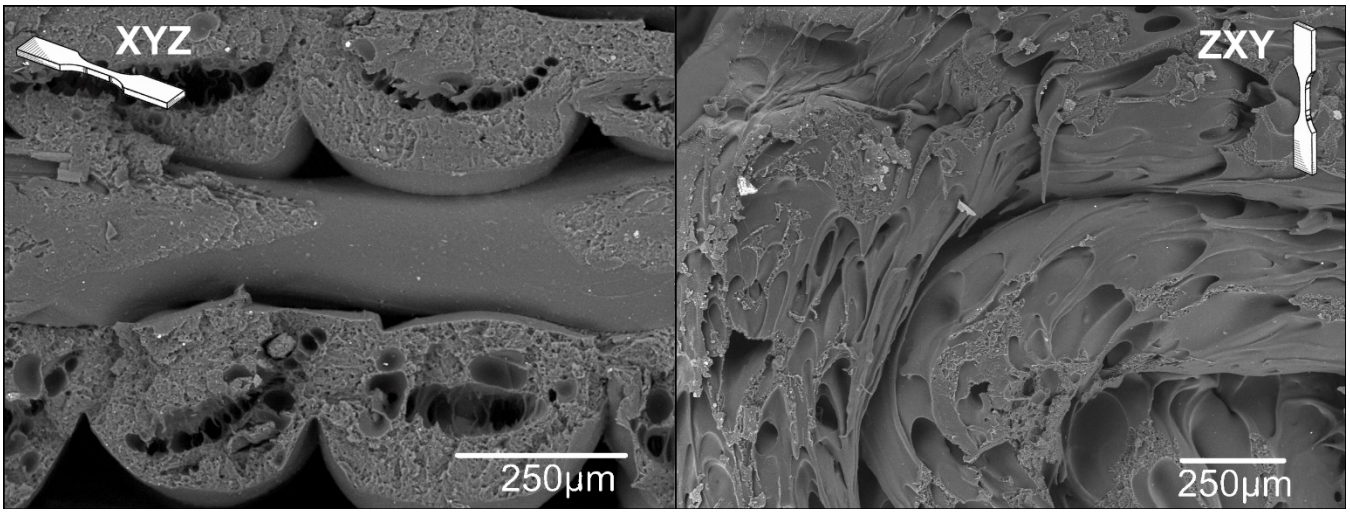

Figure 4.6: Fracture surfaces of specimens fabricated from an ABS/Jute composite in the XYZ print orientation sample and ZXY print orientation. Note the ZXY oriented sample has failed within the print raster.

4.3.3. ABS/MayaCrom® Blue Composite

The compound of ABS with 2% by weight MayaCrom® Blue (essentially a polymer organonanoclay nanocomposite) displayed the lowest absolute difference of the composite materials tested here in terms of UTS when comparing samples printed in the vertical and horizontal orientations (9.52 ±2.66 MPa). The %EL of tensile specimens printed in the XYZ orientation from this composite was also greatest of all the composite materials tested in this study (8.86 ±1.4%), however this value is not significantly greater than the amount of plastic deformation endured by the ABS specimens (8.6 ±3.3%).

The fracture surfaces of samples printed in the XYZ plane from the ABS/MayaCrom® Blue nanocomposite (Figure 4.7) exhibited a brittle fracture mode similar to the jute fiber system. MayaCrom® Blue is blue in color due to the presence of indigo (a plant derived pigment) and the similarity in fracture surface morphology to that of the jute system is potentially due to the indigo component of the pigment

decomposing in a similar fashion as the jute plant fiber. The deposited filament also exhibited a large amount of interior voids in the cross-section, which were more dispersed as compared to the jute fiber composite. The morphology of the MayaCrom® Blue pigment is that of a powder rather than the fiber nature of the jute additive which leads to a different dispersion behavior within the polymer matrix; facilitating the generation of isolated pockets of gas, leading to a more diffuse distribution of the voids within the print rasters.

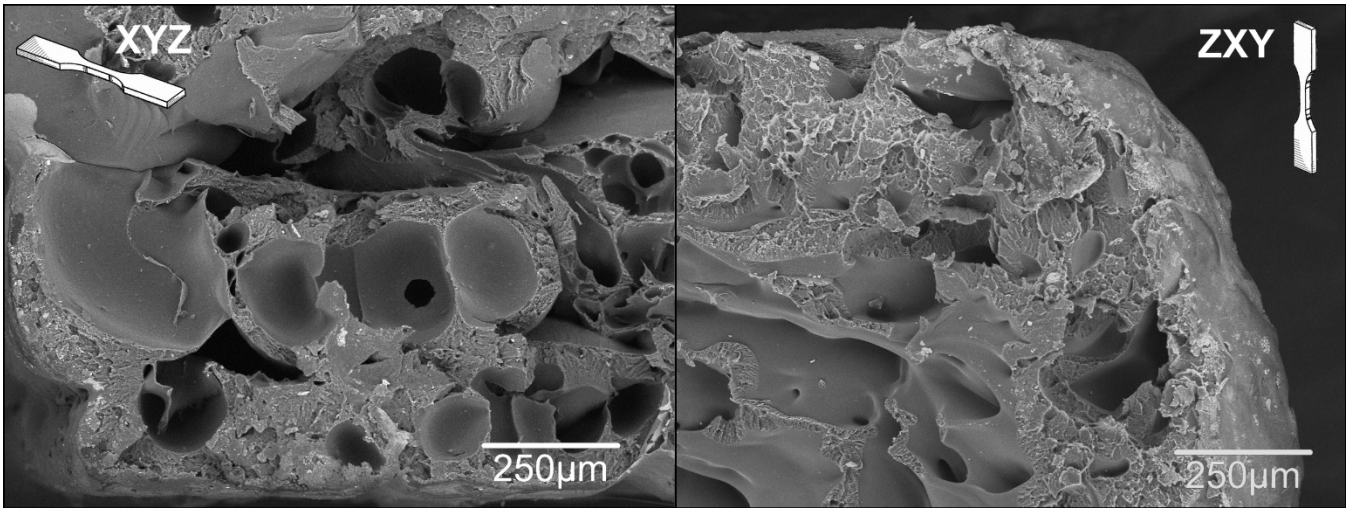

Figure 4.7: Fracture surfaces for the ABS/MayaCrom® Blue composite for both the XYZ and ZXY build orientations. Note the presence of large cup-like cusps indicative of rapid crack propagation.

Specimens printed in the ZXY build orientation from the ABS/MayaCrom® Blue nanocomposite exhibited a similar fracture mode (Figure 4.7) to that observed on the fracture surfaces of ABS/jute plant fiber composite specimens, but the increased dispersion of the voids generated led to a larger area of the fracture surface to be dominated by failure of the interface between layers, however the UTS values of the ZXY oriented samples were statically similar to those of the ABS/Jute composite samples (7.79 ±2.61 MPa).

4.3.4. ABS/TiO_2 Composite

Compounding TiO_2 with ABS led to the greatest UTS values as compared to the other PMCs and polymer blends tested in this study for samples printed in both the horizontal and vertical directions (UTS of 32.9 ±1.4 and 16.7 ±3.2 MPa respectively), however, as compared to samples printed from the base

ABS resin, the UTS values were slightly lower for samples printed in both orientations. In terms of absolute difference in UTS between print orientations, the ABS/TiO_2 composite was virtually equal to ABS (16.23 ±3.07 MPa for ABS compared to 16.22 ±3.53 MPa for the ABS/TiO_2 composite), but the relative difference in UTS was slightly higher than that of samples printed from ABS (49.32 ±9.78% for the ABS/TiO_2 composite compared to 47.79 ±7.23%) though not in a statistically significant manner. In terms of %EL, samples printed from the ABS/TIO_2 blend in the XYZ build orientation underwent less plastic deformation prior to failure as compared to samples printed from ABS (3.77 ±1.93% for the ABS/TiO_2 composite compared to 8.6 ±3.35%), but the absolute and percent (relative) difference in %EL between horizontally and vertically printed samples was lower than ABS. However, the absolute and relative differences were not statically significantly different as seen in Table 4.5.

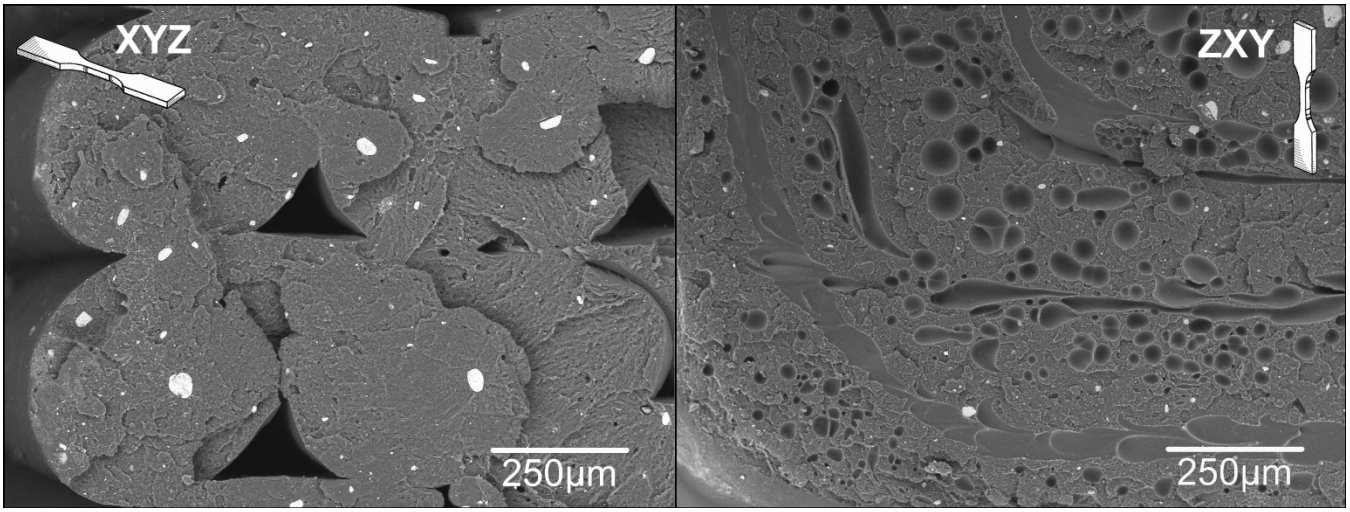

Figure 4.8: SEM micrographs of the fracture surfaces of the ABS/TiO_2 composite for both XYZ and ZXY build orientations. Note the presence of large conglomerates of TiO_2 within the ABS matrix.

The addition of TiO_2 did little to alter the fracture morphology as compared to ABS, which agrees well with the numerical results. The most notable difference is that the fracture surface is riddled by conglomerated masses of TiO_2, in diameters of ~50μm (Figure 4.8). While the addition of TiO_2 nanoparticles would typically result in an increase in tensile strength, the agglomerated particles essentially acted as stress concentrators which decreased the amount of deformation the material could withstand prior to failure. The presence of these stress concentrators lowered the UTS values observed for

this composite as compared to ABS (32.90 ±1.43 MPa for this composite as compared to 33.96 ±1.94 MPa for ABS) although, the difference is not statically significant. It should be noted that there was no functionalization of the additives tested in this study prior to compounding. Subsequent work by Roberson *et al*. [28] has demonstrated a decrease in agglomerate size and an increase in particle dispersion as a result of the functionalization of TiO_2 particles prior to compounding.

The specimens printed in the ZXY orientation from the ABS/TiO_2 composite exhibited a similar fracture mode to the specimens printed from ABS alone as revealed by SEM analysis (Figure 4.8). The presence of the metal oxide particles within the matrix did not seem to have had an effect on the interlayer adhesion between print rasters, however their presence led to the control of the formation of the microvoids observed on the fracture surface as they are of a more constant diameter and in greater number than those observed on the ZXY oriented ABS fracture surface as seen in Figure 4.5. The microvoids are the result of craze cracks whose growth was arrested by the particles.

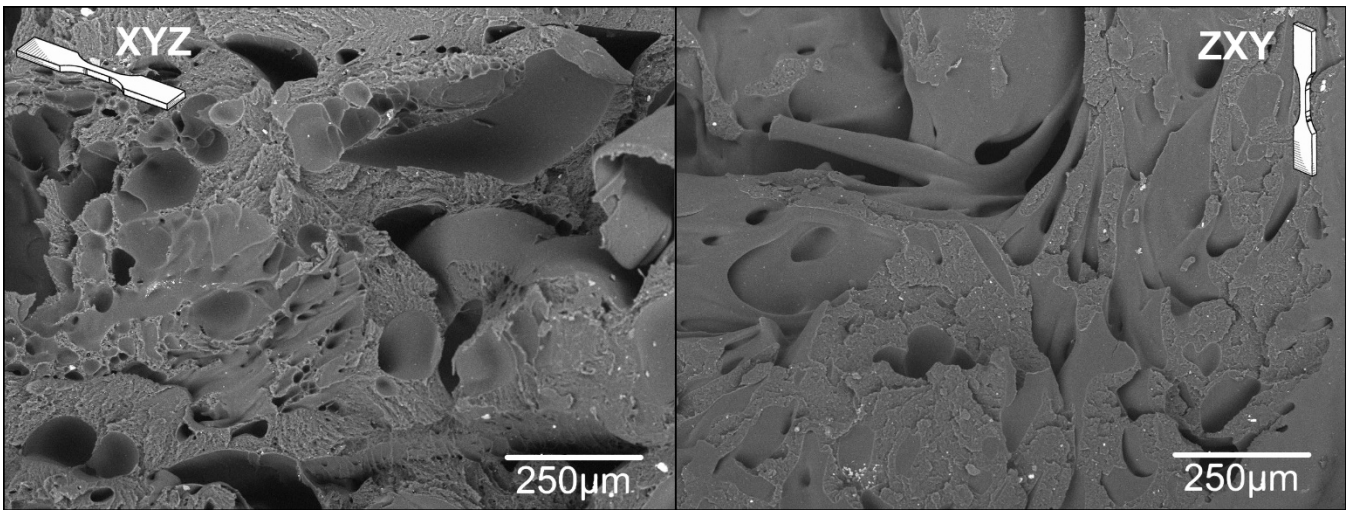

Figure 4.9: Fracture surfaces of the ABS/ZnO composite from representative samples of the XYZ and ZXY build orientations. Note the microvoids within the polymer matrix as indicated by the white arrows. ABS/$SrTiO_3$ Composite

4.3.5. ABS/ZnO Nano-rod Composite

Representative fracture surfaces of the ABS/ZnO composite sample sets (Figure 4.9) exhibited features indicative of a brittle fracture mode as compared to the morphology of the fracture surfaces of the ABS base resin. Key notable characteristics of this composite were the presence of microvoids

(highlighted by white arrows) as well as a greater surface area of smooth material. These features were not observed in the case of the ABS samples. The presence of the microvoids and evidence of a more brittle fracture mode agree well with the decrease in UTS values (20.70 ±0.55 MPa as compared to 33.96 ±1.74 MPa for ABS). In terms of mechanical property anisotropy, the ABS/ZnO composite produced the second highest relative difference between ZXY and XYZ specimens (64.2%). It should be noted that the ABS/ZnO composite was one of only two material systems tested here that possessed statically significantly lower %EL values for ZXY oriented specimens when comparing tensile test results to ABS (1.07 ±0.24% compared to 2.08 ±0.55% for ABS) meaning that the addition of ZnO may have compromised the interlayer adhesion properties between print rasters.

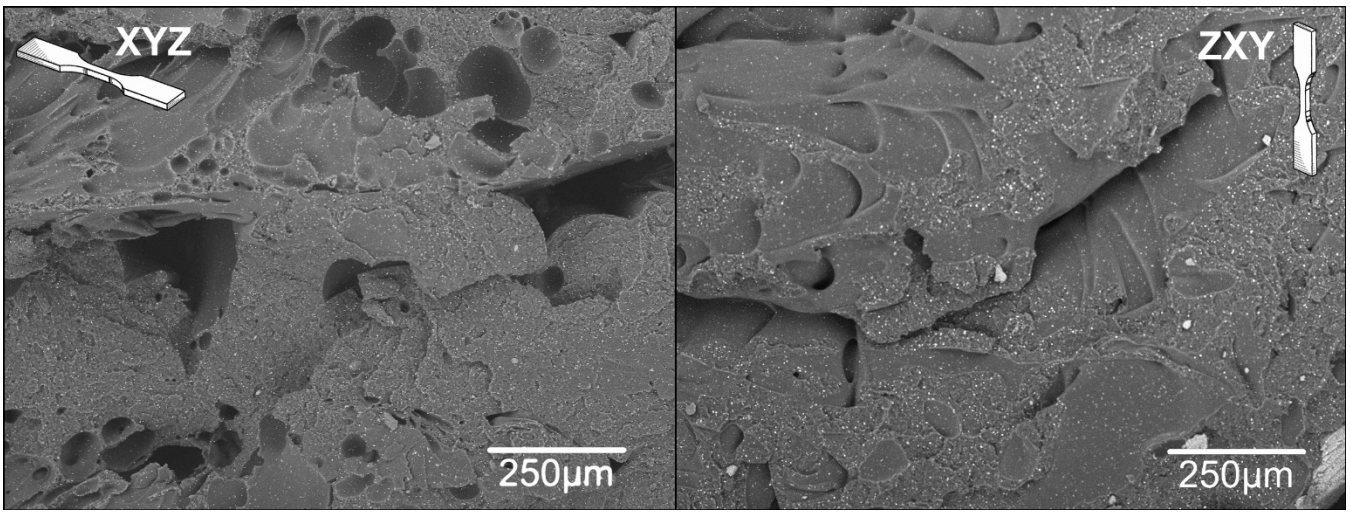

Figure 4.10: Fracture surfaces of the ABS/$SrTiO_3$ composite from representative samples of the XYZ and ZXY build orientations. Note the microvoids within the polymer matrix as indicated by the white arrows.

Examination of the fracture surface of samples printed from the $SrTiO_3$ composite material (Figure 4.10) displayed a fracture surface morphology indicative of a brittle mode failure and the presence of microvoids (indicated by white arrows) was also observed. As was the case with ZnO composite, the microstructure of the material led to an overall decrease in strength as compared to samples printed form the ABS base resin. The UTS values for the $SrTiO_3$ were comparable with those of the ZnO composite and the similarity is most likely due to the corresponding microsctrual characteristics. The relative difference in UTS between the vertical and horizontal samples printed from this composite material was

72.46 ±28.28% making it the poorest performing material in terms of mechanical property anisotropy. Another similarity between the ABS/$SrTiO_3$ composite and the ABS/ZnO composite was the poor performance in terms of %EL as compared to ABS. The ABS/$SrTiO_3$ composite was the other material system in this study to possess %EL values statically significantly lower than ABS for samples printed in the ZXY direction (1.06 ±0.047% compared to 2.08 ±0.55% for ABS) again indicating that this additive potentially lowered the strength of adhesion between print rasters.

4.3.6. ABS/Al_2O_3 Composite

The addition of Al_2O_3 produced a fracture surface with the highest level of plastic deformation of all the inorganic additive composites. As can be seen in Figure 4.11, the morphology of the fracture surface is dominated by crests. Also notable is the presence of microvoids (highlighted by white arrows). The presence of microvoids along with the potential of the Al_2O_3 particles to act as stress crack initiation sites led to a decrease of UTS values (28.8 ±2.62 MPa for the XYZ sample set and 12.14 ±4.82 MPa for the ZXY sample set) as compared to ABS. When comparing the anisotropy of strain values (%EL) between build orientations, ABS compounded with 5% by weight Al_2O_3 exhibited the lowest values of both absolute (%EL of 1.34 ±0.77) and relative percentage (45.7 ±13.3%).

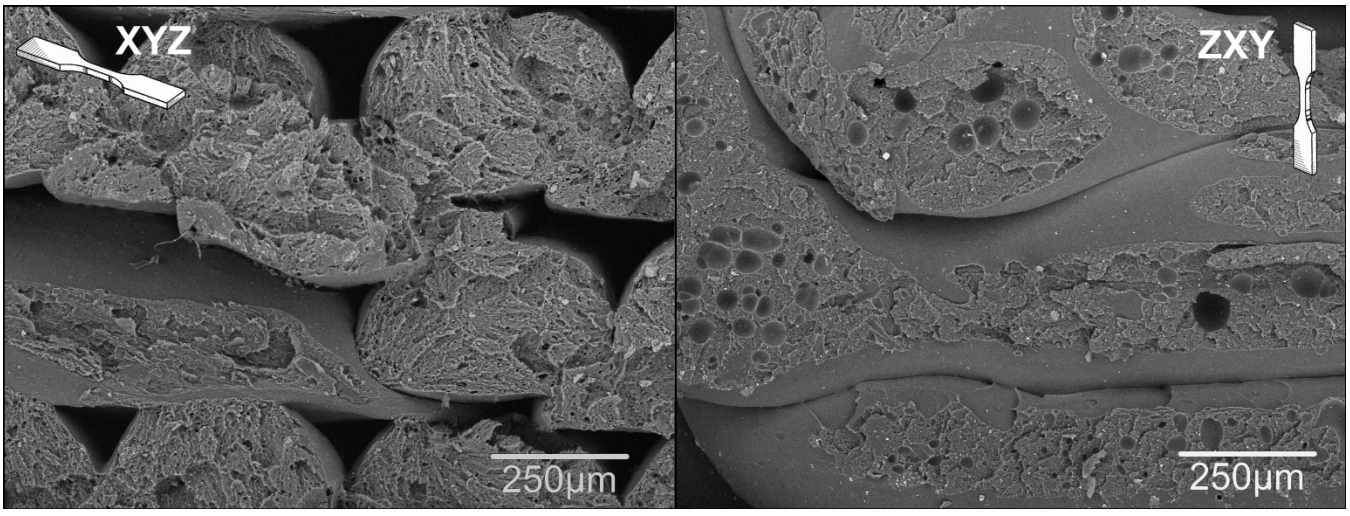

Figure 4.11: SEM micrographs of the fracture surfaces from representative samples of the ABS/ Al_2O_3 composite printed in the XYZ and ZXY build orientations. Note the microvoids within the polymer matrix as indicated by the white arrows.

4.3.7. ABS/SEBS Blends

Samples printed from the ABS/SEBS polymer blends, in the XYZ direction, exhibited a ductile fracture with the greatest amount of plastic deformation of the materials tested in this study. The fracture surfaces are characterized by the manifestation of fibrils. For the 95:5 by weight rato of ABS:SEBS blend (Figure 4.12) the print raster deformed to the point where a bottleneck-like feature was created. At the center of the necked area, a morphology dominated by the presence of fibrils was observed. Figure 4.13 demonstrates the ductile fracture mode observed for the 80:20 by weight ratio ABS:SEBS polymer blend which exhibited an even greater level of plastic deformation due to the higher concentration of SEBS; a thermoplastic rubber.

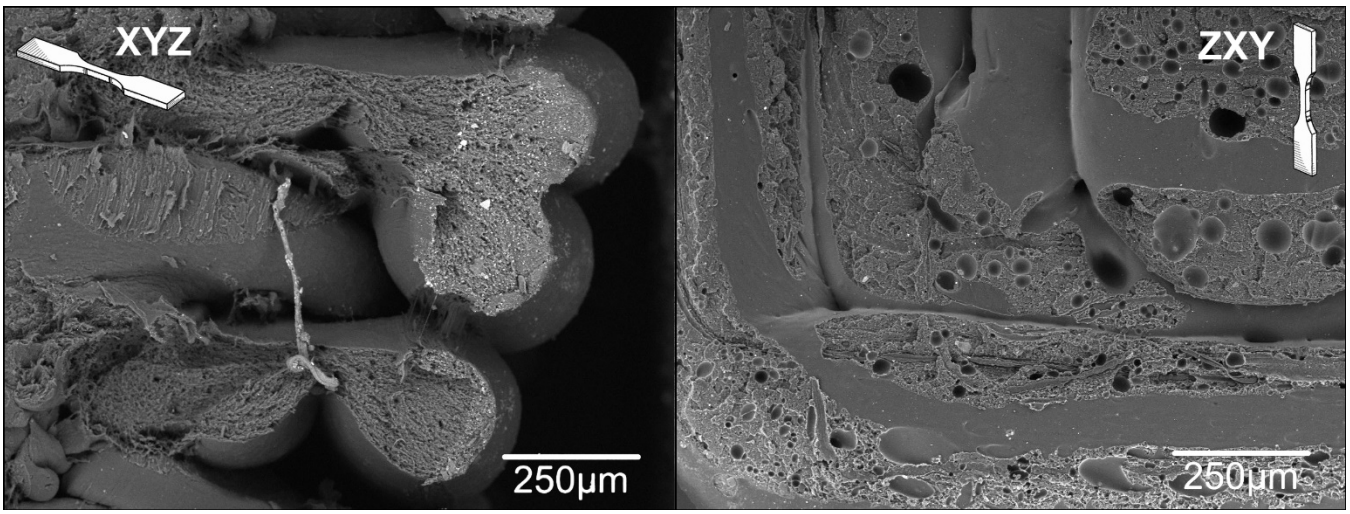

Figure 4.12: SEM micrographs of the fracture surfaces from representative samples of the 95:5 by weight ratio ABS:SEBS blend printed in the XYZ and ZXY build orientations. Note the bottleneck feature indicative of a larger amount of plastic deformation on the XYZ sample.

The polymer blend of 95:5 by weight ratio ABS:SEBS possessed the second lowest values pertaining to strain isotropy of the materials tested in this study with an absolute difference in %EL of 1.64 ±0.75% and relative difference of 46.07 ±13.51%, values which are virtually the same as those reported for the ABS/Al_2O_3 composite. Blending ABS with 5% by weight SEBS did not greatly affect the fracture morphology of specimens printed in the ZXY direction (Figure 4.12) as compared to ABS, however increasing the SEBS concentration to 20% by weight SEBS altered the fracture morphology to a mixed fracture mode where the smooth areas are indicative of rapid crack propagation (Figure 4.13) mixed

with regions of high plastic flow. The large smooth areas on the fracture surface indicate a more brittle mode fracture and is somewhat misleading due to the higher ductility of this material as compared to ABS alone. Though the fracture morphology agrees well with the numerical results for tensile testing, it is the result of poor interlayer adhesion between print rasters rather than a lack of material ductility.

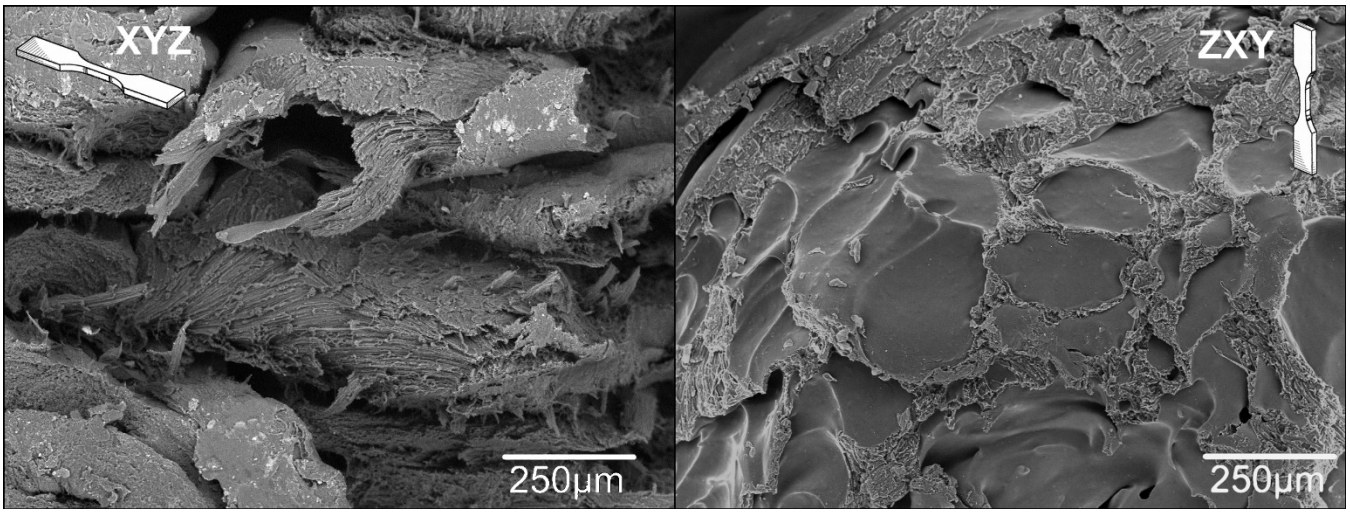

Figure 4.13: SEM micrographs of the fracture surfaces from representative samples of the 80:20 by weight ratio ABS:SEBS blend printed in the XYZ and ZXY build orientations. Note the large amount of smooth area on the ZXY specimen indicating rapid crack propagation.

4.3.8. ABS:UHMWPE:SEBS Blends

The third lowest %EL (strain) anisotropy values reported here were observed in test data obtained from samples printed from the 75:25:10 blend of ABS:UHMWPE:SEBS as these values were 3.4 ±0.88% absolute difference and 60.2 ±17.12% relative difference. Fracture surface analysis of samples printed from ABS:UHMWPE:SEBS blends in the XYZ direction revealed information about the effectiveness of blending the three polymeric materials together as it was observed that this system was essentially a polymer/polymer composite of UHMWPE particles with sizes from 50 to 150um of diameter, embedded in an ABS/SEBS matrix.. The fracture surfaces in the matrix region displayed characteristics indicating ductile mode fracture (namely, fibrils) however, there are distinct spheroids dispersed within the matrix. Characterization performed by Rocha *et al*. [25] confirmed these spheroids to be UHMWPE particles

which did not blend with ABS and SEBS during the compounding process. Deformed voids of the same dimensions can be observed where more UHMWPE particles were located were then dislodged during the tensile testing process (indicated by white arrows in Figure 4.14).

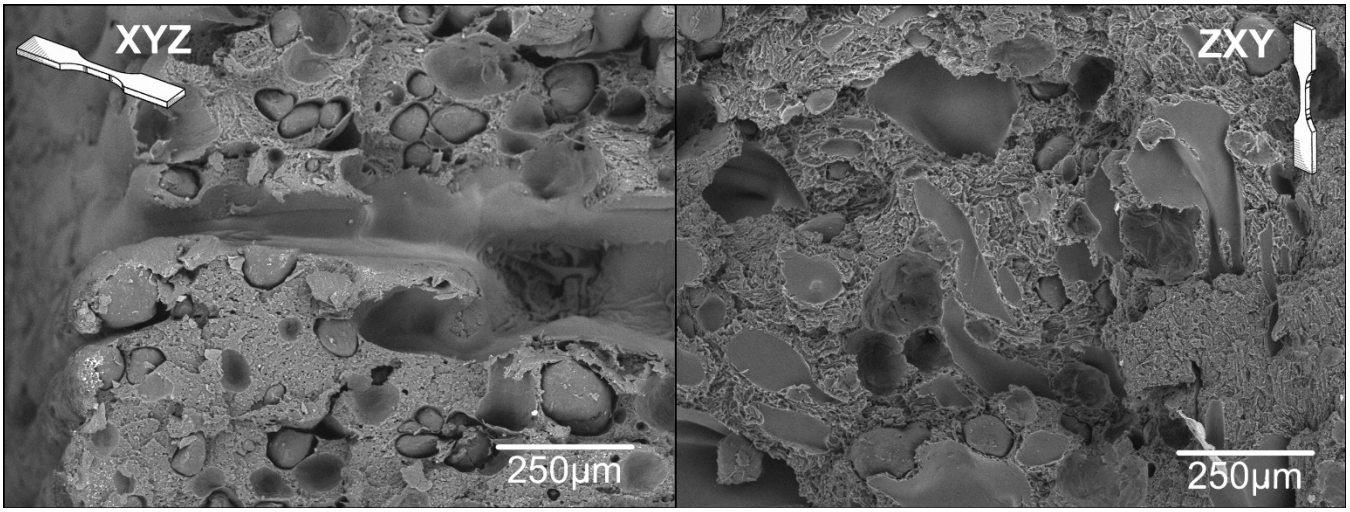

Figure 4.14: SEM micrographs of the fracture surfaces from representative samples of the 90:10:10 by weight ratio ABS:UHMWPE:SEBS blend printed in the XYZ and ZXY build orientations. The large particles are undissolved UHMWPE and the craters (indicated by white arrows) are sites where the particles became dislodged during mechanical testing.

Overall, the polymer blend of 75:25:10 by weight ratio ABS:UHMWPE:SEBS produced the lowest relative and absolute anisotropic values as compared to ABS. While, compared to ABS, there is a steep reduction in the UTS of horizontally (14.7 ±0.6 MPa) and vertically (11.5 ±1.0 MPa) printed tensile test specimens, both the relative (22.02 ±2.07%) and absolute difference (3.42 ±0.88 MPa) between horizontal and vertical strength are the lowest values presented in this study in terms of the difference in UTS based on build orientation.

The specimens printed from this ternary blend (75:25:10 ABS:UHMWPE:SEBS) presented a very homogeneous fracture surface with undiscernible interfaces between the rasters (Figure 4.15). Essentially, there is an intermingling with a given print layer with subsequent layers leading to a more solid microstructure with little to no air gap (sparsity) between print layers. The particles of UHMWPE can be seen along with the voids of particles which were dislodged during the mechanical testing process within a matrix of ABS and SEBS which underwent a high amount of plastic deformation. The similarity between

the fracture morphology and material microstructure observed on fracture surfaces for specimens printed on both the XYZ and ZXY directions along with the better adhesion and blending of the rasters, are due to the rheological differences of the ternary blend as compared to the other material systems evaluated here.

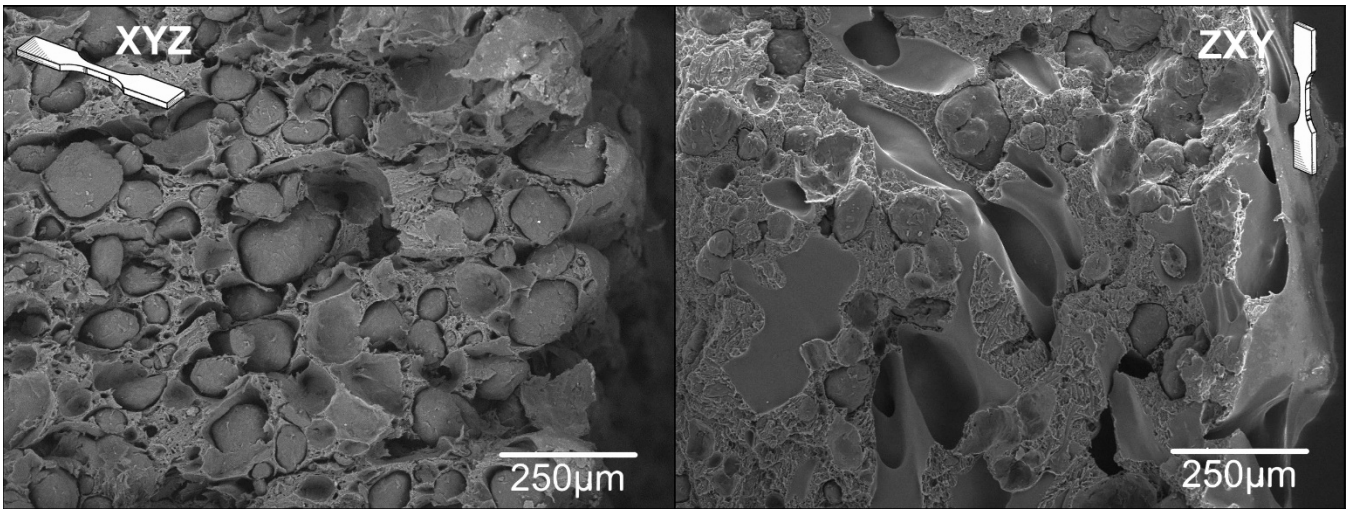

Figure 4.15: SEM micrographs of the fracture surfaces from representative samples of the 75:25:10 by weight ratio ABS:UHMWPE:SEBS blend printed in the XYZ and ZXY build orientations. Note the blending of material between print rasters for both build orientations.

Of particular pertinence to the goal of this paper —the decrease in build orientation-caused mechanical property anisotropy— is the 75:25:10 ABS:UHMWPE:SEBS blend. As noted earlier, though the tensile strength is diminished as compared to ABS, the difference in mechanical property anisotropy based on build orientation was the lowest as compared to ABS and the other material systems tested in this study. As shown by Rocha et al., [25] there is little distinction between raster layers, which is an indication of the different rheological properties of this blend as compared to ABS. The difference in the way the material flows alters the interface between print layers. Further evaluation of the 75:25:10 ABS:UHMWPE:SEBS blend via dynamic material analysis (DMA) revealed the ternary blend to have a complex viscosity of 27.92 MPa·sec as compared to 80.21 MPa·sec for ABS at 40 °C. Both materials were tested at 100Hz with a TA Instruments DMA (Model Q 800, TA Instruments, New Castle DE, USA). Further analysis via DMA of ABS and the 75:25:10 ternary blend revealed that the ternary blend is more reactive to an increase in temperature than ABS; at 100°C the complex viscosity decreased by 15.85% to

67.47 MPa·sec for ABS while the ternary blend experienced a 23.03 % drop in complex viscosity to 21.49 MPa·sec at the same temperature. The glass transition temperature ($T_{g)}$ of both materials was also determined from plots of storage modulus vs. temperature derived from DMA analysis at 100 Hz and it was found that the ABS used in this study had a T_g of 112.62 °C and the ternary blend had a T_g of 115.47 °C. DMA Analysis at 140 °C (above the T_g of both materials) reveals the ternary blend to still be less viscous than ABS (0.21 MPa·sec for ABS as compared to 0.17 MPa·sec for the ternary blend). Results of DMA testing are tabularized in Table 4.6.

Table 4.6: Results of DMA analysis from selected material systems.

	ABS			ABS:UHMWPE:SEBS 75:25:10		
Temperature (°C)	40	100	140	40	100	140
Storage Modulus (MPa)	1511.00	1349.00	*	530.40	436.10	*
Complex Viscosity (MPa·sec)	80.21	67.49	0.21	27.92	21.49	0.17
Glass Transition Temperature (°C)		112.62			115.47	

The higher propensity to flow is a key aspect which drives the ability of the ternary 75:25:10 blend to produce parts with a more homogenous microstructure which obscures the raster layers as observed under SEM. Rocha *et al*. [25] noted the rheological differences of this ternary blend also led to the printing of smoother inclined planes as compared to ABS due to the greater propensity of the ternary blend to spread out during the printing process. The lack of distinction and air gap between print rasters led to a decrease in the mechanical property anisotropy when comparing tensile specimens printed in the XYZ and ZXY directions. A critical finding of the results presented above is, that for the 75:25:10 ABS:UHMWPE:SEBS blend which exhibits a smaller difference in UTS values when comparing the ZXY and XYZ build orientations, there is an obscuring of the print rasters caused by the individual material properties which alters the mode of failure. The altering of the failure mode leads to a decrease in mechanical property anisotropy as the failure becomes less dependent upon the printing process and more dependent on the bulk material properties. It should be noted that here the difference in failure mode decreased anisotropy where in the case of the ABS/jute composite this was not the case as here, the

material was altered in a way that it was substantially weaker in the ZXY orientation than in the XYZ orientation whereas in the case of the ternary blend, the material was made to be weaker in both directions.

4.4. Summary and Conclusions

The mechanical property anisotropy associated with build direction is an issue that manifests in virtually all 3D printing technologies. Here, the effort to mitigate this problem centered around understanding the effect of various additives to ABS on the resulting mechanical property anisotropy. A total of six ABS-based polymer matrix composites and four polymer blends tested in terms of mechanical property anisotropy where the metric was the UTS of samples printed in the XYZ and ZXY build orientations.

Of the material systems tested here, ABS blended with UHMWPE and SEBS at a 75:25:10 (by weight) ratio demonstrated the lowest mechanical property anisotropy in terms of UTS (a relative difference of 22.02 ±2.07%) while samples printed from ABS demonstrated a greater difference in UTS between XYZ and ZXY (47.79 ±7.23%). However, the reduction of mechanical property anisotropy for the ternary blend came at the expense of UTS as the samples printed from the ternary blend possessed UTS values of 14.70 ± 0.63 MPa and 11.47 ± 0.96 MPa for samples printed in the XYZ and ZXY directions respectively whereas specimens printed from the same ABS base resin alone demonstrated UTS of 33.96 ± 1.74 MPa and 17.73 ± 2.52 MPa for samples printed in the XYZ and ZXY build orientations.

In terms of the % elongation to break, the polymer matrix composite of ABS compounded with 5% by weight Al_2O_3 exhibited the lowest relative difference at 45.68 ±13.30%. Also near this value of % difference was the binary blend of ABS mixed with 5% by weight SEBS (46.07 ±13.51%). In most cases, the blending of ABS with a reinforcing agent had a detrimental effect on the %EL at break while blending with SEBS in an 80:20 by weight ratio led to an improvement to the amount of elongation tensile specimens printed in the XYZ endured prior to rupture, though this amount was not statically significantly greater than specimens printed in the same orientation from ABS.

The work presented here was performed to determine what material properties are relevant to anisotropy. In particular, the work was done to determine the impact of composite loading on interlayer adhesion and material rheology. The results in turn show a relationship between complex viscosity and

anisotropy. Specifically, this work shows a lower complex viscosity above T_g would improve anisotropy by creating a stronger layer-to-layer bond (failure occurs in the raster and not at the raster-raster boundary) and increased surface area contact between layers. Thus the ABS:UHMWPE:SEBS ternary polymer blend shows the greatest promise for improving anisotropy by exhibiting failure mechanisms within a printed raster, and not the raster-raster boundary. The development of this ternary blend will be further explored and potentially lead to future material systems compatible with ME3DP that are immune to build orientation-caused mechanical property anisotropy.

4.5. Supplemental Information

Supplemental information related to this study consists of representative stress-strain plots of the materials tested here. The plots, seen in Figures 4.16 and 4.17, were generated by a MatLab program and are composite graphs of each sample's stress-strain plot for a given sample pool. The process for creating these plots is described in more detail in Torrado *et al*. [1]. Also included here are DMA plots. Figures 4.18 and 4.19 are representative DMA plots illustrating the calculation of glass transition temperature for the selected materials analyzed here.

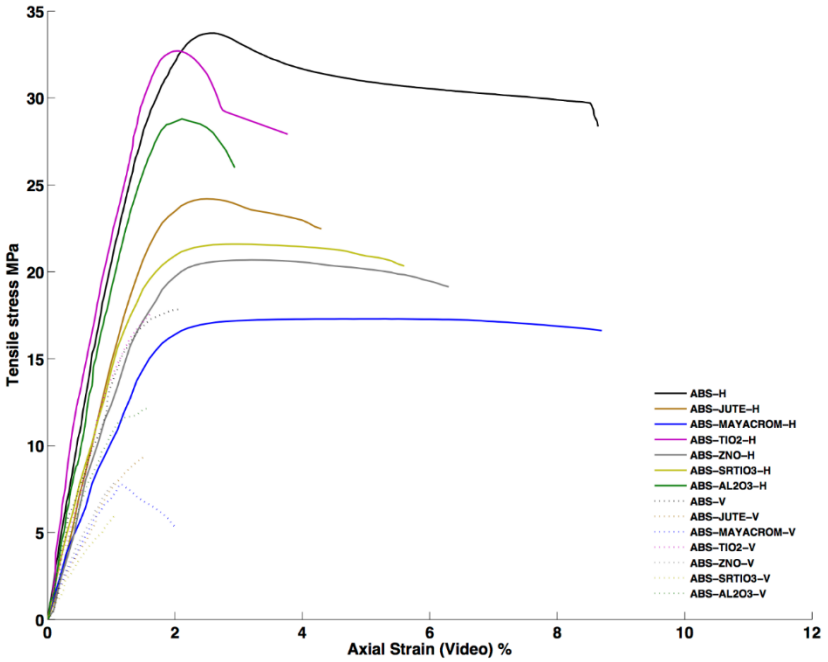

Figure 4.16: Composite stress strain plots for all the polymer matrix composites tested in this study compared to ABS where (H) indicates horizontal or XYZ build orientation and (V) indicates vertical or ZXY build orientation.

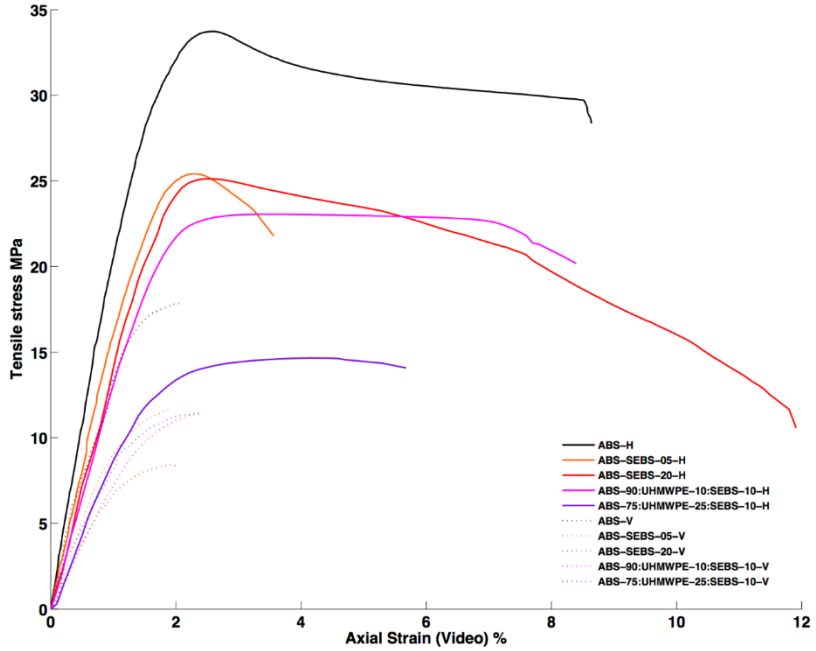

Figure 4.17: Composite stress strain plots for all the polymer blends tested in this study compared to ABS where (H) indicates horizontal or XYZ build orientation and (V) indicates vertical or ZXY build orientation.

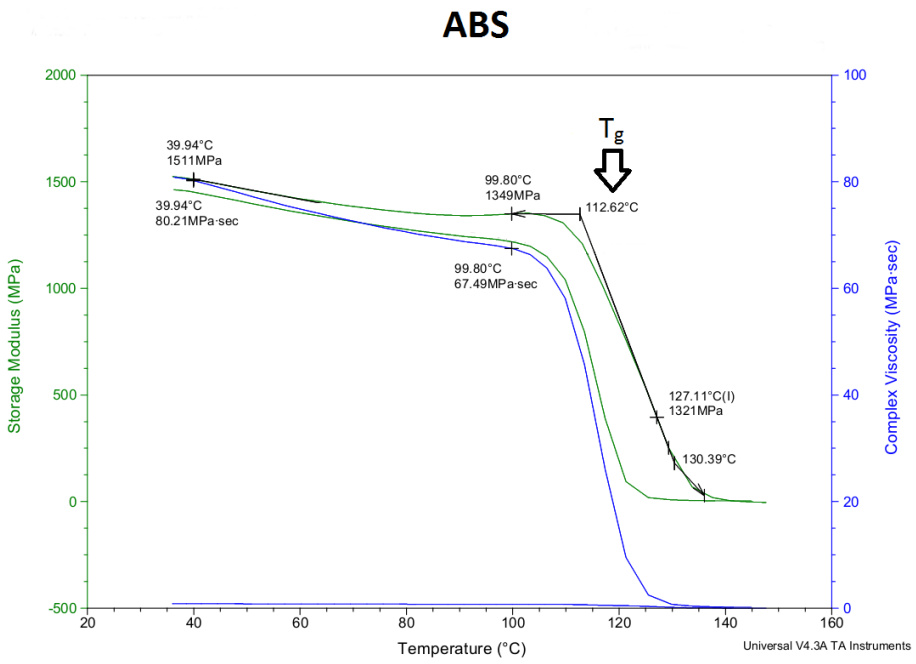

Figure 4.18: DMA plot of ABS where the glass transition temperature (T_g) is determined by tangential plots of slope differences in the storage modulus curve.

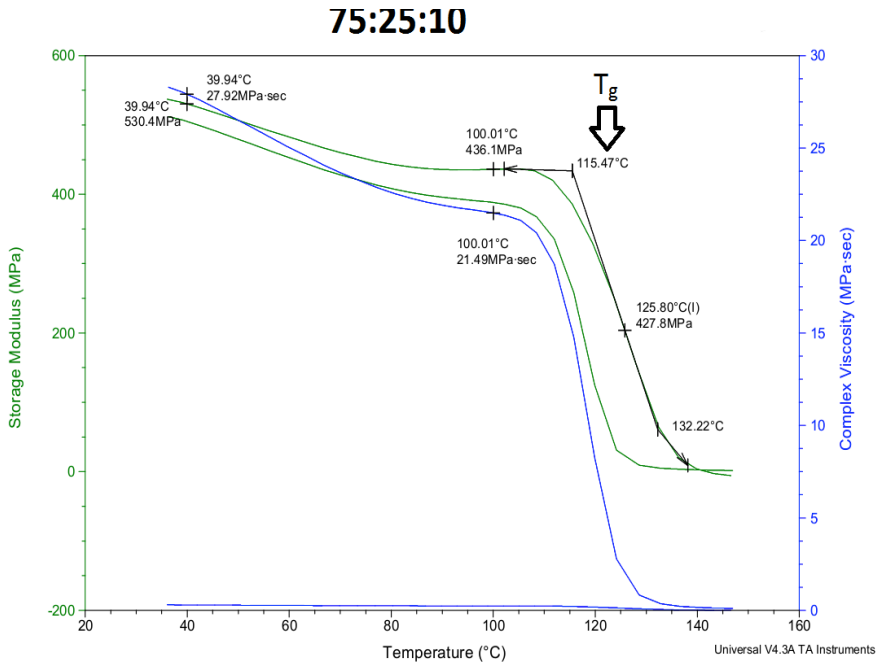

Figure 4.19: DMA plot of ABS the 75:25:10 ABS:UHMWPE:SEBS ternary polymeric blend where the glass transition temperature (T_g) is determined by tangential plots of slope differences in the storage modulus curve.

4.6. References

[1] A.R.Torrado-Perez, D.A. Roberson, R.B. Wicker, Fracture Surface Analysis of 3D-Printed Tensile Specimens of Novel ABS-Based Materials, J Fail. Anal. and Preven. 14 (2014.) 343–353. doi:10.1007/s11668-014-9803-9.

[2] S.-H. Ahn, M. Montero, D. Odell, S. Roundy, P.K. Wright, Anisotropic material properties of fused deposition modeling ABS, Rapid Prototyping Journal. 8 (2002) 248–257. doi:10.1108/13552540210441166.

[3] A. Bellini, S. Güçeri, Mechanical characterization of parts fabricated using fused deposition modeling, Rapid Prototyping Journal. 9 (2003) 252–264. doi:10.1108/13552540310489631.

[4] O.S. Es-Said, J. Foyos, R. Noorani, M. Mendelson, R. Marloth, B.A. Pregger, Effect of Layer Orientation on Mechanical Properties of Rapid Prototyped Samples, Materials and Manufacturing Processes. 15 (2000) 107–122. doi:10.1080/10426910008912976.

[5] R. Hague, S. Mansour, N. Saleh, R. Harris, Materials analysis of stereolithography resins for use in Rapid Manufacturing, Journal of Materials Science. 39 (2004) 2457–2464. doi:10.1023/B:JMSC.0000020010.73768.4a.

[6] V. Vega, J. Clements, T. Lam, A. Abad, B. Fritz, N. Ula, et al., The Effect of Layer Orientation on the Mechanical Properties and Microstructure of a Polymer, J. of Materi Eng and Perform. 20 (2011) 978–988. doi:10.1007/s11665-010-9740-z.

[7] A. Bagsik, V. Schoeppner, E. Klemp, FDM Part Quality Manufactured with Ultem* 9085, in: 14th International Scientific Conference on Polymeric Materials, September, 2010.

[8] R. Hague *, S. Mansour, N. Saleh, Material and design considerations for rapid manufacturing, International Journal of Production Research. 42 (2004) 4691–4708. doi:10.1080/00207840410001733940.

[9] Shaffer S, Yang K, Vargas J, Di Prima MA, Voit W, On reducing anisotropy in 3D printed polymers via ionizing radiation, Polymer (2014), doi: 10.1016/j.polymer.2014.07.054.

[10] B. Caulfield, P. E. McHugh, and S. Lohfeld, Dependence of mechanical properties of polyamide components on build parameters in the SLS process, Journal of Materials Processing Technology, 182.1 (2007): 477-488.

[11] Takaichi, Suyalatu, T. Nakamoto, N. Joko, N. Nomura, Y. Tsutsumi, S. Migita, H. Doi, S. Kurosu, A. Chiba, N. Wakabayashi, Y. Igarashi, and T. Hanawa, Microstructures and mechanical properties of Co–29Cr–6Mo alloy fabricated by selective laser melting process for dental applications, Journal of the mechanical behavior of biomedical materials, 21 (2013): 67-76.

[12] L. E. Murr, K. N. Amato, S. J. Li, Y. X. Tian, X. Y. Cheng, S. M. Gaytan, E. Martinez, P. W. Shindo, F. Medina, and R. B. Wicker, Microstructure and mechanical properties of open-cellular biomaterials prototypes for total knee replacement implants fabricated by electron beam melting, Journal of the mechanical behavior of biomedical materials 4.7 (2011): 1396-1411.

[13] L. E. Murr, S. A. Quinones, S. M. Gaytan, M. I. Lopez, A. Rodela, E. Y. Martinez, D. H. Hernandez, E. Martinez, F. Medina, and R. B. Wicker, Microstructure and mechanical behavior of Ti–6Al–4V produced by rapid-layer manufacturing, for biomedical applications, Journal of the mechanical behavior of biomedical materials, 2.1 (2009): 20-32.

[14] M. L. Griffith, D. M. Keicher, C. L. Atwood, J. A. Romero, J. E. Smugeresky, L. D. Harwell, and D. L. Greene, Free form fabrication of metallic components using laser engineered net shaping

(LENS), Proceedings of the Solid Freeform Fabrication Symposium. University of Texas at Austin, 1996.

[15] J.F. Rodrı´guez, J.P. Thomas, J.E. Renaud, Design of Fused-Deposition ABS Components for Stiffness and Strength, J. Mech. Des. 125 (2003) 545–551. doi:10.1115/1.1582499.

[16] S.. Masood, W.. Song, Development of new metal/polymer materials for rapid tooling using Fused deposition modelling, Materials & Design. 25 (2004) 587–594. doi:10.1016/j.matdes.2004.02.009.

[17] M. Nikzad, S.H. Masood, I. Sbarski, Thermo-mechanical properties of a highly filled polymeric composites for Fused Deposition Modeling, Materials & Design. 32 (2011) 3448–3456. doi:10.1016/j.matdes.2011.01.056.

[18] A. Safari, E.K. Akdogan, Rapid Prototyping of Novel Piezoelectric Composites, Ferroelectrics. 331 (2006) 153–179. doi:10.1080/00150190600737727.

[19] M.L. Shofner, K. Lozano, F.J. Rodríguez-Macías, E.V. Barrera, Nanofiber-reinforced polymers prepared by fused deposition modeling, Journal of Applied Polymer Science. 89 (2003) 3081–3090. doi:10.1002/app.12496.

[20] M.. Shofner, F.. Rodrı´guez-Macı´as, R. Vaidyanathan, E.. Barrera, Single wall nanotube and vapor grown carbon fiber reinforced polymers processed by extrusion freeform fabrication, Composites Part A: Applied Science and Manufacturing. 34 (2003) 1207–1217. doi:10.1016/j.compositesa.2003.07.002.

[21] Y. Li, H. Shimizu, Co-continuous Polyamide 6 (PA6)/Acrylonitrile-Butadiene-Styrene (ABS) Nanocomposites, Macromol. Rapid Commun. 26 (2005) 710–715. doi:10.1002/marc.200400654.

[22] B. Majumdar, H. Keskkula, D.R. Paul, Morphology of nylon 6/ABS blends compatibilized by a styrene/maleic anhydride copolymer, Polymer. 35 (1994) 3164–3172. doi:10.1016/0032-3861(94)90117-1.

[23] A. Misra, G. Sawhney, R.A. Kumar, Structure and properties of compatibilized blends of polyamide-6 and ABS, J. Appl. Polym. Sci. 50 (1993) 1179–1186. doi:10.1002/app.1993.070500708.

[24] J.-D. Nam, J. Kim, S. Lee, Y. Lee, C. Park, Morphology and thermal properties of PPS/ABS blend systems, J. Appl. Polym. Sci. 87 (2003) 661–665. doi:10.1002/app.11401.

[25] C. Rocha, A. R. Torrado Perez, D. A. Roberson, C Shemelya, E. MacDonald, R. B. Wicker, Novel ABS-based Binary and Ternary Polymer Blends for Material Extrusion 3D Printing, Journal of Materials Research, 2014, Accepted In press.

[26] Y. Lin, G. Ehlert, H.A. Sodano, Increased Interface Strength in Carbon Fiber Composites through a ZnO Nanowire Interphase, Adv. Funct. Mater. 19 (2009) 2654–2660. doi:10.1002/adfm.200900011.

[27] ASTM D638, Test Method for Tensile Properties of Plastics, ASTM International, (2010)

[28] D.A. Roberson, C.M. Shemelya, R.B. Wicker, E. MacDonald, Expanding the Applicability of FDM-type Technologies through Materials Development, in Proceedings of the 25th Annual Solid Freeform Fabrication Symposium, Austin, TX, August 4-6, 2014.

CHAPTER 5: CHARACTERIZATION OF ABS:UHMWPE:SEBS BLENDS IN TERMS OF ANISOTROPY

5.1. Introduction

The anisotropy in ME3DP is a characteristic still very present in all the parts generated by this methodology, minimally covered in the literature and that still remains unexplained. The works performed by Shaffer, *et al*. [1] or Horn *et al*. [2] were probably among the first ones known to diminish anisotropy, suggesting a modification of the process itself, or addition of some kind of post-processing stage to overcome the problem. The concept proposed by Shaffer is interesting and generates reasonably good results, however the study is specific to PLA and the post-processing solution is costly and time consuming, which reduces one of the main advantages of 3DP. Further investigation in compatibilizers and cross-linker additives that activate under different circumstances other than exposure to radiation is needed. On the other hand, although Horn *et al*. covered part of the effects on the mechanical properties of acetone on the final parts, they didn't study the effects on the anisotropy or more specifically, the effect on the parts fabricated in the direction of layer addition.

The work by Torrado *et al.* [3, 4] aims for the adaptation of the materials to solve the problems of anisotropy. Their previous publications suggest that this solution could come through the development of ternary blends such as those composed by acronitrile butadiene styrene (ABS), ultra high molecular weight polyethylene (UHMWPE) and styrene-ethylene-butylene-styrene (SEBS). Further work in this area is needed indeed, to better understand the characteristics of this specific blend and others. Although the final mechanical properties were worsened, ABS-UHMWPE-SEBS yielded good results in terms of lowering the anisotropy, but the blend has still not been extensively researched. More configurations need to be mapped and the compatibility between the materials further investigated. The works by Rocha *et al*. [8] already mentioned difficulties obtaining filaments with ratios of UHMWPE over the 20% by mass. The analysis of the micrographs performed in those studies for the 90:10:10 and 75:25:10 blends also revealed an insolubility of the UHMWPE within what was essentially a matrix composed of a blend composed of ABS and SEBS in which the first material appears in a globular shape embedded in a matrix blend of the other two materials. Furthermore, the studies comprised in this paper and others performed in parallel

confirmed that a higher processing temperature in the early mixing areas of the barrel diminished the formation of vermicular SEBS embedded on an ABS matrix, leading to a better mixed blend with different mechanical properties. In any case, it remains unclear if an improved blending of the materials would lead to an undesired higher anisotropy in the final results.

The incompatibility between the ABS and the UHMWPE is apparent by the differences in polarity between the two polymers. While polyethylenes are among the most non-polar thermoplastics, ABS is an engineered polymer with a high polarity due to the nitrile groups in its composition [15]. SEBS should serve as a compatibilizer between the two polymers, [9] hence it is surprising to find the UHMWPE so dispersed in a matrix of the other two materials. The use of other compatibilizers, such as maleic anhydride, could lead to a better blending of the ABS and the UHMWPE, as an alternative to processes at higher temperature. Finally, performing several re-extrusions of the same material, or masterbatching them before the final extrusion process could help as well with this goal. The use of maleic-anhydride grafted is as well explored in this study. Maleic-anhydride grafted polymers are very well known and utilized in the industry to facilitate the coupling of olefinic groups in dissimilar materials such as incompatible polymers or organic and inorganic materials for reinforcement or improvement of mechnical properties. It's been used in the past to produce bulk blending between polymers, although the outcome depends highly on the process and usually leads to diverse results. At least, a better adhesion to the matrix could provide an improved resulting composite. [10-15]

5.2. Experimental procedure

In this experiment, two Cycolac™ MG37CR and MG47 Resin acronitrile-butadiene-styrene (ABS) variants (Sabic, Pittsfield, MA, USA) were used as a based material, for comparisons with the previous tests. Two different flavors of styrene-ethylene-butylene-styrene (SEBS) supplied by Kraton were used: a first one in form of undusted powder (A1536 HU SEBS, Kraton, Houston, TX, USA), and a second one grafted with maleic anhydride (from now on MASEBS) as dusted pellet (FG1901 G (SEBS), Kraton, Houston, TX, USA). The ultra-high-molecular-weight-polyethylene (UHMWPE) used was the same for all the blends, supplied by Celeanese (GUR® 1020 UHMWPE, Celeanese, Irving, TX, USA). Five new ABS:UHMWPE:SEBS blends were fabricated using MG47 instead of MG37CR, the non-grafted SEBS

and the UHWMPE to compare with the previous study [4] and cover a broader range of compositions. Then three new ABS:UHMWPE:SEBS blends where produced in order to compare with the best performers of both experiments, but this time using the MASEBS variant (and the corresponding grade of ABS of the best performer). A total of twelve systems were analyzed in this work: Three blends of ABS:UHMWPE:SEBS based on MG37CR and a MG37CR baseline, and seven ABS:UHMWPE:SEBS based on MG47 based on MG47 with the corresponding baseline. The blends presented in this study are listed in Table 5.1 with the corresponding weight proportions for each of the constituents.

Table 5.1: A total of twelve systems are compared in this study:
Ten ABS:UHMWPE:SEBS blends and two ABS baselines.

Blend combinations	Weight percentage		
	ABS	UHMWPE	SEBS
ABS MG37CR	100.0%	0.0%	0.0%
ABS MG37CR (90) : UHWMPE (10) : SEBS (10)	81.8%	9.1%	9.1%
ABS MG37CR (75) : UHWMPE (25) : SEBS (10)	68.2%	22.7%	9.1%
ABS MG37CR (75) : UHWMPE (25) : MASEBS (10)	68.2%	22.7%	9.1%
ABS MG47	100.0%	0.0%	0.0%
ABS MG47 (90) : UHWMPE (10) : SEBS (10)	81.8%	9.1%	9.1%
ABS MG47 (75) : UHWMPE (25) : SEBS (10)	68.2%	22.7%	9.1%
ABS MG47 (75) : UHWMPE (25) : SEBS (50)	60.0%	20.0%	20.0%
ABS MG47 (75) : UHWMPE (25) : SEBS (50)	50.0%	16.7%	33.3%
ABS MG47 (75) : UHWMPE (25) : SEBS (75)	42.9%	14.3%	42.9%
ABS MG47 (75) : UHWMPE (25) : MASEBS (50)	50.0%	16.7%	33.3%
ABS MG47 (75) : UHWMPE (25) : MASEBS (75)	42.9%	14.3%	42.9%

All the new blends were processed using a Dr. Collin Twin Screw Extruder/Compounder Model ZK 25T (Dr. Collin GmbH, Ebersberg, Germany) equipped with a dual system with co-rotating, intermeshing screws. The materials were first dried according to the manufacturer recommendations, in an oven or a dehumidifier to ensure they were free of moisture. The filaments were produced targeting a diameter of 1.75 ±0.05mm, for which such rough filaments are found better for later printability. The processing parameters used for each of the combinations produced are listed in Table 5.2. The 90:10:10 and 75:25:10 combinations based on MG37CR were extracted from a previous work by Torrado *et al*. [4]. A new MG37CR baseline was produced with the bigger nozzle to make the results comparable. The blends based on MG47 were processed at a higher temperature in zones 1, 2 and 3, to help with the ensure a better blending during the first extrusion phase between the SEBS and the ABS, and the melting of the

UHMWPE to facilitate the interaction between the materials. The best performing combinations for each ABS flavor were processed again with MASEBS instead of SEBS to analyze the impact in the blending during the extrusion process.

Table 5.2: Extrusion processing parameters for each combination.

Material	T Zone 1 (ºC)	T Zone 2 (ºC)	T Zone 3 (ºC)	T Zone 4 (ºC)	T Zone 5 (ºC)	T Zone 6 (ºC)	Main Screw Speed (rpm)	Melting Pump Speed (rpm)	Feed Screw Speed (%)	P Main Screw (Bar)	P Pump (Bar)
ABS MG37CR											
100%	240	280	280	240	215	215	40	15	5	90	36
ABS MG37CR:UHMWPE:SEBS											
90:10:10	155	195	195	195	190	NMP*	40	NMP*	6	72	NMP*
75:25:10	155	185	185	185	185	NMP*	40	NMP*	6	80	NMP*
ABS MG37CR:UHMWPE:MASEBS											
75:25:10	240	280	280	240	125	215	30	15	5	90	72
ABS MG47											
100%	230	230	220	210	205	195	80	18	7	90	110
ABS MG47:UHMWPE:SEBS											
90:10:10	250	280	275	230	195	190	75	15	7	90	130
75:25:10	250	280	275	230	195	190	48	15	5	90	220
75:25:25	250	280	275	235	215	200	37	15	8	90	97
75:25:50	250	280	275	235	215	200	65	15	17	90	97
75:25:75	250	280	275	235	215	200	60	15	16	90	95
ABS MG47:UHMWPE:MASEBS											
75:25:50	250	280	275	235	215	200	65	15	17	90	97
75:25:75	250	280	275	235	215	200	60	15	16	90	95

*NMP: No melting pump installed

In order to keep consistency with the previous studies, a MakerBot Replicator (MakerBot Industries, Brooklyn, NY USA) was used to print five specimens for each of the different combinations produced, in both XYZ (or horizontal) and ZXY (or vertical) directions, following the dimensions for specimens Type V specified by the ASTM Standard D638-10. The parameters used to print the specimens can be found in Table 5.3.

The tensile testing was performed in an Instron® 5866 (Instron, Norwood, MA) tensile testing machine equipped with a 10kN load cell and an Instron® 2663-821 advanced video extensometer (AVE) to measure % elongation (%EL), in which the specimens were tested at a strain rate of 10mm/min at room temperature.

Table 5.3: Printing parameter for each material in MakerBot Replicator

Material	Object Infill (%)	Layer Height (mm)	Number of Shells	Feedrate (mm/s)	Travel Feedrate (mm/s)	Print Temperature (°C)	Filament Diameter (mm)	G-code Nozzle Diameter (mm)	Actual Nozzle Diameter (mm)	Raft
ABS MG37CR	100	0.27	1	40	55	240	1.8	0.6	0.8	No
ABS MG47	100	0.27	1	40	55	240	1.8	0.6	0.8	No
ALL ABS:UHMWPE:SEBS BLENDS	100	0.27	1	40	55	240	1.8	0.6	0.8	No

A Hitachi TM-1000 (Hitachi High-Technologies Europe GmbH, Germany) operating at a 15kV accelerating potential was used to analyze the fracture surfaces via scanning electron microscopy (SEM) The specimens were previously coated with platinum to improve the image quality and resolution.

5.3. Tensile test results.

The results of the tensile test can be found in Tables 5.4 and 5.5 and graphically represented in Figures 5.1 and 5.2 to provide an easy and quick evaluation. The anisotropy was quantified absolutely through the difference in UTS found for each blend, and relatively by comparison to the main UTS value of the XYZ specimens. The same equations utilized by Torrado et al. in [4] were used to analyze the anisotropy, rewritten below for reference:

$$\Delta(\%)_{UTS} = \frac{UTS_{XYZ} - UTS_{ZXY}}{UTS_{XYZ}} \quad [4]$$

and

$$\Delta(\%)_{\%\mathrm{EL}} = \frac{\%\mathrm{EL}_{XYZ} - \%\mathrm{EL}_{ZXY}}{\%EL_{XYZ}} \quad [4]$$

The two variants of ABS performed similarly in the tensile test, with very close values of UTS, but with a clear advantage in favor of MG37CR for the elongation to break of XYZ specimens. Their relative anisotropy is equivalent with values of 41.4 and 40.6%, close to anisotropy values showed elsewhere.

In comparison with the previously studied blends based on MG37CR [4], the new materials provided the lowest anisotropy for the 75:25:50 mix, shifting the result to a higher SEBS content in the material. With values of relative anisotropy of 22.0±2.1 and 24.8±3.5%, the best two performers can be considered equivalent in terms of strength, but the MG47(75):UHMWPE(25):SEBS(50) blend showed a higher anisotropy in the elongation to break department. Aditionally, the elongation to break is not greatly affected by the addition of small proportions of SEBS, and the effects can only be appreciated for relationships close or over a 1:1 ratio of SEBS to ABS.

Table 5.4: UTS results for both XYZ and ZXY directions, absolute and relative anisotropy.

Material	UTS_{XYZ}		UTS_{ZYX}		Δ		Δ	
	Mean (MPa)	σ (MPa)	Mean (MPa)	σ (MPa)	Mean (MPa)	σ (MPa)	Mean (%)	σ (%)
ABS MG37CR	41.1	1.2	24.1	1.3	17.0	1.8	41.4%	2.6%
90 MG37CR: 10 UHMWPE: 10 SEBS	23.1	0.8	10.2	3.8	12.8	3.9	55.6%	20.9%
75 MG37CR: 25 UHMWPE: 10 SEBS	14.7	0.6	11.5	1.0	3.2	1.1	22.0%	2.1%
75 MG37CR: 25 UHMWPE: 10 MASEBS	17.8	1.1	7.9	1.5	9.9	1.9	55.5%	11.1%
ABS MG47	44.4	1.9	26.4	0.8	18.0	2.1	40.6%	2.1%
90 MG47: 10 UHMWPE: 10 SEBS	26.4	0.2	14.6	1.3	11.8	1.4	44.8%	4.1%
75 MG47: 25 UHMWPE: 10 SEBS	17.1	0.2	10.9	1.1	6.3	1.1	36.6%	3.8%
75 MG47: 25 UHMWPE: 25 SEBS	15.5	0.4	10.3	0.5	5.2	0.7	33.8%	2.0%
75 MG47: 25 UHMWPE: 50 SEBS	12.0	0.3	9.0	1.2	3.0	1.3	24.8%	3.5%
75 MG47: 25 UHMWPE: 75 SEBS	11.0	0.2	6.7	0.3	4.3	0.3	39.2%	1.7%
75 MG47: 25 UHMWPE: 50 MASEBS	13.7	0.2	3.7	0.4	10.0	0.5	72.7%	8.3%
75 MG47: 25 UHMWPE: 75 MASEBS	13.5	0.1	2.9	0.1	10.5	0.1	78.1%	2.1%

Table 5.5: Elongation results for both XYZ and ZXY directions, absolute and relative anisotropy.

Material	$\%EL_{XYZ}$		$\%EL_{ZYX}$		Δ		Δ	
	%	%	%	%	%	%	%	%
ABS MG37CR	18.0	3.2	2.0	0.3	16.1	3.2	89.2%	19.7%
90 MG37CR: 10 UHMWPE: 10 SEBS	8.4	0.9	2.4	1.0	6.0	1.4	71.3%	30.3%
75 MG37CR: 25 UHMWPE: 10 SEBS	5.7	0.7	2.4	0.4	3.3	0.8	57.3%	12.0%
75 MG37CR: 25 UHMWPE: 10 MASEBS	6.0	0.7	1.9	0.6	4.1	0.9	69.1%	23.2%
ABS MG47	6.6	1.9	2.3	0.3	4.2	2.0	64.8%	21.0%
90 MG47: 10 UHMWPE: 10 SEBS	9.5	1.5	4.6	0.6	5.0	1.6	52.2%	10.8%
75 MG47: 25 UHMWPE: 10 SEBS	6.2	1.4	2.8	1.2	3.4	1.8	54.5%	26.0%
75 MG47: 25 UHMWPE: 25 SEBS	7.8	0.7	3.4	0.9	4.4	1.1	56.9%	15.2%
75 MG47: 25 UHMWPE: 50 SEBS	18.3	4.6	5.4	1.3	13.0	4.8	70.7%	24.7%
75 MG47: 25 UHMWPE: 75 SEBS	48.0	4.0	7.6	3.6	40.4	5.4	84.1%	40.8%
75 MG47: 25 UHMWPE: 50 MASEBS	7.5	1.1	2.5	0.7	5.0	1.3	66.4%	21.3%
75 MG47: 25 UHMWPE: 75 MASEBS	17.8	2.0	5.9	0.7	12.0	2.1	67.1%	10.7%

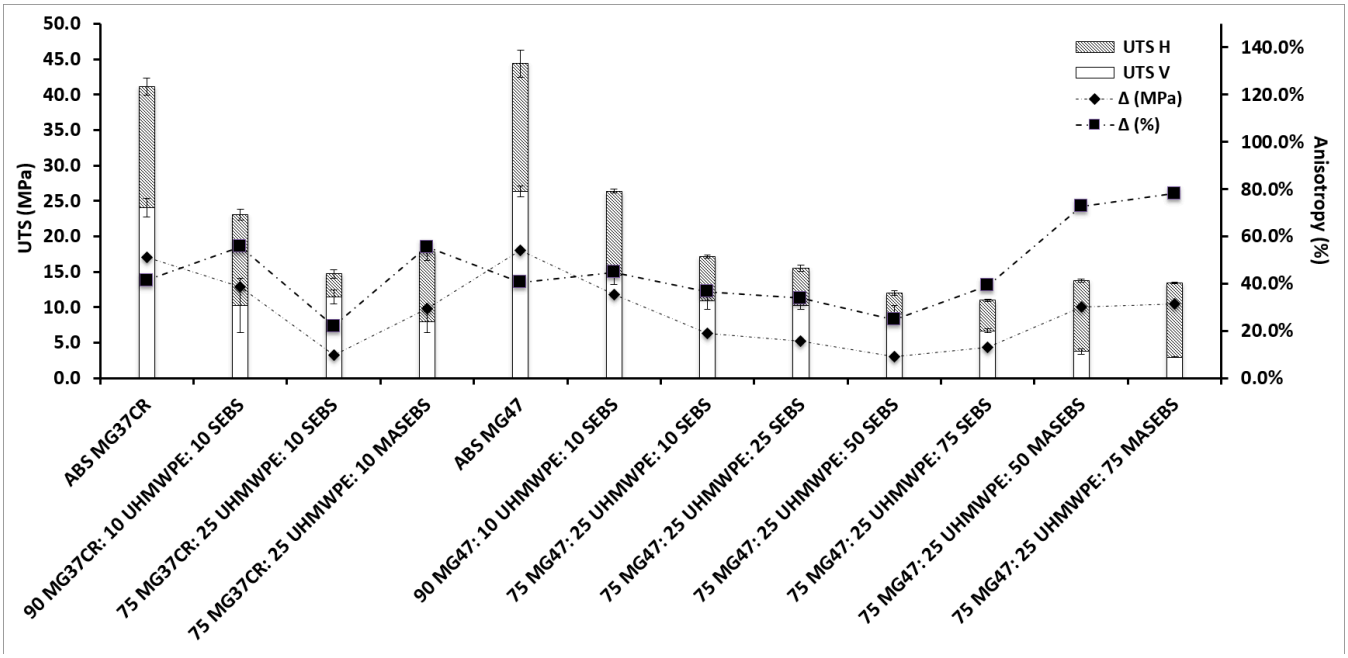

Figure 5.1: UTS anisotropy for ABS:UHMWPE:SEBS systems.

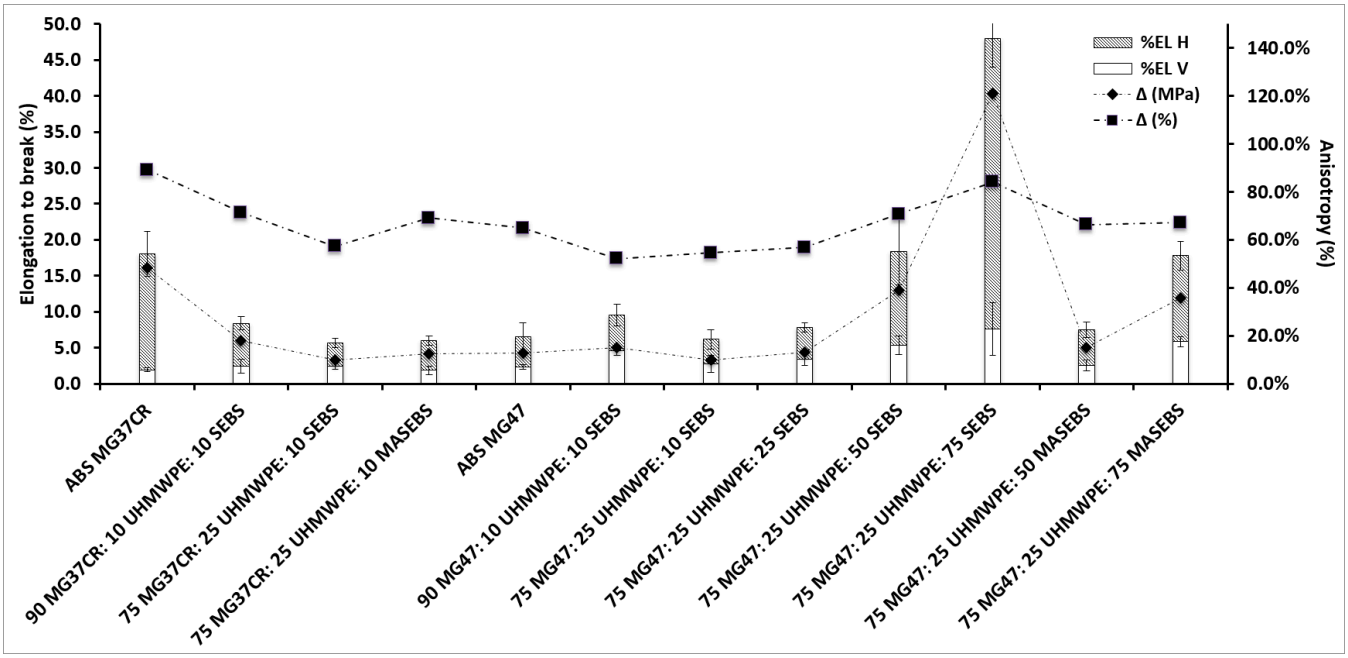

Figure 5.2: Elongation to break anisotropy for ABS:UHMWPE:SEBS systems.

It should be noted that although the relative anisotropy was not greatly decreased in all the cases, the difference between XYZ and ZXY UTS was decreased for all the ABS(75):UHMWPE(25):SEBS(x) blends. On the other hand, the blends produced with MASEBS showed values of anisotropy among the highest in all the variants. The reason for this is that the use of MASEBS leads to a slightly higher UTS results in the ZXY direction, but decreases it in the ZXY direction, an outcome not desirable for ME3DP.

All XYZ specimens showed necking, crazing deformation and cold drawing to different extends prior to the fracture. These characteristics were not present in ZXY specimens that broke in a much more brittle manner without necking or cold drawing. These strain mechanisms correlate with the results of elongation at break. [5, 6]

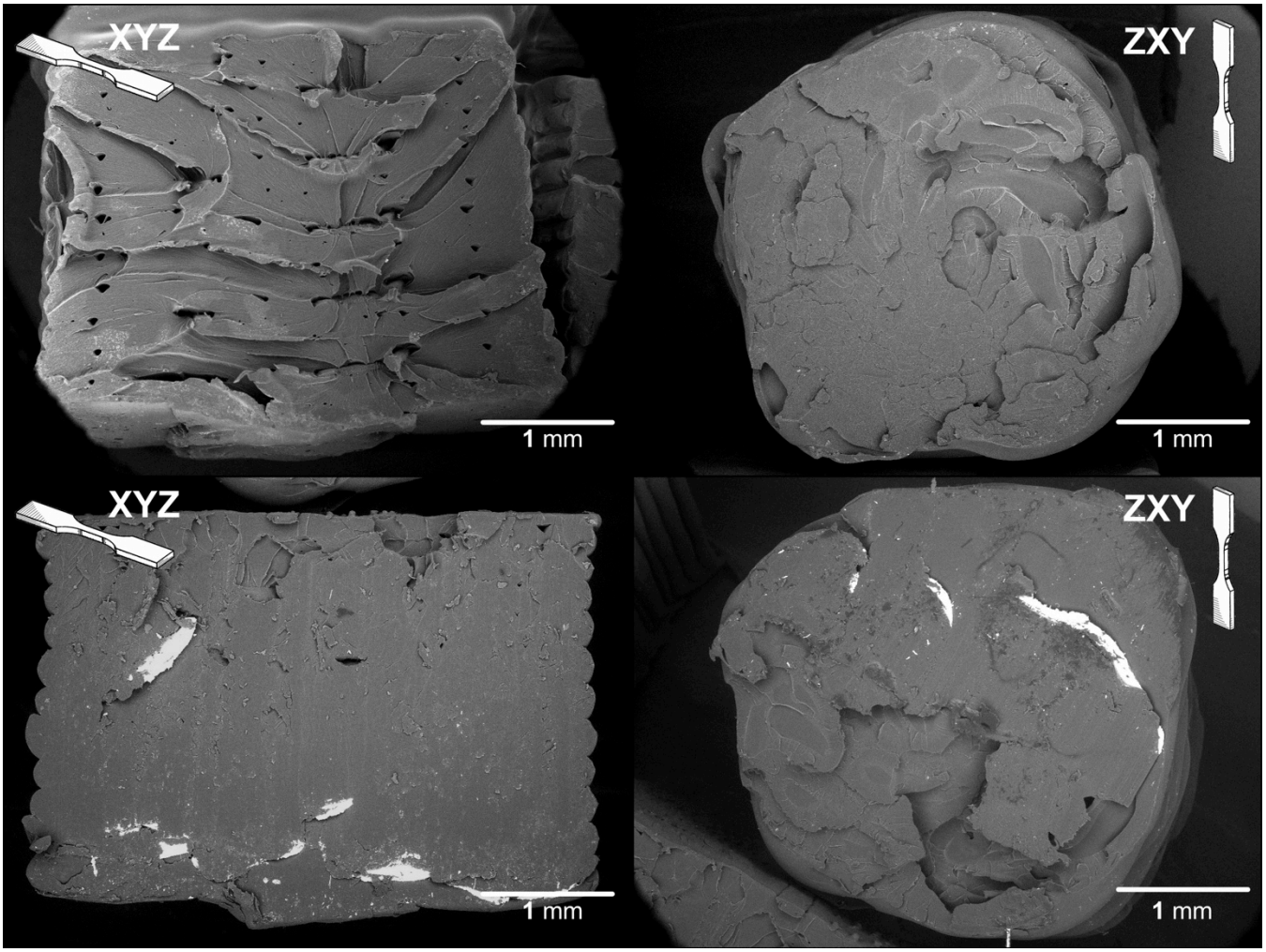

Figure 5.3: Comparison of cross sections for MG47 ABS specimens in XYZ and ZXY directions: At top, tensile specimens after being tested; at bottom, untested cut tensile specimens.

5.4. Comparison of cross sectional areas

The standard specifies tolerances for each of the dimensions defining a specimen. The truth is that these tolerances are difficult to achieve during the 3D prototyping processes that provides a dispersion in their repeatability that is already larger than the tolerance itself. In the end, the manufacturing process does not meet the specifications of the standard, so there is still a need to somehow evaluate its outcome.

The rectangular shape obtained for the cross-section of specimens printed in the XYZ direction is relatively close to design dimensions, but the analysis of the fracture surfaces of specimens printed in the ZXY revealed a rather oval shape. In order to verify that the shape of the fracture surface was the result of plastic deformation during the testing process, two specimens of ABS MG47 were printed and cut to compare the original cross sectional area. Figure 5.3 shows a comparison between the cross sectional area of untested specimens that has been cut and the resulting fracture surface after the test. The result indicates that tested specimens keep a similar profile after being tested. In the case of XYZ specimens a higher plastic deformation can be observed. A similar tendency to create oval shapes during the printing process was found to be true for the rest of the materials tested in this study. Figure 5.4 shows the cross-sectional area for XYZ and ZXY directions of the most representative materials.

The data acquisition during the testing process is performed in real time with the proprietary software provided by Instron®. The values obtained during the test correspond to the definition of engineering tensile stress σ, that is defined as the load W over the original cross sectional area A_0. This original cross sectional area A_0 is supposed to be rectangular and is provided to the machine through the original width w_0, and thickness t_0, of each of the specimens tested.

$$\sigma = \frac{W}{A_0} = \frac{W}{w_o t_o}$$

The problem that this approach presents is that the resulting values for the tensile strength of ZXY specimens are always decreased by a factor. An optimistic estimation of that factor would be the relationship given by the area of a rectangle with w_0 and t_0 for sides, and the ellipse of maximum area that can be inscribed in it, which is the one with the axis of the same size than the sides of such rectangle. The ratio between said areas is of approximately 0.79. This value indicates that tensile stress values provided by the test for ZXY specimens would be up to 21% smaller than the real values. Although a correction

using this factor would only provide an optimistic best case scenario, the implications of this analysis indicate that the anisotropy of the parts is actually smaller than initially estimated. Table 5.6 reflects how the values of Table 5.4 are altered if this correcting factor is applied to the tensile strength of ZXY specimens. The same way, Figure 5.5 is a modified version of Figure 5.1 that graphically represents the corrected values.

$$\frac{A_{0\ ELLIPSE}}{A_{0\ RECTANGLE}} = \frac{\frac{\pi}{4} w_o t_o}{w_o t_o} = \frac{\pi}{4} \approx 0.79 \xrightarrow[W=cte.]{} \frac{\sigma_{ELLIPSE}}{\sigma_{RECTANGLE}} = \frac{4}{\pi} \approx 1.27$$

Table 5.6: UTS corrected results for both XYZ and ZXY directions, absolute and relative anisotropy.

Material	UTS_{XYZ}		UTS_{ZYX}		Δ		Δ	
	Mean (MPa)	σ (MPa)	Mean (MPa)	σ (MPa)	Mean (MPa)	σ (MPa)	Mean (%)	σ (%)
ABS MG37CR	41.1	1.2	30.5	1.7	10.6	2.0	25.8%	1.6%
90 MG37CR: 10 UHMWPE: 10 SEBS	23.1	0.8	13.0	4.8	10.1	4.9	43.8%	16.4%
75 MG37CR: 25 UHMWPE: 10 SEBS	14.7	0.6	14.5	1.2	0.2	1.4	1.3%	0.1%
75 MG37CR: 25 UHMWPE: 10 MASEBS	17.8	1.1	10.0	1.9	7.8	2.2	43.7%	8.8%
ABS MG47	44.4	1.9	33.4	1.0	11.0	2.1	24.8%	1.3%
90 MG47: 10 UHMWPE: 10 SEBS	26.4	0.2	18.4	1.7	8.0	1.7	30.2%	2.8%
75 MG47: 25 UHMWPE: 10 SEBS	17.1	0.2	13.8	1.4	3.4	1.4	19.7%	2.1%
75 MG47: 25 UHMWPE: 25 SEBS	15.5	0.4	13.0	0.7	2.5	0.8	16.2%	0.9%
75 MG47: 25 UHMWPE: 50 SEBS	12.0	0.3	11.4	1.6	0.6	1.6	4.9%	0.7%
75 MG47: 25 UHMWPE: 75 SEBS	11.0	0.2	8.4	0.3	2.5	0.4	23.1%	1.0%
75 MG47: 25 UHMWPE: 50 MASEBS	13.7	0.2	4.7	0.5	9.0	0.6	65.4%	7.5%
75 MG47: 25 UHMWPE: 75 MASEBS	13.5	0.1	3.7	0.1	9.7	0.2	72.3%	2.0%

The corrected table put the values for XYZ and ZXY UTS closer, reducing the effective anisotropy for all blends. The new results for the anisotropy, specifically for MG37CR (75) : UHMWPE (25) : SEBS (10) and MG47 (75) : UHMWPE (25) : SEBS (50) are very significant. The first blend that initially showed an anisotropy of 22%, now shows complete isotropy (1.3% theoretical anisotropy). The anisotropy for the blend based on ABS MG47 decreased from 24.8% to a practically nonexistent difference of 4.9%. These results explain the tendencies shown in the graphs for the anisotropy in the different combinations and explain why it was so difficult to get values under 20%.

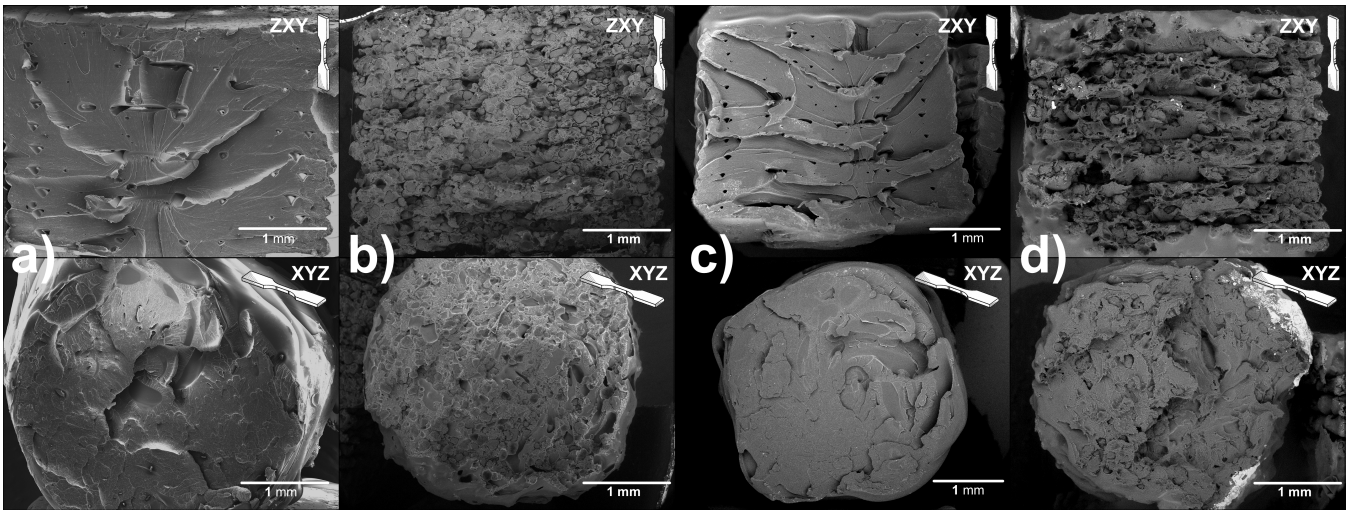

Figure 5.4: Comparison of fracture surfaces of 3D printed specimens of different materials for XYZ and ZXY directions: a) ABS MG37CR, b) ABS MG37CR (75) : UHMWPE (25) : SEBS (10), c) ABS MG47, d) ABS MG47 (75) : UHMWPE (25) : SEBS (50)

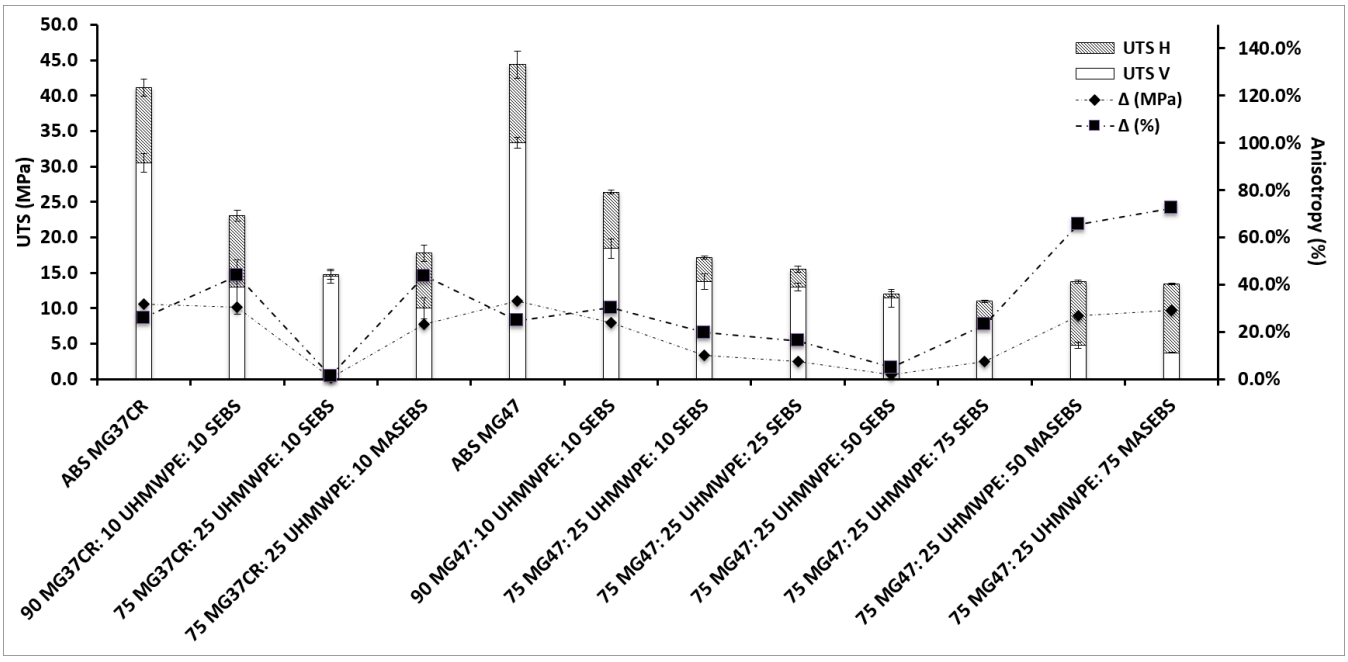

Figure 5.5: UTS anisotropy of the corrected values for ABS:UHMWPE:SEBS systems.

5.5. Fractography

The fracture surface of one representative specimen for each different blend and printing direction was analyzed via SEM. Only the most relevant results in terms of anisotropy are included in this section, due to the similarity of the fracture surfaces among the blends: that is, the two baselines (Figures 5.6 and 5.7), the two best performers (Figures 5.8 and 5.9) and the equivalent MASEBS blends of the best performers (Figures 5.1 and 5.11). The rest of the images and analysis can be found under section 5.10, "additional information" in Figures 5.16 to 5.21.

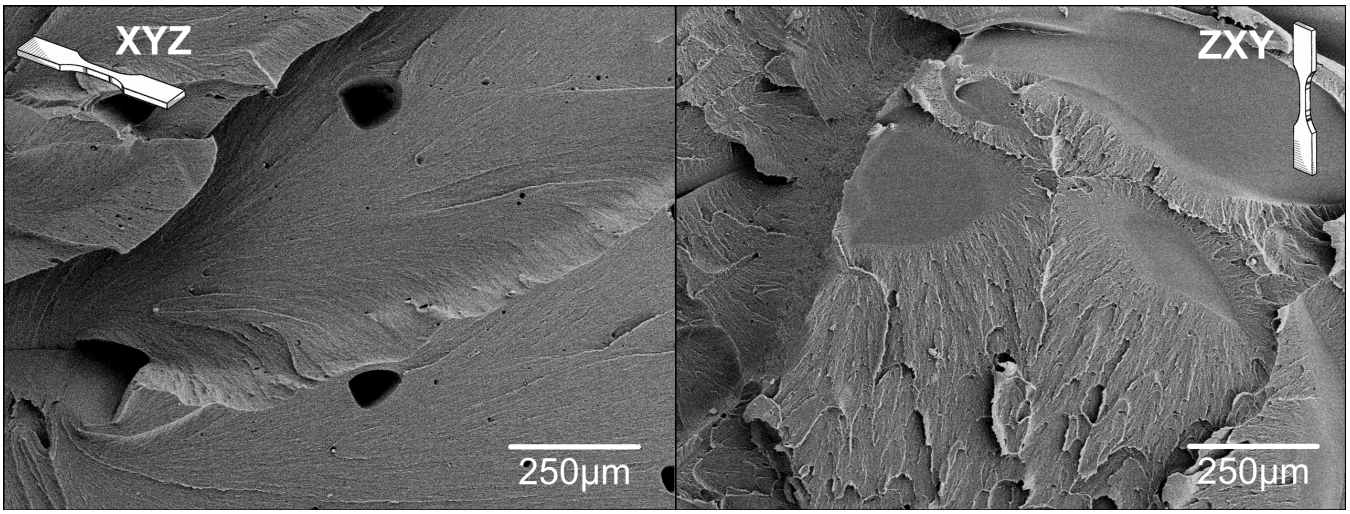

Figure 5.6: SEM micrographs of the fracture surfaces from representative samples of ABS MG37CR printed in the XYZ and ZXY build orientations.

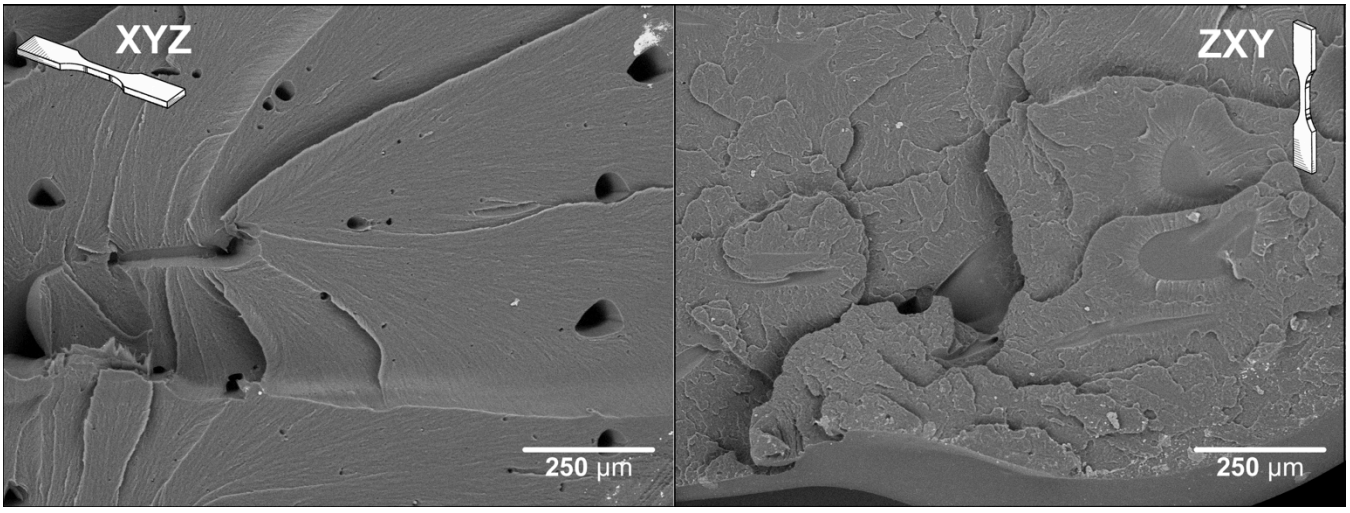

Figure 5.7: SEM micrographs of the fracture surfaces from representative samples of ABS MG47 printed in the XYZ and ZXY build orientations

The comparison between the two ABS baselines shows equivalent rheological properties. Both fracture surfaces (Figures 5.6 and 5.7) show very smooth and compact cross-sections in which the threads blend together to the point of completely unifying the material. The borders between them are indistinguishable and their positions can only be noticed by the small air gaps present in the surface. The XYZ specimens undergone a big amount of deformation in the whole gauge section, reducing the effective transversal area, to suddenly break in the end in a brittle way. The body of the ZXY specimens barely deformed in comparison and broke in a still more brittle manner. The surfaces show less plastic deformation and a more abrupt morphology full of tearing sections. The crack propagated mainly through the bonding interface between rasters but found as well its way through them in some sections. The better rheological properties demonstrated by the use of a thicker tip and a slightly higher temperature, lead to better filled, more compacted specimens.

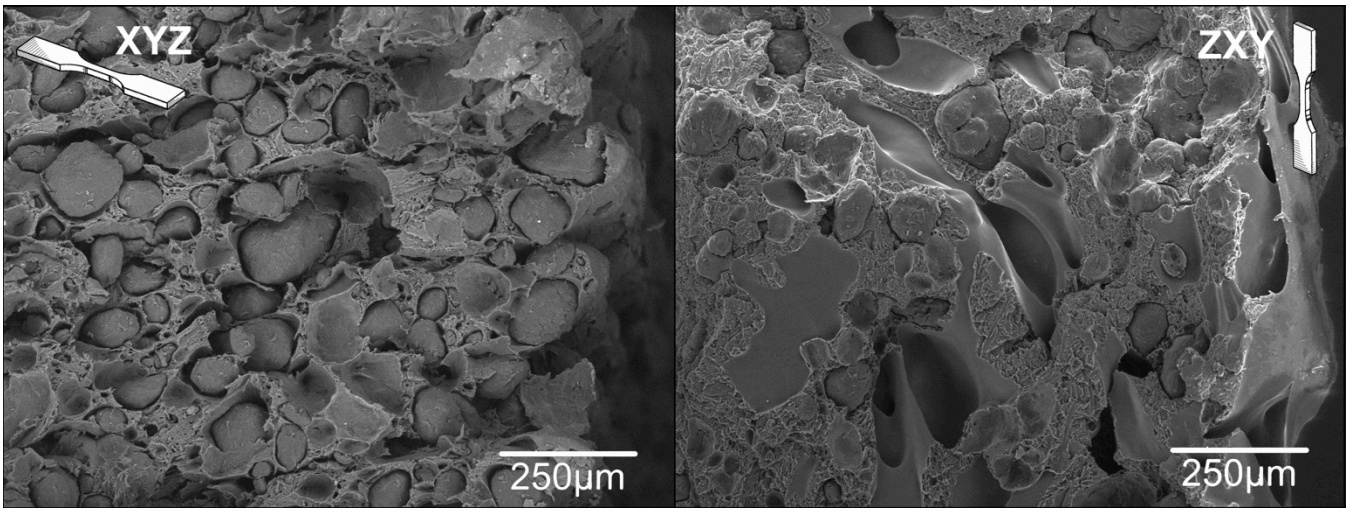

Figure 5.8: SEM micrographs of the fracture surfaces from representative samples of the 75:25:10 by weight ratio ABS MG37CR:UHMWPE:SEBS blend printed in the XYZ and ZXY build orientations. Extracted from [4]

All the tested ABS:UHMWPE:SEBS and ABS:UHMWPE:MASEBS mixes showed similar fracture surfaces in which spheroidal particles of diverse sizes were present (Figures 5.6 to 5.11 and 5.16 to 5.21) indicating an incomplete blend in all the cases, and a more composite-like resulting material. The increase of SEBS in the blends produces a more rubbery matrix that leads to an increase of the elongation during the tensile test, which correlates with the amount of plastic deformation present in the fracture

surfaces of the specimens. At the same time, the increase of SEBS entails a reduction of the proportion of UHMWPE in the mix, therefore less particulates can be observed in the micrographs. The increase of proportion of SEBS translates fracture surfaces with more plastic deformation. MASEBS based specimens showed less deformation for the specimen in the gauge region, but a much higher deformation in fracture surface than their SEBS counterparts.

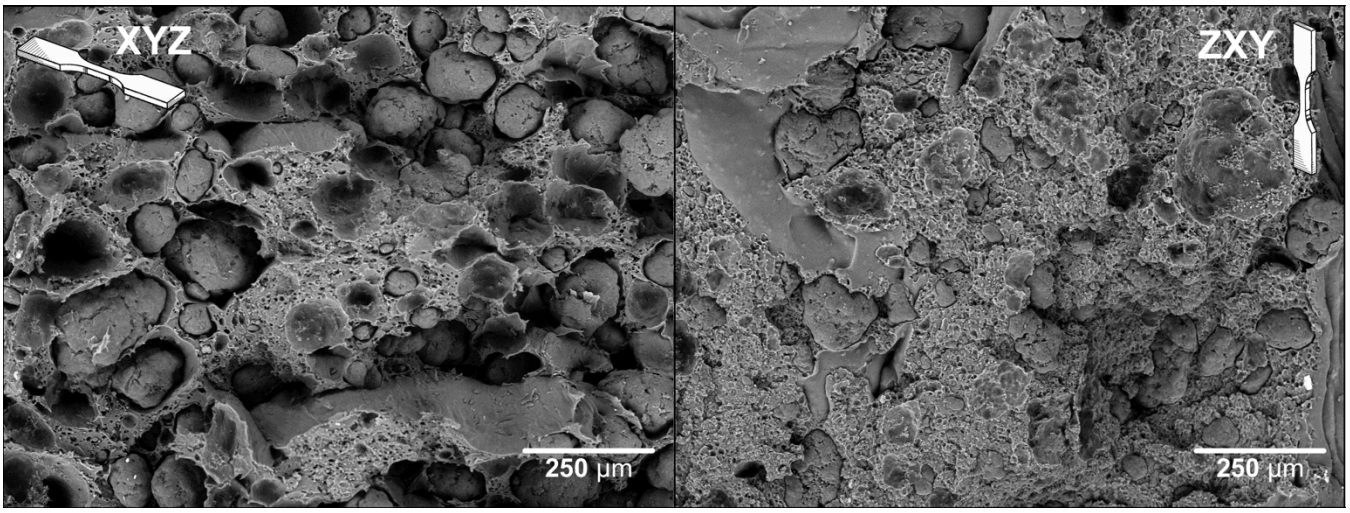

Figure 5.9: SEM micrographs of the fracture surfaces from representative samples of the 75:25:10 by weight ratio ABS MG37CR:UHMWPE:MASEBS blend printed in the XYZ and ZXY build orientations.

A closer look to the images will reveal the differences in the morphology of the spheroidal particles among the materials. Figure 5.12 shows a comparison of high magnification micrographs for the most representative combinations. The MG37CR:UHMWPE:SEBS blend surfaces exhibit particles with a non-globular, smooth surface that didn't adhere well to the matrix. In the case of MASEBS variant, the particles have a more globular appereance to them while keeping the smoothness of their surface, but still with a poor adhesion to the matrix. The MG47:UHMWPE:SEBS blend shows particles with a rough surface and a less compacted, aggregated body, that were more integrated with the matrix. The MASEBS variant shows smoother particles with a deformed coating with the same consistency as the matrix covering their whole surface. This combination of materials show the best interaction between the different plastics.

It is of special interest that blends based on MG37CR show particles of smaller sizes (diameters of 1 to 10μm) dispersed within the matrix while in blends based on MG47 these particles are not present

in any of the combinations. This fact demonstrates again a different interaction between the materials for ABS MG47 based combinations and both types of SEBS, and shows that blends based on MG37CR produce a system with particulates in a bimodal size distribution.

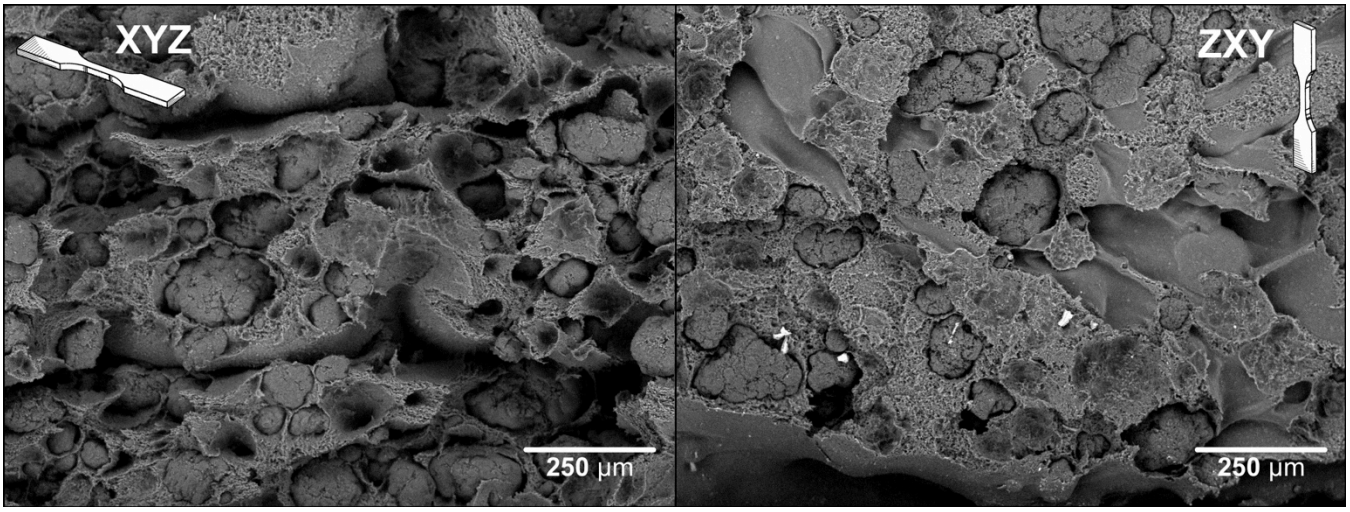

Figure 5.10: SEM micrographs of the fracture surfaces from representative samples of the 75:25:50 by weight ratio ABS MG47:UHMWPE:SEBS blend printed in the XYZ and ZXY build orientations.

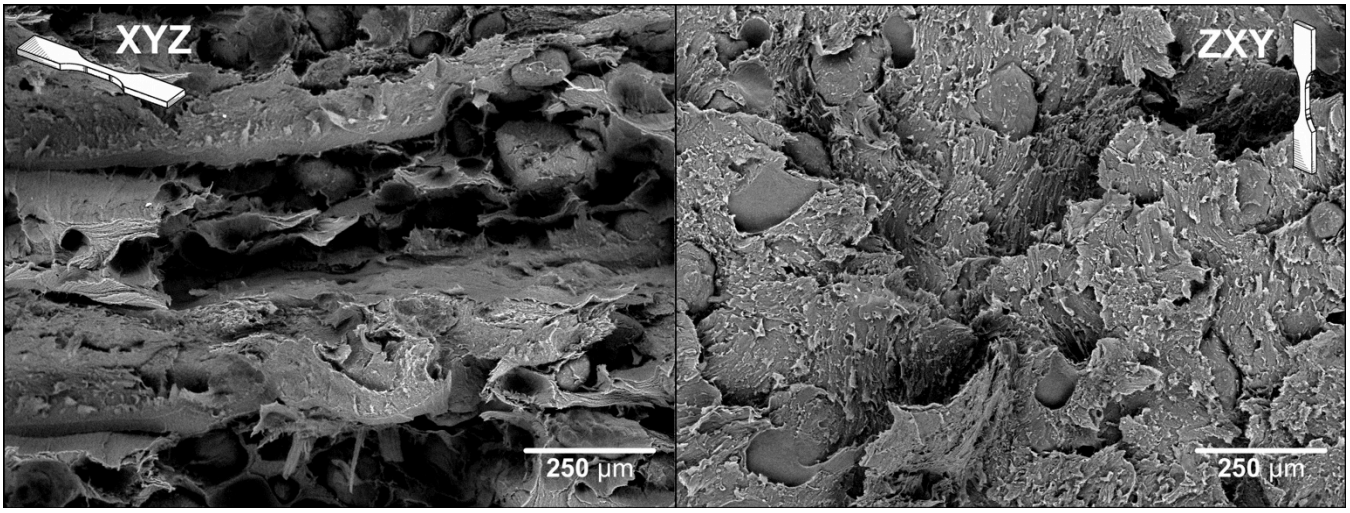

Figure 5.11: SEM micrographs of the fracture surfaces from representative samples of the 75:25:50 by weight ratio ABS MG47:UHMWPE:MASEBS blend printed in the XYZ and ZXY build orientations.

UHMWPE is a thermoplastic constituted by very long polymeric chains over 100.000 ethene units with a low degree of branching. [7] The ethilene is a rather stable molecule that polymerizes in chains

very difficult to break down. This characteristic combined with its low polarity complicates its blending with other materials. Both grades of ABS blend well with both flavors of SEBS, therefore the only possible explanation for the results showed in Figure 5.12 is that ABS is the one working as compatibilizer between the SEBS and the UHMWPE, and not the other way around. The analysis of the differences in the topography of the particulates surfaces suggests that the ABS MG47 grade interacts better with the UHMWPE, while MG37CR shows little to none compatibility. This becomes especially relevant when considering that the different processing temperatures didn't improve solubility for blends based on MG37CR (comparison between SEBS and MASEBS), while a completely different topography is shown by the particles in MG47 based blends. This is the reason why the MG37CR micrographs show particulates of mostly pure, smooth UHMWPE, with isolated small particles in the matrix, while MG47 fracture surfaces show coated particles, covered in the surface with ABS-SEBS that stick better to the matrix and aggregate with eachother. These aggregated particles do not have the same toughness as compacted, 100% UHMWPE particles, consequently dimishing the effect of big particle composite, and allowing the cracks to easily go through them. The same is true with big particles coated with a bigger layer of "rubberized" plastic: While it would help with the prevention of stress concentrators as well as the growth of new microcracks from the local plastic deformation of the material, it would also reduce the composite like effect.

The lowest anisotropy exhibited by ABS MG47 blends appears for the 75:25:50 combination. The reason can be found in the reduction of ABS in the mix that again reduces the solubility of UHMWPE therefore providing tougher, more compacted particles than in the blends with less SEBS. The 75:25:50 combination produces a material too flexible in which the deformation before failure eliminates the beneficial effect of the particles in the mix. The low proportion of UHMWPE causes the particles to no longer play a role under these circumstances.

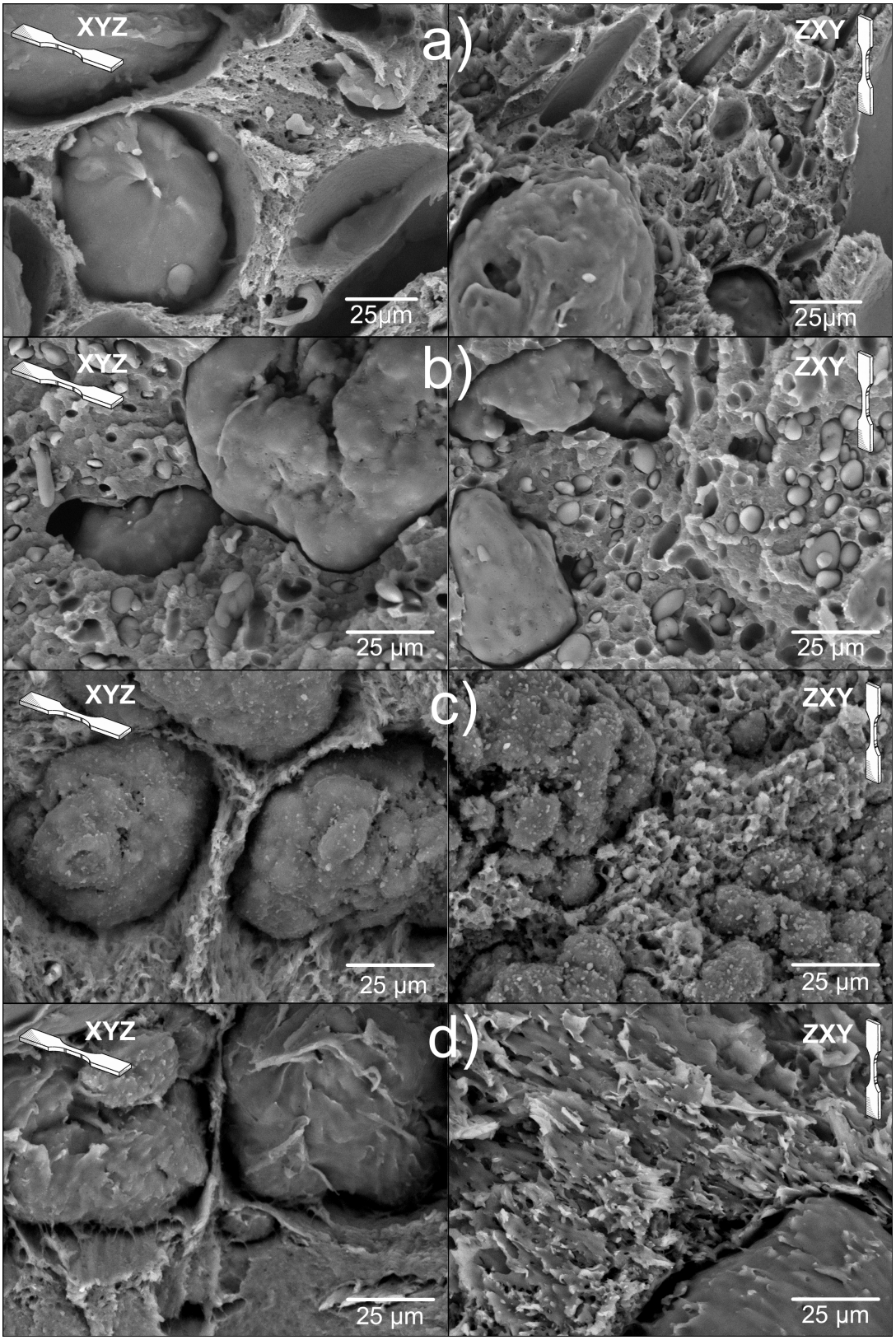

Figure 5.12: Close-up to the spheroidal particles present in the most representative blends of this study: a) ABS MG37CR(75):UHMWPE(25):SEBS(10), b) ABS MG47(75):UHMWPE(25):SEBS(50), c) ABS MG37CR(75):UHMWPE(25):MASEBS(10), d) ABS MG47(75):UHMWPE(25):MASEBS (50)

5.6. DMA Analysis

A dynamic mechanical analysis (DMA) test was performed on a TA DMA Q800 by TA Instruments (New Castle, PA USA) using 59.74x12.85x3.14mm^3 3D printed specimens for each of the systems in this work. Values for the transition temperature, storage modulus, complex viscosity and peak of tan delta were obtained with this test, and tabularized in Table 5.7.

According to the results, ABS:UHMWPE:SEBS blends show a transition temperature 5º higher, shifted from 115 to 120ºC. This is corroborated by the peaks of maximum tan delta and loss modulus.

Table 5.7: DMA results: Glass Transition temperature, storage modulus, complex viscosity and tan delta.

Material	Glass Transition Temperature (ºC)	Storage Modulus (MPa)			Complex Viscosity (MPa•s)			Max Tan Delta		Max Loss Modulus	
		40ºC	100ºC	140ºC	40ºC	100ºC	140ºC		ºC	Mpa	ºC
ABS MG37CR	115.3	1451	1219	3.43	80.2	67.5	0.210	2.14	125.4	287	117.3
90 MG37CR: 10 UHMWPE: 10 SEBS	119.1	843.8	653.7	4.192	46.7	36.2	0.294	1.52	127.2	172	119.1
75 MG37CR: 25 UHMWPE: 10 SEBS	119.7	849.8	627.7	5.311	47.0	34.8	0.369	1.30	129.2	124	122.5
75 MG37CR: 25 UHMWPE: 10 MASEBS	119.6	801.8	625.9	4.854	44.3	34.7	0.335	1.34	129.2	114	122.6
ABS MG47	115.4	1446	1222	4.24	79.9	67.6	0.251	1.99	125.5	300	116.6
90 MG47: 10 UHMWPE: 10 SEBS	117.9	987.2	789.8	4.408	54.6	43.7	0.316	1.64	126.3	168	120.3
75 MG47: 25 UHMWPE: 10 SEBS	117.0	847.0	614.8	5.525	46.84	43.07	0.359	1.35	127.7	129	119.1
75 MG47: 25 UHMWPE: 25 SEBS	119.3	736.8	515.7	5.460	40.74	28.59	0.346	1.29	126.4	110	120.7
75 MG47: 25 UHMWPE: 50 SEBS	119.8	603.3	395.6	6.381	33.36	21.95	0.435	1.15	125.8	87.7	119.8
75 MG47: 25 UHMWPE: 75 SEBS	119.0	473.9	314.1	4.681	26.20	17.43	0.286	1.12	126.2	71.1	119.9
75 MG47: 25 UHMWPE: 50 MASEBS	119.9	401.4	243.1	3.702	22.21	13.53	0.248	1.21	126.3	53.9	119.3
75 MG47: 25 UHMWPE: 75 MASEBS	119.9	318.1	180.9	2.938	17.60	10.08	0.196	1.13	126.8	38.6	121.0

The results reported by the manufacturers for the melt index (ASTM D1238) indicate a better flow for MG37CR (4.4g/10min at 230°C) than for MG47 (5.6g/10min at 230°C). The grafted MASEBS is reported to have as well flow better (22g/10min at 230°C) than the much more viscous regular SEBS (7g/10min at 260°C). In general, ABS:UHMWPE:SEBS blends show lower storage modulus and lower loss modulus when compare with pure ABS before and after the glass transition temperature. Although the chart indicates higher storage modulus at 140ºC for ABS:UHMWPE:SEBS blends, this is only due to the shifted glass transition temperature. This means that the blends behave more elastically or less rigidly, and that they disipate less energy during its deformation. Basically less viscous, or in other words, they behave more like a rubbery solid and less like a liquid, but at the same time, much easier to deform than ABS. It has been demonstrated elsewhere that a lower viscosity improves rheological weldability in

thermoplastics, which directly affects the strength of the bonding between rasters [16]. ABS:UHMWPE:SEBS blends show better interfatial adhesion, rheology and weldability. These results correlate with the tensile test results because, again, although the relative anisotropy is improved only in some cases, the absolute difference between XYZ and ZXY UTS for the blends is reduced, indicating that a better bonding is being achieved.

5.7. XRD Analysis

Squared 3D printed specimens of 20x20x2mm^3 were prepared out of the filaments to perform an XRD test. The test was conducted in a Bruker® XSX-D8 Discover (Bruker, Billerica, MA, USA), at room temperature, using Cu Kα radiation (λ = 1.5406Å). Increments of 0.02º and a scanning speed of 15º/min were used to run a coupled emisor and detector test covering 2θ angles from 10 to 80º. Resulting XRD patterns were analyzed unaltered, with no background noise removed or smoothing applied. All the raw materials were analyzed as provided by the manufacturers, whether that meant pellet or powder form. Figure 5.13 shows the the resulting spectra.

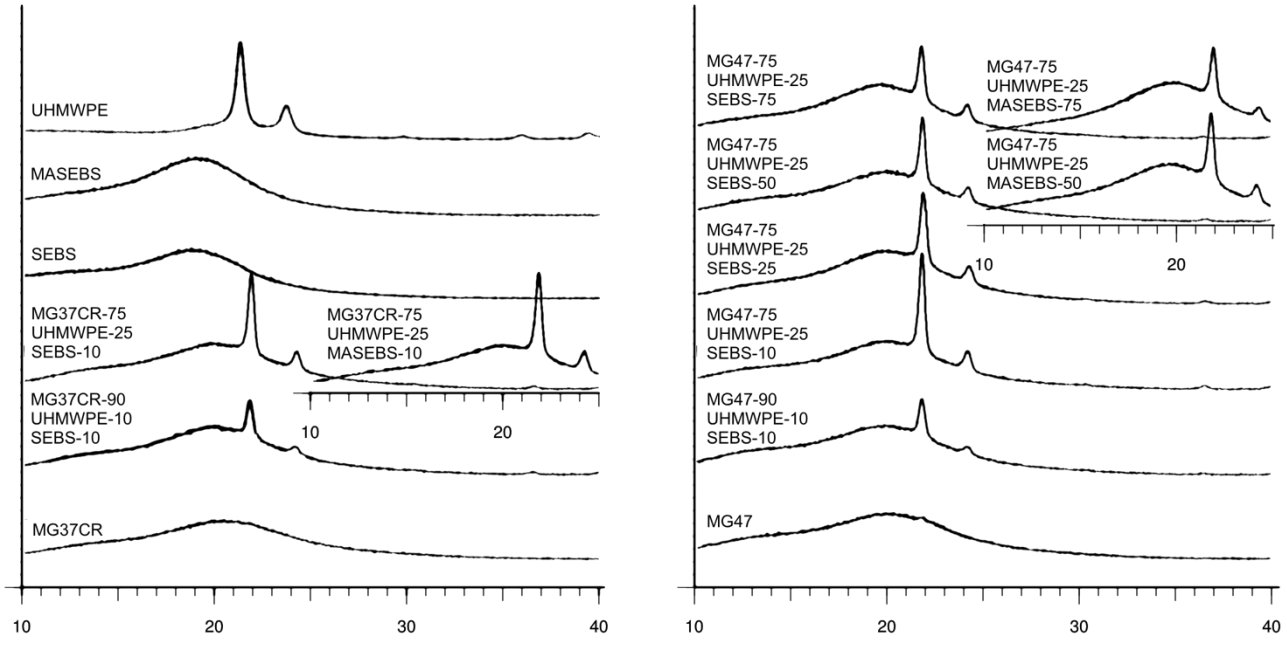

Figure 5.13: XRD spectra for MG37CR, MG47, SEBS, MASEBS, UHMWPE, and all the different ABS:UHMWPE:SEBS combinations

MG37CR and MG47 showed only an amorphous phase, characterized by a smooth XRD curve with no abrupt or sharp peaks, defined by a broad non-crystalline halo peak whose maximum could be located at 20.5º in both cases [17]. Although the spectra produced by both resins is very similar, MG47 halo is up to 15% more intense below two-theta 24º, while overlapping completely after that value all the way up to 80º.

SEBS and MASEBS showed only an amorphous phase as well but in this case the halo maximum was located at 19º; a narrower, more leftward shifted peak when compared with ABS spectra. MASEBS's halo was up to a 20% more intense than SEBS halo below 65º.

The UHMWPE powder showed two well defined peaks at 21.3 and 23.7º, revealing a predominant orthorhombic phase structure, and matching the standard spectrum of JCPDS No.53-1859 for HDPE and other results for UHMWPE of previous studies [18, 19] that located those peaks at 21.5 and 23.8º. These peaks correspond to the orthorhombic reflections o(110) and o(200) and define a lattice of dimensions 7.33, 4.88 and 2.51Å. A very subtle rise at 19.4º corresponding with the m(001) reflection discloses a monoclinic phase in a very low percentage. The following m(002) m(-201) reflections are disguised below o(200) and the non-crystalline halo representative of the amorphous phase of the material.

The XRD spectra of ABS:UHMWPE:SEBS blends is the result of the combination of the spectra of each of the components in the mixes, showing both amorphous and crystalline phases. The non-crystalline halo reflects the characteristics of the constituents in the mix. The crystalline phase reveals an orthorhombic structure such as that of the UHMWPE but with shifted o(110) and o(200) peaks from 21.3 and 23.7º to 22.1 and 24.7º in all the cases. The dimensions of the lattice for the blends are therefore slightly reduced to 7.18, 4.79 and 2.48Å. The intensity of the orthorhombic reflections correlates with the percentage in weight of UHMWPE. The spectra of the blends provide shaper peaks when compared with those of UHMWPE, indicative of larger crystalline regions, or in other words, larger UHMWPE particle sizes as a consequence of the agglomeration of UHMWPE during the extrusion process.

5.8. Surface energy

A test was designed to calculate the surface energy of the different blends following the recommendations of the ASTM D7490 standard. A Canon EOS 20D with a Canon 40mm f/2.8 macro lens was used to acquire the images. An elevator stage was used to garantee a leveled platform at a the proper height. Thin films were generated out of the different materials by hot-pressing pelets obtained from the extruded filaments. The raw materials were directly processed out of their supplied forms. Three of the materials weren't evaluated in this test. The films produced for MASEBS and the material combinations with the highest proportion of it in them would break while peeling process Droplets of 10µl of water and ethylene glycol were deposited over the samples with a calibrated pipettor. The drop contact angles were measured using photo editing software. Three drops at both edges for a total of six contact angles were analyzed per probe liquid.

Table 5.8: Contact angles for distilled water and ethylene glycol with the different blends. Surface energy, and polar and dispersive components.

	θ_{water}		$\theta_{e.\ glycol}$		γ_s^p		γ_s^d		γ_s	
	m	σ	m	σ	m	σ	m	σ	m	σ
	°	°	°	°	mJ/m²	mJ/m²	mJ/m²	mJ/m²	mJ/m²	mJ/m²
ABS MG37CR	82.0	0.8	51.2	1.0	5.1	1.1	29.3	2.7	34.5	3.8
ABS MG37CR (90) : UHWMPE (10) : SEBS (10)	82.3	0.6	49.5	1.4	4.3	1.0	32.2	3.1	36.5	4.1
ABS MG37CR (75) : UHWMPE (25) : SEBS (10)	81.9	0.8	59.6	0.9	9.2	1.5	18.2	2.2	27.3	3.7
ABS MG37CR (75) : UHWMPE (25) : MASEBS (10)	81.7	0.5	63.7	1.1	11.9	1.5	13.2	1.9	25.1	3.4
ABS MG47	89.7	0.5	54.5	1.3	1.2	0.5	37.9	3.1	39.1	3.6
ABS MG47 (90) : UHWMPE (10) : SEBS (10)	81.0	1.4	53.9	1.0	7.3	2.0	24.0	3.5	31.3	5.4
ABS MG47 (75) : UHWMPE (25) : SEBS (10)	72.6	1.3	60.2	0.9	23.0	3.3	7.8	1.9	30.8	5.2
ABS MG47 (75) : UHWMPE (25) : SEBS (50)	76.6	0.6	49.9	0.8	10.0	1.2	22.7	1.9	32.7	3.1
ABS MG47 (75) : UHWMPE (25) : SEBS (50)	80.4	0.6	56.3	0.7	9.0	1.1	20.3	1.8	29.3	2.9
ABS MG47 (75) : UHWMPE (25) : SEBS (75)	78.7	0.7	55.4	1.1	10.5	1.6	19.1	2.3	29.6	3.9
ABS MG47 (75) : UHWMPE (25) : MASEBS (50)	-	-	-	-	-	-	-	-	-	-
ABS MG47 (75) : UHWMPE (25) : MASEBS (75)	-	-	-	-	-	-	-	-	-	-
UHMWPE	80.9	1.7	60.4	0.7	10.8	2.7	15.9	3.0	26.8	5.7
SEBS	90.0	0.0	71.7	0.8	7.3	0.5	13.5	0.9	20.8	1.4
MASEBS	-	-	-	-	-	-	-	-	-	-

The surface energy was calculated following the methodologies by Owens, Wendt, Rabel and Kaelble (OWRK, which divide the surface energy into two components: one due to dispersive interaction and another one due to polar interactions. The dispersive and polar components can be obtained by solving a system of two equations based on the Owens-Wendt-Kaelble relationship (equation (3)).

$$\frac{\gamma_l(1+cos\theta)}{2} = \left[\left(\gamma_l^d \gamma_s^d\right)^{1/2} + \left(\gamma_l^p \gamma_s^p\right)^{1/2}\right] \quad (3)$$

The outcome of this test can be found in Table 5.8. Figures 5.14 and 5.15 show a graphical representation of those results. Both grades of ABS show the highest surface energy values (34.5±3. and 39.1±3.6mJ/m^2), with the exception of MG37CR(90):UHMWPE(10):SEBS(10), which is in between with 36.5±4.16mJ/m^2. In general, it can be said that ABS:UHMWPE:SEBS show a total energy that is lower than pure ABS, dropping from 5 to 10mJ/m^2. The lower free surface energy means that the blends are more malleable than ABS, and therefore that the material adapts bettwen to new shapes, something already confirmed by both the fracture analysis and the DMA results. This translates into more filled parts or less air gaps in the parts. The lower surface energy needed to break the surface should easen the rheological weldability between rasters at higher temperature.

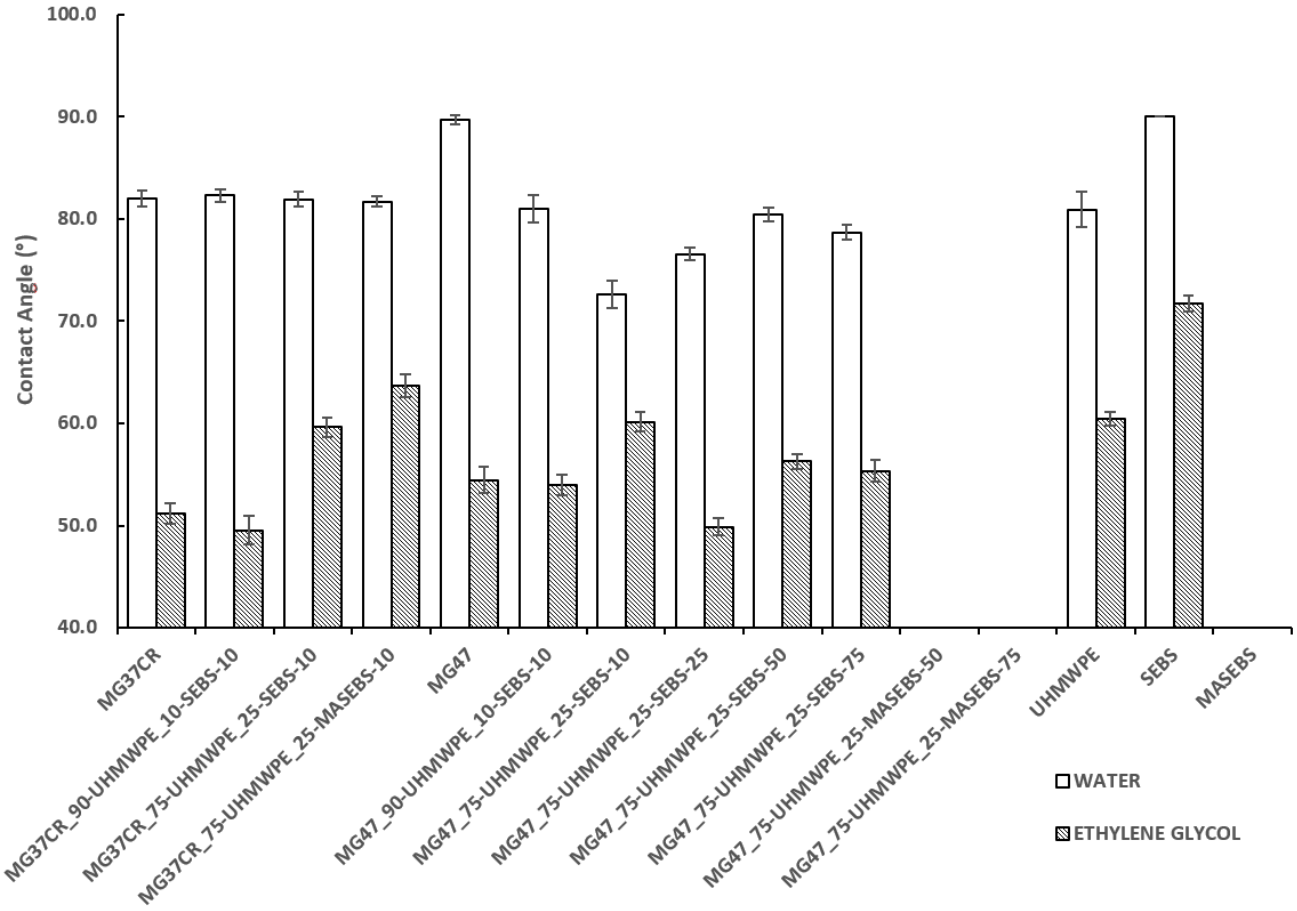

Figure 5.14: Contact angle for water and ethylene glycol droplets.

It is interesting that again both grades of ABS show the lowest values for the polar component (5.1±1.1 and 1.2±0.5mJ/m^2) with the same exception. The remaining ABS:UHMWPE:SEBS blends present similar values to that of neat UHMWPE (10.86±2.7mJ/m^2). Polyethilenes are among the most non-polar thermoplastics avalaible, sharing this characteristic with polypropylene, and its incompatibility with ABS, a rather polar copolymer, is very well-known [15]; thus, these results are shocking. On the other hand, the work performed by Carré [20] proposes that the polar component of the surface energy relates more with how the polymer interacts with the probe liquid rather than with the actual polarity of the polymer itself. This is, the polar component would be indicative of surface polarizability in interaction with a specific environment. Carré goes further suggesting that an absolute value of surface free energy could not be achieved with contact angle measurement techniques, and recommends the introduction of a surface polarizability coefficient. Following Carré's line of thought we could say that ABS:UHMWPE:SEBS has a higher tendency to adapt their surface polarity to their environment.

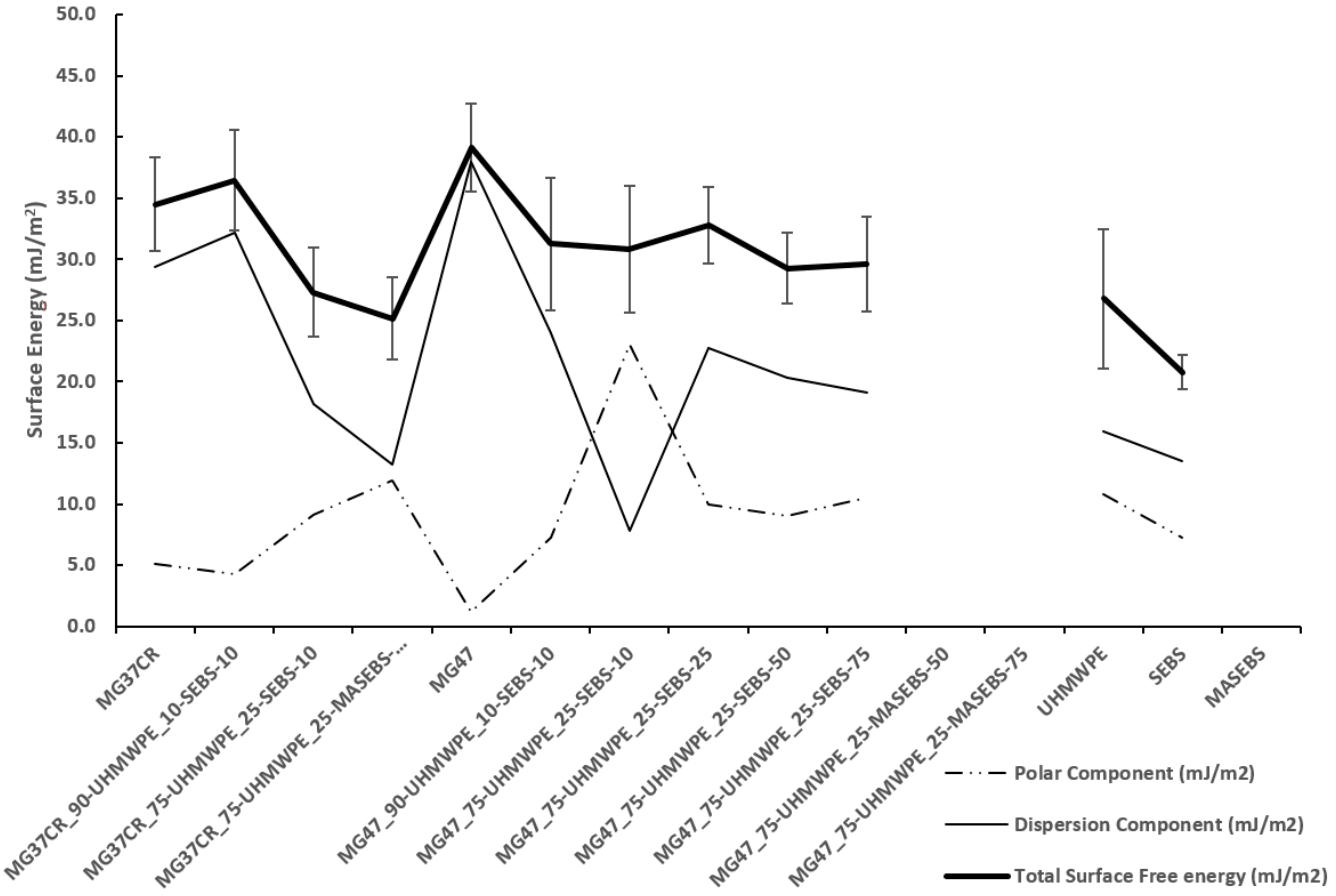

Figure 5.15: Surface free energy, polar and dispersive components.

5.9. Conclusions and final thoughts.

The development of materials that produce near zero relative anisotropy for the ultimate tensile strength of 3D printed parts has been demonstrated to be possible; however, it is at the expense of a significant reduction in that same property. On the other hand, the elongation to brake keeps showing an anisotropy that has barely decreased in most of the cases, and at times even worsened.

The incomplete blending between the materials leads to a composite-like behavior in which the larger, stronger particulates hinder the propagation of the crack withing the layer-to-layer bonding interface in favor of a trans-raster failure of the part. A better blending, even if it is only partial in localized areas of the material such as the surroundings of particles, is actually not beneficial in terms of isotropy. Instead it rather weakens these particulates leading again to a layer-to-layer interface failure. The size of these particles needs to be of the order of magnitude of the rasters being created. In this case, the raster size was of 0.6 by 0.27mm, while the particle size ranged between 0.05 and 0.15mm. Better results were obtained with ABS MG37CR as a matrix, due to the bimodal distribution of particles resulting of the incompatibility between the materials.

It is especially notable, that all the ABS(75):UHMWPE(25):SEBS(X) blends show minimum values for the absolute difference between XYZ and ZXY specimens, which translates into improved weldability between the rasters. Increasing the UTS while keeping the good rheological properties should lead to more isotropic materials. This cannot be said of ABS(75):UHMWPE(25):MASEBS(X),

It should be possible to reproduce these results with different materials, as long as the material used for the particulates is of a higher strength than the resulting matrix, and the size of the particulates is adequate. The lowered anisotropy might be a result of a combination of a weakened matrix and the deviation of the cracks through the rasters, but improved blends with better overall properties should be possible as well if the adhesion between the matrix and the particles is improved while ensuring a bimodal size distribution or, equivalently, avoiding the total disolution of the smallest particles.

5.10. Additional information

Micrographs of representative specimens of the remaining combinations of ABS:UHMWPE:SEBS have been included in this section for reference purposes, and can be found in Figures 5.16 to 5.21. They corroborate the higher deformation presented by the blends based on MASEBS

in comparison with ungrafted SEBS, and the similarities in the morphology of the particles among blends based on the same materials. The correlation between increasing proportions of SEBS and higher plastic deformation further supports the previous results.

The contrast between the ductile fracture of the XYZ specimens and the brittle fracture of ZXY specimens is still present in all the cases.

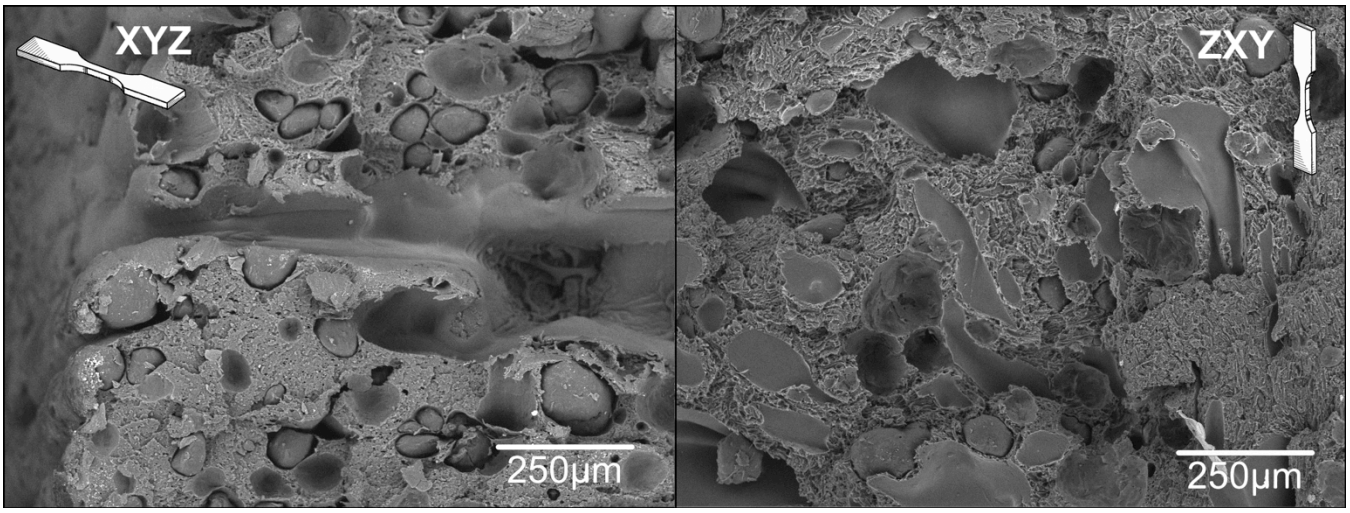

Figure 5.16: SEM micrographs of the fracture surfaces from representative samples of the 90:10:10 by weight ratio ABS MG37CR:UHMWPE:SEBS blend printed in the XYZ and ZXY build orientations. Extracted from [4]

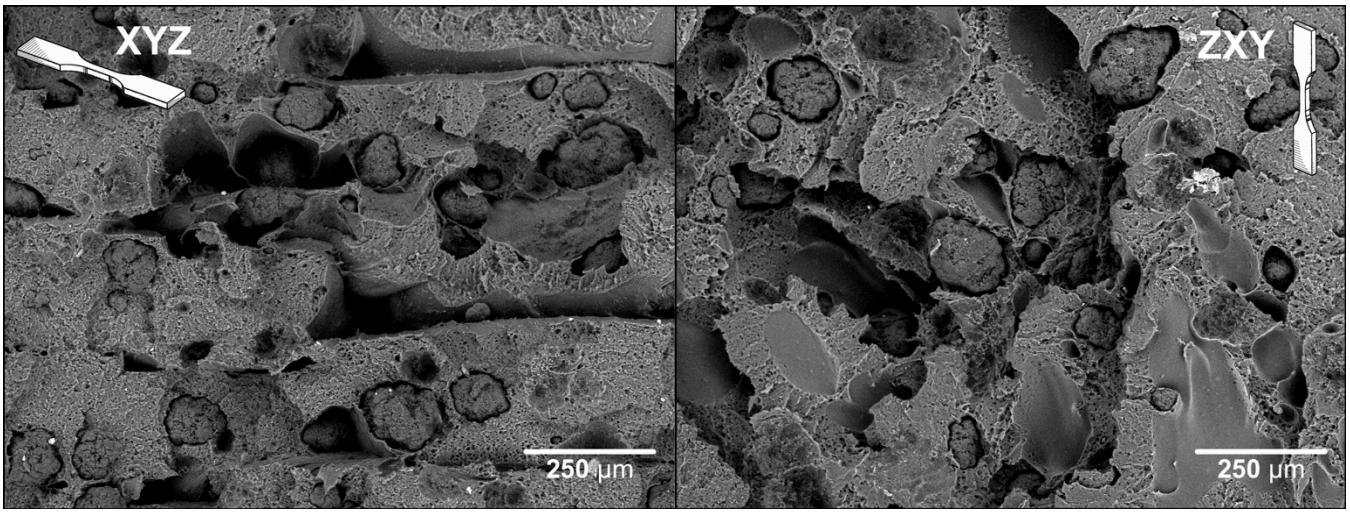

Figure 5.17: SEM micrographs of the fracture surfaces from representative samples of the 90:10:10 by weight ratio ABS MG47:UHMWPE:SEBS blend printed in the XYZ and ZXY build orientations.

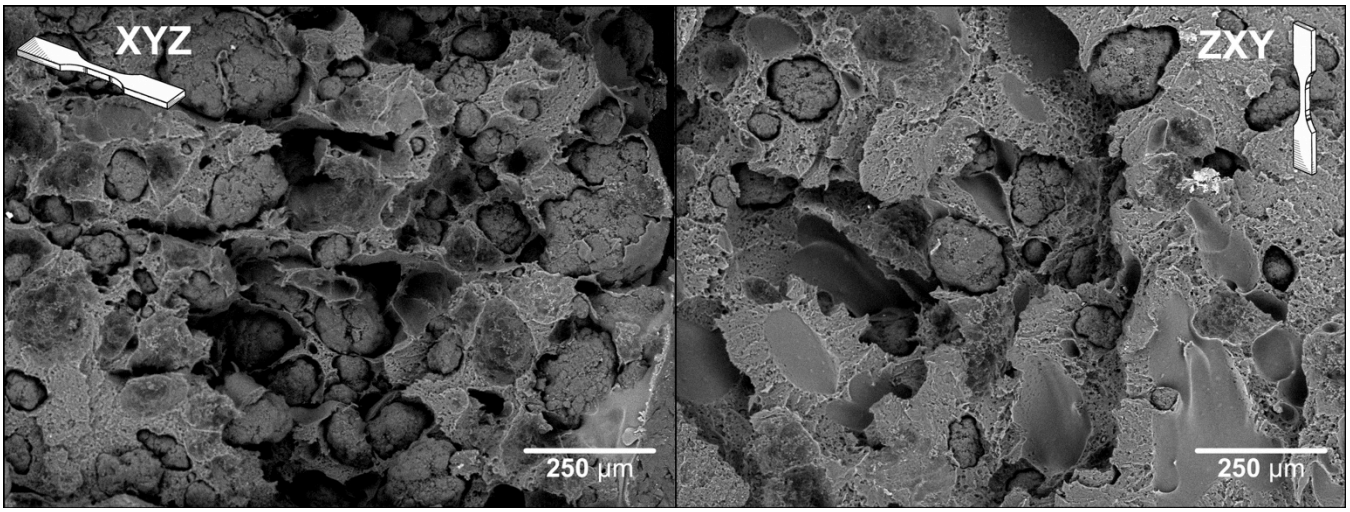

Figure 5.18: SEM micrographs of the fracture surfaces from representative samples of the 75:25:10 by weight ratio ABS MG47:UHMWPE:SEBS blend printed in the XYZ and ZXY build orientations.

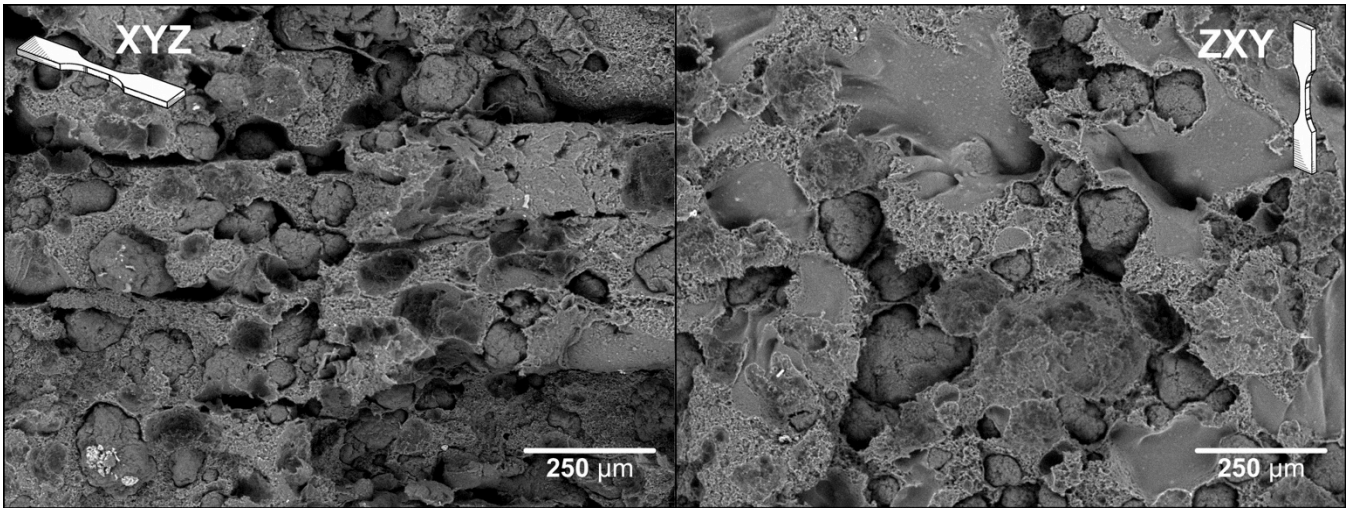

Figure 5.19: SEM micrographs of the fracture surfaces from representative samples of the 75:25:25 by weight ratio ABS MG47:UHMWPE:SEBS blend printed in the XYZ and ZXY build orientations.

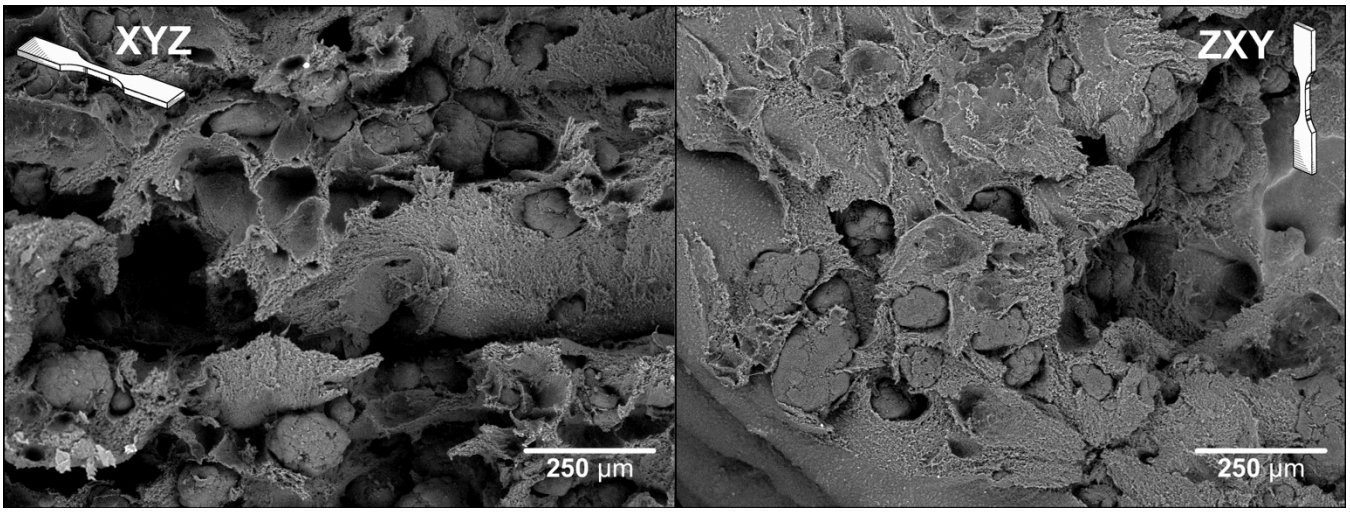

Figure 5.20: SEM micrographs of the fracture surfaces from representative samples of the 75:25:75 by weight ratio ABS MG47:UHMWPE:SEBS blend printed in the XYZ and ZXY build orientations.

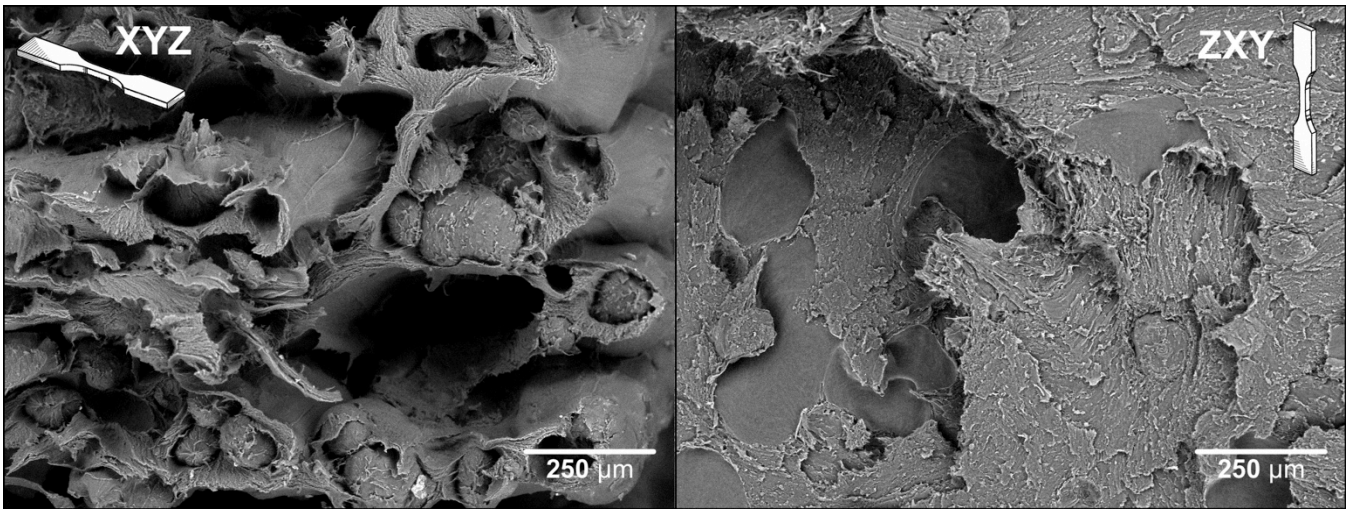

Figure 5.21: SEM micrographs of the fracture surfaces from representative samples of the 75:25:75 by weight ratio ABS MG47:UHMWPE:MASEBS blend printed in the XYZ and ZXY build orientations.

5.11. References

[1] Shaffer, S., Yang, K., Vargas, J., Di Prima, M. A., & Voit, W. "On reducing anisotropy in 3D printed polymers via ionizing radiation." *Polymer*, 2014.

[2] T. Horn, R. Aman, O. Harrysson, H. West, C. Keough, J. Brennan, D. Davis "Effect of Acetone Vapor Polishing Parameters for on the Properties of 3D Printed ABS Components" *25th Annual International Solid Freeform Fabrication Symposium, 2014 Aug 4-6, Austin, TX*

[3] Torrado, A. R., Roberson, D. A., & Wicker, R. B. "Fracture surface analysis of 3D-printed tensile specimens of novel ABS-based materials". *Journal of Failure Analysis and Prevention, 14(3), 343-353, 2014*.

[4] Torrado, A. R., Shemelya, C. M., English, J. D., Lin, Y., Wicker, R. B., & Roberson, D. A. (2015). "Characterizing the Effect of Additives to ABS on the Mechanical Property Anisotropy of Specimens Fabricated by Material Extrusion 3D Printing". *Additive Manufacturing. Accepted 6 February 2015*

[5] Brydson, J. A. "Plastics materials." *Butterworth-Heinemann, 1999*

[6] Ward, I. M., & Sweeney, J. "Mechanical properties of solid polymers". *John Wiley & Sons, 2012*

[7] Fang, H. W., Hsu, S. M., & Sengers, J. V. "Ultra-high molecular weight polyethylene wear particle effects on bioactivity." *University of Maryland, College Park, 9-10,* 2003

[8] Rocha, C., Torrado, A., Roberson, D. A., Shemelya, C., MacDonald, E., Wicker, R. B., "Novel ABS-Based Binary and Ternary Polymer Blends for Material Extrusion 3D Printing," *Journal of Materials Research, submited, 2014*.

[9] Jelčić, Ž., Vranješ, N., & Rek, V. "Long-Range Processing Correlation and Morphological Fractality of Compatibilized Blends of PS/HDPE/SEBS Block Copolymer". *In Macromolecular Symposia, 2010, 290(1), 1-14*

[10] Ha, C. S., Park, H. D., Kim, Y., Kwon, S. K., & Cho, W. J. "Compatibilizer in polymer blends for the recycling of plastics waste I: preliminary studies on 50/50 wt% virgin polyblends". *Polymers for Advanced Technologies, 1996, 7(5-6), 483-492*.

[11] Borggreve, R. J. M., & Gaymans, R. J. "Impact behaviour of nylon-rubber blends: 4. Effect of the coupling agent, maleic anhydride. Polymer", *1989, 30(1), 63-70*.

[12] Araújo, E. M., Hage Jr, E., & Carvalho, A. J. F. "Morphological, mechanical and rheological properties of nylon 6/acrylonitrile-butadiene-styrene blends compatibilized with MMA/MA copolymers". *Journal of materials science, 2003, 38(17), 3515-3520*.

[13] Wilkinson, A. N., Clemens, M. L., & Harding, V. M. "The effects of SEBS-g-maleic anhydride reaction on the morphology and properties of polypropylene/PA6/SEBS ternary blends". *Polymer, 2004, 45(15), 5239-5249*.

[14] Rzayev, Z. M. "Graft copolymers of maleic anhydride and its isostructural analogues: High performance engineering materials". *arXiv preprint arXiv:1105.1260. 2011*

[15] Yang, H. "Compatibilized blends of ABS copolymer and polyolefin". *U.S. Patent Application 11/202,594, 12 Ago. 2005*.

[16] Balkan, O., Demirer, H., Ezdeşir, A., & Yıldırım, H. "Effects of welding procedures on mechanical and morphological properties of hot gas butt welded PE, PP, and PVC sheets." *Polymer Engineering & Science, 2008, 48(4), 732-746.*

[17] Mulla, S. M., Phale, P. S., Saraf, M. R. "Use of X-Ray Diffraction Technique for Polymer Characterization and Studying the Effect of Optical Accessories" *AdMet,* 006, 2012

[18] Joo, Y. L., Han, O. H., Lee, H. K., Song, J. K., "Characterization of ultra high molecular weight polyethyelene nascent reactor powders by X-ray diffraction and solid state NMR". *Polymer, 2000, 41(4), 1355-1368.*

[19] Bakshi, S. R., Tercero, J. E., & Agarwal, A., "Synthesis and characterization of multiwalled carbon nanotube reinforced ultra high molecular weight polyethylene composite by electrostatic spraying technique." *Composites Part A: Applied Science and Manufacturing, 2007, 38(12), 2493-2499.*

[20] Carré, A. "Polar interactions at liquid/polymer interfaces." *Journal of Adhesion Science and Technology,* 2007, *21(10), 961-981.*

CHAPTER 6: COMPARISON OF FILLING AND THE DIFFERENT STANDARD SPECIMEN SIZES IN TENSILE STRENGTH AND ELONGATION TO BREAK

6.1. Introduction

Additive manufacturing (AM) has been around since the early 1980s when the term stereolithography was first utilized in a U.S patent by Charles W. Hull in 1986 [1]. Since then, many different techniques have been invented, developed and evaluated, and during this evaluation process, the available standards for traditional manufacturing techniques have continued to be applied without much update. Most of the standards specific to additive manufacturing are directed to powder bed fusion, [2-10] and only some of them are general to all AM or specific for polymer-based AM technologies. [8-10]

The tensile properties are without question among the most important characteristics to understand when evaluating a material for 3D printing technologies. The anisotropic nature of 3D printing techniques adds another important element which must be understood when performing materials characterization activities on 3D printed parts. Here, the mechanical property anisotropy is related to the build orientation of a specimen, for example ZXY as compared to XYZ. Typically, ZXY (or vertical) specimens tend to produce parts with decreased tensile strength as compared to vertically printed counterparts for polymeric-based 3D printing technologies such as fused deposition modeling (FDM), stereolithography (SLA), and selected laser sintering (SLS) [11-20]. How the manufacturing process translates into the final mechanical properties of a printed part needs to be better understood, but the lack of standarization and research still leaves many possible variables in the decision making process of a part designer.

The ASTM D638-10 [21] standard provides five different type dimensions (Types I through IV) for the determination of tensile properties of plastics, whether the polymeric materials are reinforced or un-reinforced. The standard specifies the preference for Type I specimens over the alternatives, and provides a guidance for which cases allow for the use of the other specified dimensions dimensions. Although none of the recommendations made by the standard directly specifies a reccommended type to be used in the evaluation of parts fabricated through materials extrusion 3D printing (ME3DP) or FDM technology, Type V offers many advantages over the other available dimensions as it allows for a faster evaluation of the material, less printing time, higher number of samples for the same use of material, less

variability due to lack of quality in the filaments being used, and —perhaps the most pertinent reason to those performng research related to ME3DP— the dimensions of the Type V specimen are the smallest as compared to the others which gives the possibility of being used in a higher number of small build envelope machines. This aspect is especially important when when specimens are printed in a build orientation perpendicular to the platform or in ZXY direction. However, the disadvantage of using small specimens in 3D printing in general, and in ME3DP in particular, is that the dimensions of the cross sectional area are within or very near to a factor of ten as compared to the print raster sizes. This is, a cross-sectional area of $3.2x3.18mm^2$ (thickness by width) compared to a normal raster size of $0.27x0.4mm^2$ (layer height by tip size). The raster dimension limits the overall number of layers in the cross sectional area of the specimen and increases the influence of the air-gaps in the final results. Other common dimensions are 0.1, 0.2 and 0.3mm for the layer heights, or 0.35, 0.6 or 0.8mm for the layer width (or diameters for the hotend tips).

The effects of print raster direction on the mechanical properties of parts printed through the use of FDM-type technologies has been evaluated in literature [13-15] and the accepted methodology for evaluating mechanical property anisotropy has been printing a standard tensile test specimen in various print orientations and/or raster patterns, for example Ahn, *et. al* [22] utilized the Type I specimen of the ASTM standard D638 to evaluate the effect of raster pattern on the tensile strength of test coupons printed from ABS while Bellini and Güçeri [14] evaluated the effect of both build orientation and raster pattern on the tensile strength of specimens printed by FDM following the ASTM D537-96 standard. Previous works by Torrado *et al*. [11, 12] have made use of the Type V specimen dimensions specified in the ASTM D638-10 standard; printed in a direction parallel to the platform, (horizontal or XYZ build orientation), and a direction perpendicular to the platform, (vertical or ZXY build orientation) to evaluate the mechanical property anisotropy of novel ABS-based composites and polymer blends printed through the use of ME3DP. The main difference between the two resulting specimens is the lack of continuous threads or rasters in the same direction of the tensile force, for ZXY specimens. Therefore, a more robust bond between the layers (or equivalently the print rasters) would be necessary in order to lower the anisotropy, along with a more homogenous distribution of the air gaps among the part. The problem with this

methodology is that printing a vertical sample can be a tedious, time-consuming process, if at all possible in some cases; for example, the previously mentioned works by Torrado, *et al.*, utilized the Type V dimensions due to an inability to print larger sized specimens in the ZXY direction due to printer build volume restrictions.

The work presented in this study proposes an alternative method for the evaluation of mechanical property anisotropy for parts printed using material extrusion 3D printing technologies. Here, the alternative was be to print a XYZ specimen with an adapted slicing that more closely resembles the raster morphology of a ZXY oriented printed specimen. Here we seek to better understand the relationship between the raster patterning and the mechanical properties of the printed part.

6.2. Experimental

The experiments in this study were designed to find a correlation between printing directions, dimensions and filling employing the ASTM standard D638-10 for tensile testing of polymers as a metric. Specimens 3D printed according to the Type I, Type IV and Type V dimensions were utilized to represent the different cross-sectional areas proposed by the standard. Type II was excluded due to its similarities to Type IV and V, and Type III was excluded due to size constrictions. Figure 6.1 depicts the relative size differences between the specimens. For comparison purposes, the main dimensions for the specimens are tabulated in Table 6.1.

In order to compare the influence or the raster direction in the mechanical properties, three different g-code recipes with different infill patterns were prepared for each type of specimen printed all in XYZ direction: 1) Longitudinal, 2) cross-hatched, and 3) transversal. An additional printing pattern set was produced only for Type V in the ZXY direction, in order to evaluate the effectiveness of printing "faux vertical" samples as well as provide a comparison to previous works by Torrado et al. [11, 12]. The slicing parameters used to generate the g-code can be found in Table 6.2. The cross-hatched filling pattern alternated the direction of the raster in 90º for each new layer generated, resulting in odd layers printed with rasters parallel to the axis of application of the tensile force and even layers printed with perpendicular rasters. This code was used in the machine without any further modification, the way it was generated by the g-code engine. The longitudinal variant was generated through the manual modification

of the cross-hatched code, by substituting the layers with transversal rasters with more longitudinal raster layers. These two versions were generated with a perimeter raster to avoid the crack to be generated outside the gauge length portion of the specimen. The transversal filling was generated from the same code used for the cross-hatched filling, but eliminating the external perimeter. The transversal filling tries to emulate a specimen printed perpendicular to the platform. Lastly, the vertical or ZXY printing was sliced from a modified STL for the Type V specimen dimensions with four additional ribs at the base to facilitate the printability. A graphical rendering representation of Type V specimens for each of the g-code filling patterns is shown in Figure 6.2.

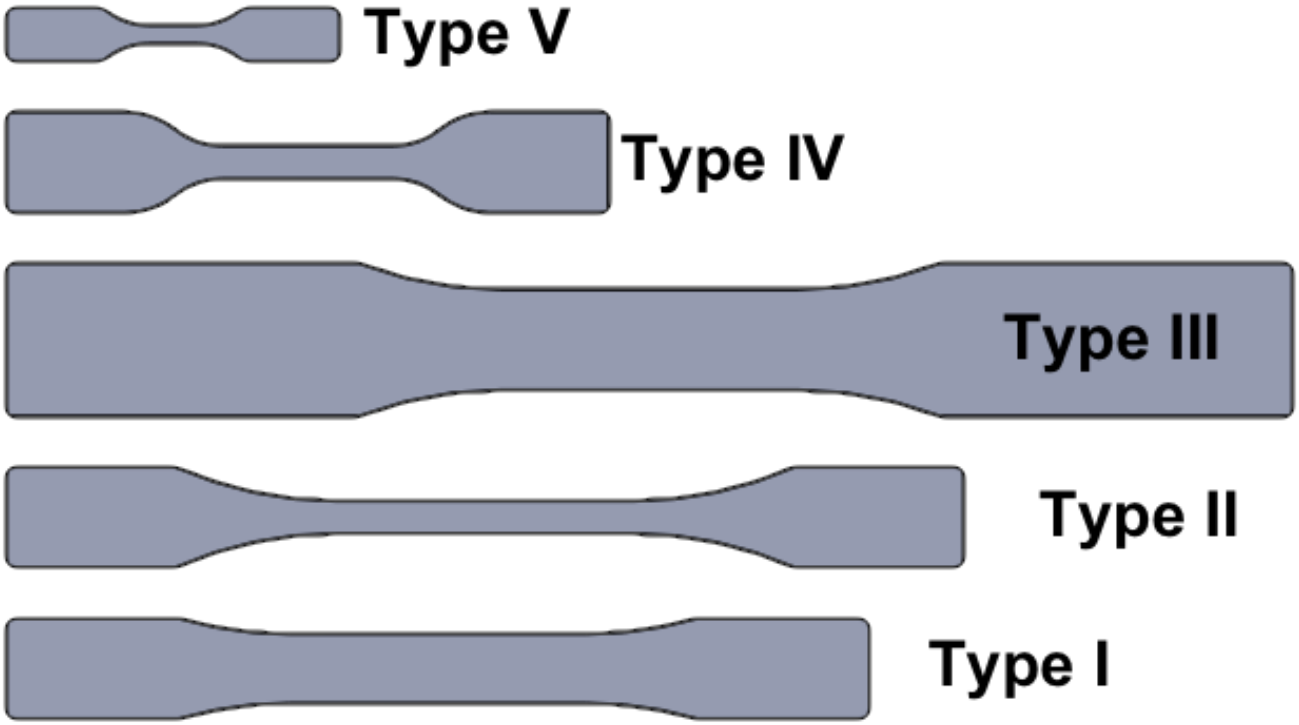

Figure 6.1: Graphical representation of the different types proposed by D638 to analyze stress-strain curves in plastic material

For this work, acrilonytrile butadiene styrene pellets (Cycolac™ grade MG47, Sabic, Pittsfield, MA, USA) were extruded into a filament with a target diameter of 1.75±0.05mm through the use of a Collin ZK 25T twin extruder/compounder (Dr. Collin GmbH, Erbersberg, Germany) equipped with co-rotating, intermeshing screws and a filament winding system operating with a mean barrel temperature of

215°C and a screw speed of 80 RPM. A custom Lulzbot TAZ 4 3D Printer (Aleph Objects Inc., Loveland, CO) running a custom Marlin open source firmware and modified with a V6 E3D hotend (E3D-Online Limited, Chalgrove, Oxfordshire , UK) was used to print all the specimens evaluated in this study.

Table 6.1: Main dimensions for specimens described by the ASTM D638-10 standard.

Type	Cross section		Gauge Length	Overall Length	Overall Width
	Width	Thickness		(min)	(min)
I	13	3.2	50	165	19
II	6	3.2	50	183	19
III	19	3.2	50	246	29
IV	6	3.2	25	115	19
V	3.18	3.2	7.62	63.5	9.53

* All dimensions in mm.

The mechanical properties were obtained through the use of an Instron® 5866 tensile testing machine (Instron, Norwood, MA) equipped with an Instron® 2663-821 advanced video extensometer (AVE) to measure % elongation (%EL). The specimens were tested at strain rates of 5mm/min for Type I and IV, and 10mm/min for Type V specimens at room temperature.

Table 6.2: Parameter used during the slicing process for the different filling patterns used in this study.

G-Code type	Fill pattern	Print Temperature (°C)	Object Infill (%)	Layer Height (mm)	G-code Nozzle Diameter (mm)	Actual Nozzle Diameter (mm)	Filament Diameter (mm)	Perimeters	Raft
Longitudinal	Rectilinear*	230	100	0.27	0.4	0.4	1.7	1	No
Cross-hatched	Rectilinear	230	100	0.27	0.4	0.4	1.7	1	No
Transversal	Rectilinear*	230	100	0.27	0.4	0.4	1.7	0	No

* Manually modified after slicing process

Cross sections of selected specimens were examined via scanning electron microscopy (SEM) using a Hitachi TM-1000 microscope equipped with a backscatter electron detector and operating at an accelerating voltage of 15kV (Hitachi High-Technologies Europe GmbH, Germany). Prior to SEM microanalysis, the specimens were sputter-coated with a gold-palladiuum (Au-Pd) alloy to reduce charge

effects with a Gatan sputter coater (Model 682 Precision Etching Coating System, Gatan, Inc., Pleasanton, CA, USA).

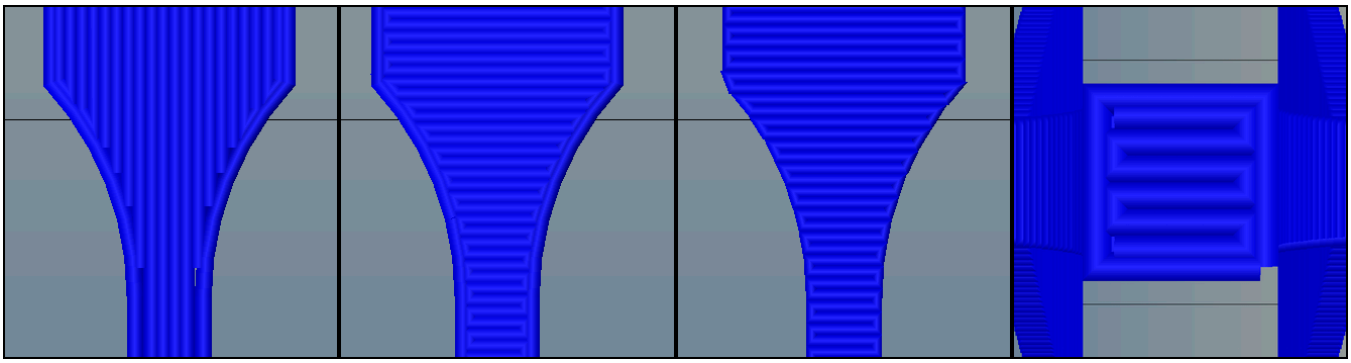

Figure 6.2: 3D rendering for the g-code of the three different filling patterns of a type V specimen. From left to right: Longitudinal rasters found in the longitudinal filling and the transversal filling even layers; transversal rasters of the cross-hatched filling; transversal rasters of the transversal filling lacking an external perimeter raster; and vertical printing with one external perimeter thread.

6.3. Discussion/Results

The results from the tensile test are presented Table 6.3 and Figure 6.3.while Figures 6.4 and 6.5 provide a graphical representation of the data. A key aspect to note is a geometric dependence on the mechanical anisotropy for different print raster types. For the Type I and Type IV dimensions, the longitudinal print raster pattern produced the strongest specimen, though the strength difference was not statistically significantly greater than the strength values for the crosshatched values. Also, for the Type I and Type IV printed specimens the transverse, or "*faux vertical*" specimens produced the lowest strength values which validates the use of this method to evaluate the mechanical property anisotropy utilizing all XYZ oriented specimens. Conversely, in the case of the Type V specimen dimension, the crosshatched raster pattern produced the strongest specimen where the longitudinal raster pattern led to tensile test results which were similar to the vertical ZXY oriented specimens and the transverse raster horizontally (XYZ oriented) specimens. The values obtained for equivalent printing patterns are very close among the different types with the exception of the Type V cross-hatched specimens, which show an elongation to brake 0.6 to 0.9% lower. The minor differences found between them can be attributed to variabilities in the effective filling of material in the specimen and differences in the slicing process.

Further validation of utilizing all XYZ oriented specimens in the evaluation of the mechanical property anisotropy of materials printed via ME3DP was the evaluation of the Type V specimens which led to a similarity in the UTS values for XYZ transversal (faux vertical) filling and vertical or ZXY printing; 28.6±0.8MPa compared to 29.5±0.8MPa, respectively. These two values are statistically equivalent. This result adds credence to the statement that an assessment of mechanical property anisotropy due to build orientation can be realized by the alteration of the raster pattern to mimic that of a vertically printed specimen.

Table 6.3: UTS mean and standard deviation values for the Types I, IV and V in longitudinal, cross-hatched, transversal and vertical printing patterns.

Material	UTS LONGITUDINAL		UTS CROSSHATCHED		UTS TRANSVERSAL		UTS VERTICAL	
	Mean (MPa)	σ (MPa)	Mean (MPa)	σ (MPa)	Mean (MPa)	σ (MPa)	Mean (MPa)	σ (MPa)
TYPE I	38.5	2.9	35.4	1.0	25.0	1.4	-	-
TYPE VI	39.9	1.4	38.2	1.4	29.6	0.9	-	-
TYPE V	29.3	1.1	37.6	1.9	28.6	0.8	29.5	0.8

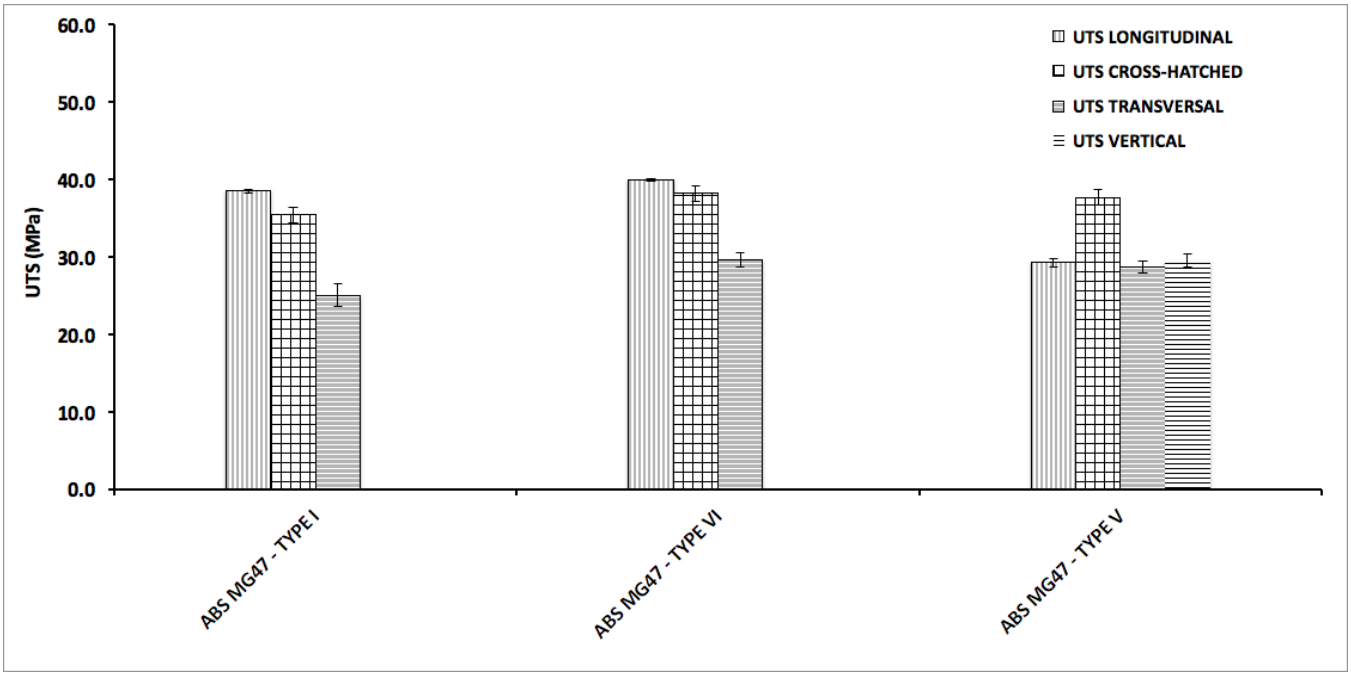

Figure 6.3: UTS mean values graphical comparison for the Types I, IV and V in longitudinal, cross-hatched, transversal and vertical printing patterns.

The same analysis conducted in Chapter 5 was repeated in this experiment, in which the cross sectional areas of tested representative specimens of transversal (XYZ) and vertical (ZXY) specimens was analyzed via SEM (Figure 6.5). The printing of the ZXY specimens was assisted with the use of cooling flow over the part provided by a fan through a duct pointing right over the last layers. Direct airflow over the tip was avoided to ensure the temperature reading was correct. The amount of material deposited by layer in a ZXY specimen is much lower than that for an XYZ specimen. Thus, the material in the later layers printed is still over the glass transition temperate and is therefore in a rubbery state. The material being printed on top drags the underneath soft material, causing imperfections on the desired shapes of the object being printed. The benefits of this technique are reflected in the quality of the cross-sectional area obtained in these specimens, whose shape is closer to a rectangle than in the previous experiments performed with a MakerBot Replicator printer. While this is true, we can still find that corners are more rounded that in XYZ specimen. This is the second reason why a slight increase in the UTS is expected for these specimens and why the analysis of ZXY UTS should always be performed with XYZ specimens.

Table 6.4: Elongation to break mean and standard deviation values for the Types I, IV and V in longitudinal, cross-hatched, transversal and vertical printing patterns.

Material	EL% LONGITUDINAL		EL% CROSSHATCHED		EL% TRANSVERSAL		EL% VERTICAL	
	Mean (%)	σ (%)	Mean (%)	σ (%)	Mean (%)	σ (%)	Mean (%)	σ (%)
TYPE I	2.5	0.2	3.0	0.1	2.0	0.2	-	-
TYPE VI	2.9	0.1	3.3	0.8	2.4	0.3	-	-
TYPE V	2.7	0.5	2.4	0.2	2.9	0.4	2.2	0.4

Table 6.5: Values of anisotropy for crosshatched specimens versus transversal and vertical specimens.

Material	UTS CROSSHATCHED		UTS TRANSVERSAL		Δ		Δ	
	Mean (MPa)	σ (MPa)	Mean (MPa)	σ (MPa)	Mean (MPa)	σ (MPa)	Mean (%)	σ (%)
TYPE I	35.4	1.0	25.0	1.4	10.4	1.7	29.28%	5.00%
TYPE VI	38.2	1.4	29.6	0.9	8.6	1.6	22.52%	4.33%
TYPE V	37.6	1.9	28.6	0.8	9.0	2.1	23.96%	5.69%
	UTS CROSSHATCHED		UTS VERTICAL		Δ		Δ	
	Mean (MPa)	σ (MPa)	Mean (MPa)	σ (MPa)	Mean (MPa)	σ (MPa)	Mean (%)	σ (%)
TYPE V	37.6	1.9	29.5	0.8	8.2	2.1	21.67%	5.72%

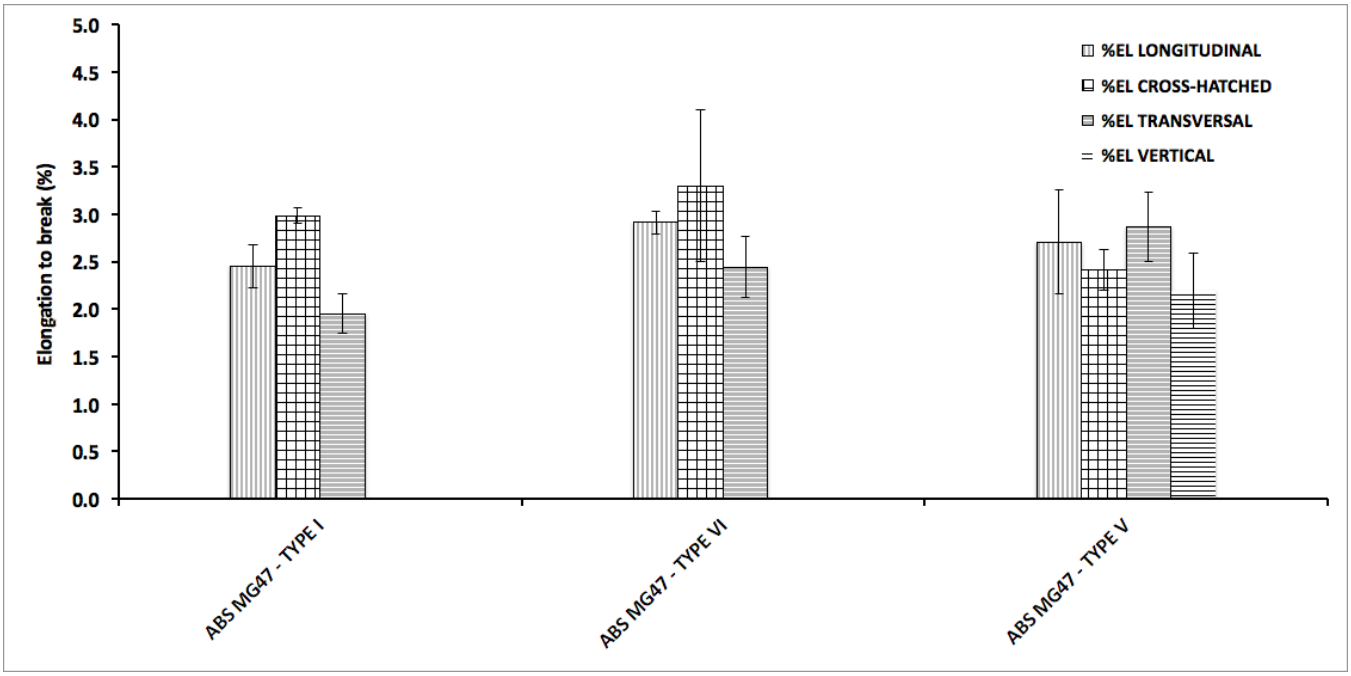

Figure 6.4: Elongation to break mean values graphical comparison for the Types I, IV and V in longitudinal, cross-hatched, transversal and vertical printing patterns.

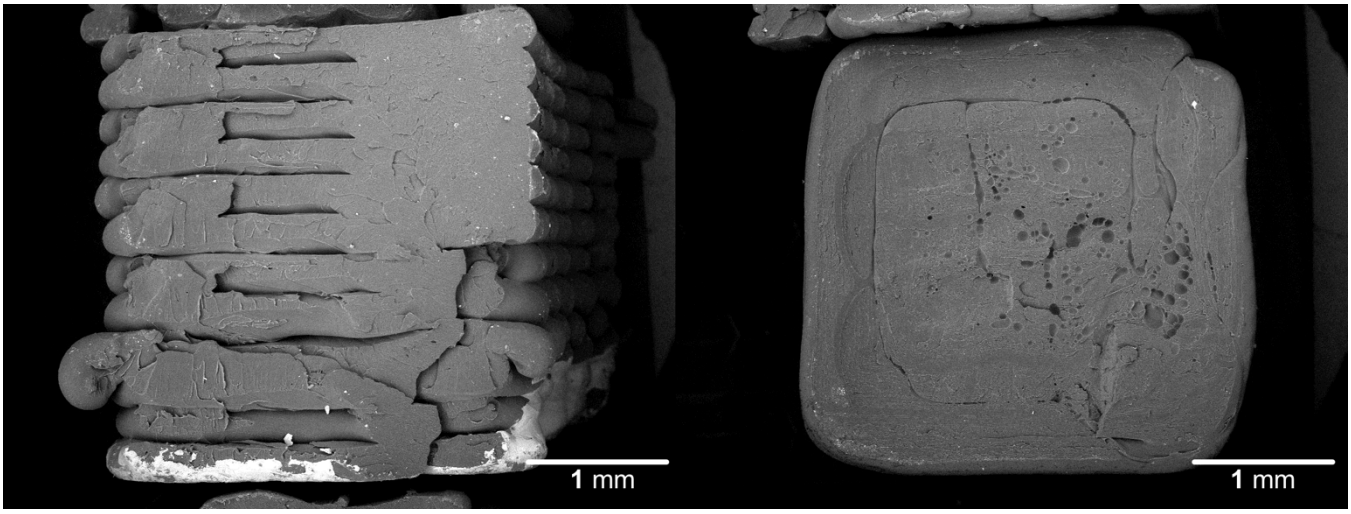

Figure 6.5: Comparison of cross-sectional areas: Fracture surfaces of tensile tested Type V specimens: On the left, transversal filling; on the right, vertical printing.

The values for the anisotropy between crosshatched specimens, and transversal and vertical specimens can be found Table 6.5. The mean value for all the types compared in that table provides an average relative anisotropy of 24.2±5.2% for ABS MG47.

6.3.1. Heat-treating test

Material extrussion additive manufacturing can be considered a discrete process since the extrusion of material is constantly interrupted and the parts are generated from the deposition of threads with a given dimension. Due to this characteristique, the strength of a raster being pulled in its longitudinal direction is not the same that the strength of several rasters bonded together being pulled in their transversal direction, especially if this "welding" process occurs between rasters at different temperature (one at printing temperature, the adjacent or bottom one at lower temperature. A previous study performed on PLA by Shaffer *et al*. [13] have demonstrated the strength improvement produced by the application of ionizing radition on these bondings at temperatures near the T_g of the material. Perhaps a question that remained unanswered was the contribution of the reheating process in the final results. The effects of a post-processing reheat over the glass transition temperature could potentially help with the redistribution of the polymeric chains and the linkages between them within the bonding. However, exposure to high temperature must be restricted to avoid big deformations of the part and ensure dimensional stability. Espalin [23] performed similar studies with Stratasys® ABS-PC blends that showed a practically total densification achieved and an increase of aprox. 25% when compared to untreated specimens. Nevertheless, the specimens undergone a not negligible dimensional change in their main dimensions, and geometric changes were not analyzed further. The main goal of this study is not to to reduce air gaps inside the part but instead improve bonding of non-continuously deposited material interfaces.

Table 6.6: Comparison between heat treated and non-treated Type V specimens.

Material	UTS CROSSHATCHED		UTS VERTICAL		Δ		Δ	
	Mean (MPa)	σ (MPa)	Mean (MPa)	σ (MPa)	Mean (MPa)	σ (MPa)	Mean (%)	σ (%)
TYPE V Not treated	37.6	1.9	29.5	0.8	8.2	2.1	21.67%	5.72%
TYPE V Heat Treated	39.0	1.3	30.9	1.7	8.1	2.1	20.74%	5.47%

Two additional Type V sets of five specimens were printed and ZXY direction and in XYZ direction with crosshatched filling. These two sets were exposed to a temperature ramp between 100 and 120ºC for 10 minutes, and then kept at that temperature for 20 minutes more. Then the specimens were carefully removed from the oven and let cool down for one hour. That heating program had previously

showed to be long enough to allow the material to freely deform in parts of a comparable size. The results of the tensile test are presented in Table 6.6 along with those of the non treated specimens.

The resulting UTS is slightly higher for the treated specimens, but this difference is within expected deviation values and cannot be considered a significant improvement, or at least and improvement derived from an optimized bonding between rasters.

6.4. Conclusions

The possibility of replacing vertically printed specimens (or in ZXY direction) with horizontal specimens printed with a transversal filling (or faux vertical specimens) to evaluate the anisotropy of the mechanical characteristics of a material has been demonstrated. The tensile results showed for them are complitely equivalent. The second methodology is recommended due to the simplicity, higher accuracy and a higher reliability of the printing process. This result predicts that the resulting bond strenght between the welded rasters is initially independent of the difference of temperature between the rasters and the thickness of the threads being welded.

The three specimen types chosen from the ASTM standard D638-10 for this experiment have provided equivalent tensile test results in both strength and elongation to brake. Although the standard recommends the use of the Type I specimen, Types IV and V should be equally suitable for evaluating the characteristic of a material extruded 3D printed material. Perhaps there should be a slight preference towards the use of Type IV in order to diminish raster dimension or other printing pattern related influence, that could affect the results. It should be possible to reduce or completely avoid these deviations in Type V specimens through a better engineered slicing of the part.

Lastly, short exposure to heat sources has not shown improvement of the bonding between rasters. Thus, all improvement generated by a so-called heat-treatment of ME3DP parts can be attributed to material densification, as long as radition or other type of environmental effect is not being used.

6.5. References

[1] Hull, Charles W. "Apparatus for production of three-dimensional objects by stereolithography." U.S. Patent No. 4,575,330. 11 Mar. 1986.

[2] "Standard Specification for Additive Manufacturing Titanium-6 Aluminum-4 Vanadium with Powder Bed Fusion," ASTM International, *F2924-14*, 2014

[3] "Standard Specification for Additive Manufacturing Titanium-6 Aluminum-4 Vanadium ELI (Extra Low Interstitial) with Powder Bed Fusion," ASTM International, *F3001-14,* 2014

[4] "Standard Guide for Characterizing Properties of Metal Powders Used for Additive Manufacturing Processes," ASTM International, *F3049-14,* 2014

[5] "Standard Specification for Additive Manufacturing Nickel Alloy (UNS N07718) with Powder Bed Fusion," ASTM International, F3055-14a, 2014

[6] "Standard Specification for Additive Manufacturing Nickel Alloy (UNS N06625) with Powder Bed Fusion", ASTM International, F3056-14e1, 2014

[7] "Standard Guide for Evaluating Mechanical Properties of Metal Materials Made via Additive Manufacturing Processes," ASTM International, *F3122-14*, 2014

[8] "Standard terminology for additive manufacturing technologies," ASTM International, *F2792-12a*, 2013.

[9] "Standard Practice for Reporting Data for Test Specimens Prepared by Additive Manufacturing," ASTM International, *F2971-13*, 2013.

[10] "Standard Specification for Powder Bed Fusion of Plastic Materials", ASTM International, *F3091M-14*, 2014

[11] Torrado, A. R., Roberson, D. A., & Wicker, R. B. "Fracture surface analysis of 3D-printed tensile specimens of novel ABS-based materials". *Journal of Failure Analysis and Prevention, 14(3), 343-353, 2014*.

[12] Torrado, A. R., Shemelya, C. M., English, J. D., Lin, Y., Wicker, R. B., & Roberson, D. A. (2015). "Characterizing the Effect of Additives to ABS on the Mechanical Property Anisotropy of Specimens Fabricated by Material Extrusion 3D Printing". *Additive Manufacturing. Accepted 6 February 2015*

[13] Shaffer S, Yang K, Vargas J, Di Prima MA, Voit W, "On reducing anisotropy in 3D printed polymers via ionizing radiation", *Polymer, 55(23), 5969-5979, 2014*

[14] A. Bellini, S. Güçeri, "Mechanical characterization of parts fabricated using fused deposition modeling", *Rapid Prototyping Journal, 9, 252–264, 2003*

[15] O.S. Es-Said, J. Foyos, R. Noorani, M. Mendelson, R. Marloth, B.A. Pregger, "Effect of Layer Orientation on Mechanical Properties of Rapid Prototyped Samples", *Materials and Manufacturing Processes. 15, 107–122, 2000*

[16] R. Hague, S. Mansour, N. Saleh, R. Harris, "Materials analysis of stereolithography resins for use in Rapid Manufacturing", *Journal of Materials Science. 39, 2457–2464, 2004*

[17] Vega, V., Clements, J., Lam, T., Abad, A., Fritz, B., Ula, N., & Es-Said, O. S., "The Effect of Layer Orientation on the Mechanical Properties and Microstructure of a Polymer", *Journal of materials engineering and performance, 20, 978–988, 2011*

[18] A. Bagsik, V. Schoeppner, E. Klemp, "FDM Part Quality Manufactured with Ultem* 9085", *in: 14th International Scientific Conference on Polymeric Materials, September, 2010.*

[19] R. Hague *, S. Mansour, N. Saleh, "Material and design considerations for rapid manufacturing", *International Journal of Production Research. 42, 4691–4708, 2004*

[20] B. Caulfield, P. E. McHugh, and S. Lohfeld, "Dependence of mechanical properties of polyamide components on build parameters in the SLS process", *Journal of Materials Processing Technology, 182.1, 477-488, 2007*

[21] "Test Method for Tensile Properties of Plastics", *ASTM International ASTM D638, 2010*

[22] S.-H. Ahn, M. Montero, D. Odell, S. Roundy, P.K. Wright, "Anisotropic material properties of fused deposition modeling ABS", *Rapid Prototyping Journal. 8, 248–257, 2002*

[23] Espalin Jr, D. "Development of a multi-material, multi-technology FDM system for process improvement experimentation." *2012, The university of Texas at El Paso*

CHAPTER 7: CONCLUDING REMARKS AND FUTURE WORK

The work presented in this document reviews the whole process of developing new blends and composites for applications in ME3DP, from the selection and processing of the materials, to the evaluation, testing and analysis of the final parts. Specifically, the text is centered on the tensile properties of the final parts, how to evaluate the resulting anisotropy and the different characteristics that lead to it, and how to lower it through material development and characterization.

During the evaluation of different composite and blend systems, a combination of ABS, UHMWPE and SEBS was found surprisingly suitable for parts with lower differences in the strength for different printed directions. This combination of materials was more deeply investigated in chapter 5, revealing two systems with values of relative strength anisotropy potentially under 5% after performing corrections. A new shape factor was introduced to correct the UTS values for specimens printed in the ZXY direction due to a limited printing quality in MakerBot machines. The 40.6% initial value for the anisotropy of MG47 ABS was recalculated through the shape factor to be 24.8%. Interestingly enough, this same value correlated with the experiment performed in chapter 6, in which the same material showed relative anisotropy values of 24.0 and 21.7% for the equivalent specimens. These results reinforce the validity of the corrections performed with the shape factor for the previous chapter, in which the anisotropy for ABS MG37CR (75) : UHMWPE (25) : SEBS (10) was recalculated from 22.0 to 1.3% and ABS MG47 (75) : UHMWPE (25) : SEBS (50) was recalculated from 24.8 to 4.9%. Although these updated values can be considered to be on the optimistic side of the scale, it should not lessen importance to the result, that demonstrates a tendency in favor of materials with very low anisotropy.

The benefits and deficits of the aplicability of the available standards was evaluated as well, and the difficulty to meet the tolerances proposed by them was exposed. This work provides recommendations for future material evaluations in ME3DP. However, experimentation in ME3DP still requires more flexibility from a slicing point of view. Slic3r is probably the most flexible slicer interface available right now, but it some manual recoding was still necessary in the elaboration of the g-code required for these studies. Furthermore, for some specific objects with small sections, the acumulation of still soft material

directs to printing quality issues. More flexibility is required as the g-code needs to be adapted to the different materials offered and to be offered.

The possible effects that an after-process reheating cycle could have in the strength of the bonding between rasters in ME3DP parts was evaluated as well with no promising results. The increase in UTS obtained with these methodologies is mostly due to a material densification of the part, although this might differ if blends based on materials other than ABS are utilized.

A compromise must always be taken between the dimensional accuracy or the mecanical properties obtained through the practical filling of material in the final part produced. This is why the research should focus in the development of materials with engineered properties specifically for ME3DP.

APPENDIX A: PERMISSION TO INCLUDE MATERIAL FROM *JOURNAL OF FAILURE ANALYSIS AND PREVENTION*

RE: Request to use material published in Journal of Failure Analysis and Prevention in a Dissertation

Absolutely.

Per the copyright transfer statement:

The author retains the following:

1 All proprietary rights other than copyright, such as patent rights.

2 The right to make oral presentation or to personally reuse all or portions of the content of the work in other works of his own authorship, including lectures, textbooks, reviews, and articles, provided proper notice of ASM International's copyright is given.

3 The right to reproduce the work or parts thereof without revision or modification for the author's personal use, for lecture or educational purposes, to the extent the Fair Use Provisions of the U.S. Copyright Act permit, provided that all copies include proper notice of ASM International's copyright and indicate the source, and that no fees are collected for distribution or publication of the work. If the work was prepared by an employee within the scope of his or her employment, the employer shall have the right to make copies of the article for the employer's own internal use.

4 The right to post an electronic form of the final ASM International file of the work without revision or modification on the author's own personal or current employer's website, provided that such posting is noncommercial in nature and the work is made available to users without a fee or charge, and provided that proper notice of ASM's copyright is included. Such posting shall include a link to the journal homepage. The following statement must appear on the first page, or screen, of the work as posted:

Copyright [year; for example, 2014] ASM International. This paper was

published in [journal bibliographic information; for example, Journal of Failure Analysis and Prevention, Vol. 14, Issue 1, pp. 99-108] and is made available as an electronic reprint with the permission of ASM International. One print or electronic copy may be made for personal use only. Systematic or multiple reproduction, distribution to multiple locations via electronic or other means, duplications of any material in this paper for a fee or for commercial purposes, or modification of the content of this paper are prohibited.
5 The right to make limited distribution of the article or portions of the article.
6 The right to reproduce Figures and extracts from the article with proper acknowledgment.

Diane Whitelaw

Production Coordinator

9639 Kinsman Road | Materials Park, Ohio | 44073-0002 USA

P 440.338.5151 ext. 5240
F 440.338.4634
E diane.whitelaw@asminternational.org
W www.asminternational.org

From: Angel Torrado [mailto:artorrado@gmail.com] **Sent:** Monday, February 23, 2015 12:56 PM**To:** Diane Whitelaw**Cc:** Roberson, David A**Subject:** Request to use material published in Journal of Failure Analysis and Prevention in a Dissertation

Dear Mrs. Whitelaw,

I am a Ph.D. candidate at The University of Texas at El Paso, El Paso, TX, USA. An article I have written was published in *Journal of Failure Analysis and Prevention*. The article at issue is cited below:

Torrado Perez, A. R., Roberson, D. A., & Wicker, R. B. (2014). Fracture surface analysis of 3D-printed tensile specimens of novel ABS-based materials. *Journal of*

Failure Analysis and Prevention, *14*(3), 343-353.
I wanted to request permission for the use of the material in the mentioned article in my dissertation. The University of Texas at El Paso would accept permission to use the material published in *Journal of Failure Analysis and Prevention* in a form of a reply to this e-mail. I appreciate your time and look forward to receiving a reply to this message.
Thank you in advance,

Ángel R. Torrado

==========

==========

APPENDIX B: PERMISSION TO INCLUDE MATERIAL FROM JOURNAL OF *ADDITIVE MANUFACTURING*

Elsevier copyright agreement allows the sharing of the article for personal (scholarly) purposes, as stated in their copyright agreement section for subscription articles. Such agreement can be found in their online website (http://www.elsevier.com/journal-authors/author-agreement). An extract of said agreement is included in following lines:

Authors can use their articles, in full or in part, for a wide range of scholarly, non-commercial purposes as outlined below:

- Share copies of the article and distribute them via email to colleagues for their research use (also known as 'scholarly sharing').
- Share the article for personal use or for the author's own classroom teaching.
- Use the article at a conference, meeting or for teaching purposes.
- Allow the author's employers to use the article for other internal purposes (such as training).
- Include the article in a printed compilation of the author's works, such as collected writings and lecture notes.
- Inclusion the article in a thesis or dissertation
- Use the article in full or in part to prepare other derivative works, including expanding the article to book-length form, with each work to include full acknowledgement of the article' original publication.

These rights apply for all Elsevier authors who publish their article as either a subscription article or an open access article. In all cases we require that all Elsevier authors always include a full acknowledgement and, if appropriate, a link to the final published version hosted on Science Direct.

CURRICULUM VITAE

Ángel Ramón Torrado Pérez was born June 4, 1984 in Madrid, Spain, to Ángel Ramón Torrado Orbe and María del Pilar Pérez Pinazo. He decided to move to the United States to pursue his Ph.D. in Materials Science and Engineering at The University of Texas at El Paso, after meeting his wife Stephanie Diebold. Ángel holds an advance degree (B.S. & M.S.) in mechanical engineering by Escuela Técnica Superior de Ingenieros Industriales (Universidad Politécnica de Madrid) after which he spent four years working with the agricultural division of Deere & Company.

Selected Publications:

Torrado, A. R., Shemelya, C. M., English, J. D., Lin, Y., Wicker, R. B., Roberson, D. A. (2015). Characterizing the Effect of Additives to ABS on the Mechanical Property Anisotropy of Specimens Fabricated by Material Extrusion 3D Printing. Additive Manufacturing. (Accepted, in press)

Torrado, A. R., Roberson, D. A., Wicker, R. B. (2014). Fracture surface analysis of 3D-printed tensile specimens of novel ABS-based materials. Journal of Failure Analysis and Prevention, 14(3), 343-353.

Rocha, C. R., **Torrado, A. R.**, Roberson, D. A., Shemelya, C. M., MacDonald, E, Wicker, R. B. (2014) Novel ABS-based binary and ternary polymer blends for material extrusion 3D printing. Journal of Materials Research, 29(17) 1859-1866.

Roberson, D. A., **Torrado, A. R.**, Shemelya, C. M. , Rivera, A., MacDonald E., Wicker, R. B., (2015) Comparison of Stress Concentrator Fabrication for 3D Printed Polymeric Izod Impact Test Specimens. Additive Manufacturing, (Accepted)

Shemelya, C. M., Rivera, A., **Torrado, A. R.**, Rocha, C., Liang, M., Yu, X., Kief, C., Alexander, D., Stegeman, J., Xin, H., Wicker, R. B., MacDonald, E., Roberson, D. A., (2015). Mechanical, Electromagnetic, and X-Ray Shielding Characterization of a 3D Printable Tungsten/Polycarbonate Polymer Matrix Composite for Space Based Applications. Journal of Electronic Materials, (Accepted, in press)

Permanent address: San Manuel 1-11-1

28011, Madrid, Spain

artorradoperez@miners.utep.edu

This dissertation was typed by Ángel Ramón Torrado Pérez